Pharmaceutical Characterization of Selected Xenobiotics Utilizing Novel Drug Delivery Systems

By

Samaa Alrushaid

A Thesis submitted to the Faculty of Graduate Studies of The University of Manitoba

in partial fulfilment of the requirements of the degree of

DOCTOR OF PHILOSOPHY

College of Pharmacy

Rady Faculty of Health Sciences

University of Manitoba

Winnipeg

ABSTRACT

Drug development is a very costly procedure. Many failed clinical trials could be prevented by optimizing drug formulations or delivery systems of an existing drug, which may be a better and less costly approach over developing a new compound. In this thesis, chemical structure modification was employed as a drug delivery optimization strategy to improve the efficacy and safety of selected xenobiotics, and examine their biodistribution and feasibility for further drug development using *in silico*, *in vitro*, and *in vivo* studies. DoxQ, a derivative of the anticancer drug doxorubicin, was developed to mitigate poor bioavailability and systemic toxicities associated with doxorubicin. The speculated mechanism of cardiac and renal toxicities induced by doxorubicin involves oxidative stress while the mechanism behind the poor bioavailability is due to doxorubicin being a substrate of a major metabolic enzyme CYP3A4 and P-glycoprotein efflux transporter. To mitigate these effects, the flavonoid quercetin was conjugated to doxorubicin (DoxQ) as it is a potent antioxidant and exhibits inhibitory effects on CYP3A4 and P-glycoprotein, and also is absorbed via intestinal lymphatics. DoxQ changed the physiochemical properties of the parent compound doxorubicin as predicted in silico by computer software packages. *In vitro* DoxQ inhibited CYP3A4, showed higher cellular uptake by MDCK-MDR cells than doxorubicin, was less toxic to cardiomyocytes, and reduced the expression of cardiac toxicity and oxidative stress markers. DoxQ administered intravenously to rats had a short half-life, was primarily eliminated via non-renal routes, less nephrotoxic than doxorubicin and did not show significantly higher cardiac toxicity than doxorubicin. Oral administration of DoxQ increased the systemic exposure of doxorubicin by ~1.5 fold compared to oral doxorubicin, and showed that Dox was partially absorbed via intestinal lymphatics. MyoNovin® is a novel skeletal muscle regenerator designed to treat muscle atrophy. *In silico*

modelling suggests that MyoNovin® is a potentially good candidate for oral or transdermal administration. In vitro MyoNovin® was not cardiotoxic < 8 μM and did not inhibit CYP3A4. A single intravenous dose of MyoNovin® to rats showed that it has a short half-life, distributes to tissues, and shows no evidence of renal or cardiac toxicity.

ACKNOWLEGMENTS

My deepest gratitude goes to my advisory committee members Dr. Frank Burczynski, Dr. Neal Davies, and Dr. Casey Sayre, who were sequentially my primary advisors during my PhD studies. The outstanding guidance and support I received from them was above and beyond what I anticipated as a graduate student, I could have not asked for better advisors. I am truly grateful for their solid knowledge, expertise, patience, kindness, time, and efforts as well as the numerous opportunities they have given me to learn new techniques, meet elite researchers and also share, present, and publish my research findings. These valuable opportunities along with the insightful conversations with my advisors have not only significantly helped me to grow as a researcher but also as a person and made my graduate experience a pleasant journey. I am also particularly grateful to Dr. Burczynski for giving me the opportunity to teach at both the undergraduate and graduate levels, Dr. Davies for his sense of humor and for introducing me to work with excellent researchers at the University of Kansas and the University of Alberta, Dr. Sayre for training me to conduct a pharmacokinetic study and use analytical instruments for the first time.

I am also thankful to my advisory committee member Dr. Donald Miller for his support, guidance, and insightful comments during committee meetings and discussions, and also for giving me an opportunity to work on a side project. I am grateful to collaborators and researcher: Dr. Laird Forrest, Dr. Sanjeewa Saneedra, Dr. Yunqi Zhao, Dr. Ayman El-Kadi, Zaid Maayah, Dr. Ramir Löbenberg, Dr. Jaime Yáñez, Dr. Hope Anderson, Dr. Ted Lakowski, Ryan Lillico, Dr. Xiaochen Gu, Sarandeep Malhi, Dr. Geoffrey Tranmer, Dr. Ousama Rachid, Dr. Judy Anderson, for their guidance, technical assistance, and valuable contributions in various projects during my studies. Special thanks to past and current members in the Davies laboratory: Dr. Stephanie Martinez for her guidance, support, and technical assistance, Tyson Le for technical

assistance and support, Ana Luísa de P. Oliveira and Júlia Novaes for their support and contribution in publishing side projects. I am also thankful to past and current graduate students: Yannick Traore, Refaat Omar, Andy Chen, and Yuhua Fang for their technical assistance and support.

I would also like to express my sincere gratitude to the College of Pharmacy at Kuwait University for the generous financial support I have received throughout my PhD program.

Lastly, I would like to express my profound gratitude to my father Sami Al-Rushaid, my mother Sabah Al-Arfaj, my son Bader, and my siblings Sharifah, Fahed, and Eithar for their endless love, care, continuous support, and for always encouraging me even at my worse days.

DEDICATION

This thesis is dedicated to my beloved parents Sami and Sabah, my son Bader, and my siblings Sharifah, Fahed, and Eithar. Without their deep love and exceptional support, I would not have been able to complete my PhD studies.

TABLE OF CONTENTS

LIST OF FIGURES

LIST OF TABLES

ABBREVIATIONS AND SYMBOLS

~	Approximately
°C	Degrees Celsius
%	Percent
α	Alpha
α-MHC	α-myocin heavy chain
β	Beta
β-MHC	β-myocin heavy chain
μ	Micro
μg	Microgram
μm	Micrometer
μM	Micromolar
ΔΔCT	Delta Delta cycle threshold (relative gene expression method)
ΣXu	Cumulative amount excreted unchanged in urine
ABCB1	ATP binding cassette B1, a gene that encodes
ABTS®	(2,2'-azino-di-[3-ethylbenzthiazoline sulphonate])
$ABTS^{\bullet+}$	(2,2'-azino-di-[3-ethylbenzthiazoline sulphonate]) radical cation
ad libitum	At one's pleasure (as desired)
ADME	Absorption, Distribution, Metabolism, Excretion
ADP	Adenosine di-phosphate
$AgNO_3$	Silver nitrate
ALT	Amino alanine transferase
ANOVA	One-way analysis of variance

AST	Aspartate amino transferase
ATP	Adenosine triphosphate
ATP	Adenosine tri-phosphate
AUC	Area under the concentration-time curve
$AUC_{(m)}$	AUC of the metabolite after IV administration of an equimolar dose of the preformed metabolite
$AUC_{(m,D)}$	AUC of the metabolite after administration of its precursor
AUC_{inf}	Area under the plasma concentration-time curve extrapolated to infinity
AUC_{last}	Area under the plasma concentration-time curve up to the last measurable concentration
AUEC	Area under the effect curve
B.W.	Body weight
BNP	Brain natriuretic peptide
BW	Body weight
C_0	Maximum serum concentration calculated by back extrapolation
CADD	Computer-aided drug design
$C_{average}$	Average calculated concentration
$CDCl_3$	Deuterated chloroform
cDNA	Complementary Deoxyribonucleic Acid
CH_3CN	Methyl cyanide (acetonitrile)
CK	Creatine kinase
CL	Clearance
C_{last}	Last measurable (observed) concentration

$CL_{hepatic}$	Hepatic clearance
$CL_{non\text{-}renal}$	Non-renal clearance
CL_{renal}	Renal clearance
CL_{tot}	Total clearance
C_{max}	Maximum plasma concentration
c-met	Tyrosine-protein kinase Met
CO_2	Carbon dioxide
Conc.	Concentration
Ct	Cycle threshold
cTnI	Cardiac troponin
CV	Coefficient of variation
CYP/CYP450	Cytochrome P450
DAPI	4',6-diamidino-2-phenylindole
DCF	Dichlorofluorescein (DCF)
DCM	Dichloromethane
DIPEA	Diisopropylethylamine
DMEM	Dulbecco’s modified Eagle’s medium
DMEM-F12	Dulbecco's Modified Eagle Medium/Nutrient Mixture F-12
DMF	Dimethylformamide
DMSO	Dimethyl sulfoxide
DNA	Deoxyribonucleic acid
dNTP	Deoxynucleotide Triphosphate
Dox	Doxorubicin

Dox-HA	Doxorubicin-hyaluronic acid conjugate
DoxQ	Doxorubicin-quercetin conjugate
E	Extraction ratio
ELISA	Enzyme-linked immunosorbent assay
EPR	Electron paramagnetic resonance
ER	Extraction ratio
EROD	Ethoxyresorufin O-deethylase
ESI	Electrospray ionization
ESI/MS	Electron spray ionization mass spectrometry
EtOAc	Ethyl acetate
EtOH	Ethanol
ex/em	Excitation/Emission
F	Bioavailability
FBS	Fetal bovine serum
FDA	United States Food and Drug Administration
f_e	Fraction excreted unchanged in the urine
FGF	Fibroblast growth factor
F_m	Fraction of the dose metabolized
g	Gram
G	Gauge
GST-A1	Glutathione S-transferase A1
h	Hour
H^1NMR	Proton nuclear magnetic resonance

HATU	1-[Bis(dimethylamino)methylene]-1H-1,2,3-triazolo[4,5-b]pyridinium 3-oxid hexafluorophosphate
HCl	Hydrochloric acid
HGF	Hepatocyte growth factor
H-Gly-OtBu-HCl	Glycine with t-butyl protected hydrogen
HO-1	Heme oxygenase
HPLC	High performance liquid chromatography
HSPs	Heparin sulfate proteoglycans
HT29	Colorectal cancer cell line
I_2	Iodine
IC_{50}	Half maximal inhibitory concentration
IP	Intraperitoneally
IS	Internal standard
IV	Intravenous
K_2CO_3	Potassium carbonate
K562	Human leukemia cell line
k_{el}	Elimination rate constant
kg	Kilograms
L	Liter
LC-ESI-MS	Liquid chromatography – electrospray ionization – mass spectrometry
LOD	Limit of detection
Log P	Partition coefficient
logD	Distribution coefficient

LogP	Partition coefficient
LOQ	Limit of quantification
m	Milli
M	Molar
MCF-7	Breast cancer cell line isolated from humans
MDCK	Multi-drug resistant canine kidney cells
MDCK-MDR	Madin-Darby canine kidney- multidrug resistance
MDR1	Multidrug resistance protein 1
mg	Milligrams
min	Minutes
mL	Milliliter
mm	Millimeters
mM	Millimolar
MMPs	Metalloproteinases
mol	Mole
mRNA	Messenger Ribonucleic Acid
MROD	Methoxyresorufin O-deethylase
MTT	3-(4,5-dimethylthiazol-2-yl)-2,5-diphenyltetrazolium bromide
MW	Molecular weight
N or n	Number
n	Nano
NA	Not applicable
NaCl	Sodium chloride

NAG	β- N-acetyl-β-D-glucosaminidase
NaOH	Sodium hydroxide
Na_3VO_4	Sodium orthovanadate
ND	Not detectable
NH2	Amine
Nm	Nanometers
nNOS	Neuronal NOS
NO	Nitric oxide
NOS	Nitric oxide synthase
OH	Hydroxyl group
P	p-value
PAR	Peak area ratio
PBS	Phosphate buffer saline
PEG	Polyethylene glycol
P-gp ATPase	P-glycoprotein ATPase
P-gp	P-glycoprotein
pH	Power of hydrogen
pKa	Acid dissociation constant
PO	Per os
PPE	Palmar plantar erythrodysesthesia
p-value	Probability value
r^2	Coefficient of determination
RBF	Round bottom flask

ROS	Reactive oxidative species
rpm	Revolutions per minute
RSD	Relative standard deviation
RT	Room temperature
RT-PCR	Real time-polymerase chain reaction
s	Seconds
SD	Standard deviation
SD	Sprague Dawley
SEM	Standard error of the mean
-SH	Thiol
SIB	Swiss Institute of Bioinformatics
t	Time
$t_{1/2}$	Half-life
TCA	Trichloroacetic acid
TFA	Trifluoroacetic acid
THF	Tetrahydrofuran
T_{last}	Time at the last measurable (observed) concentration
TLC	Thin layer chromatography
T_{max}	Time required to reach maximum serum concentration after dosing
Trolox®	(6-hydroxy,2,5,7,8-tetramethylchroman-2-carboxylic acid
U	Unit
UV	Ultraviolet
UV-VIS	Ultra-violet visible

v/v	Volume by volume
VCCLAB	Virtual Computational Chemistry Laboratory
Vd	Volume of distribution
V_{ss}	Volume of distribution at steady state

CHAPTER 1

LITERATURE REVIEW AND BACKGROUND

1.1. ABSTRACT

This is an introductory chapter to the research findings discussed in this thesis. It provides background and literature review on two major projects: DoxQ and MyoNovin®. DoxQ is a derivative of the anti-cancer drug doxorubicin designed for lymphatic delivery, while MyoNovin® is a skeletal muscle regenerator and a derivative of guaifenesin designed for skeletal muscle drug delivery. The two compounds were synthesized utilizing a pro-drug approach with a potential to improve drug delivery to target tissues and limit systemic toxicities. Here, an overview of the drug development process, utilization of a pro-drug approach in drug delivery, lymphatics and skeletal muscles as target tissues for drug delivery.

1.2. DRUG DEVELOPMENT

The drug development process is a lengthy multi-step process starting with target identification followed by target validation, lead identification, lead optimization, pre-clinical evaluation, and finally clinical evaluation (1). During the early drug discovery phase, thousands of compounds are initially identified as pharmacologically active but only a few get approved for clinical use. Many active compounds fail before reaching clinical trials due to their unacceptable toxicities, limited efficacy compared to other drugs in the market, difficulty in dosage form design, chemical stability limitations or other issues. Therefore, extensive pre-clinical evaluation of pharmacologically identified compounds for their efficacy and safety, usually takes place before it can be approved for clinical use by regulatory authorities.

To increase the likelihood of translating a pharmacologically active compound for human use, extensive pre-clinical investigations at the *in silico*, *in vitro*, and *in vivo* level are undertaken. These investigations may be carried out sequentially or simultaneously to examine

the efficacy, safety, disposition, and toxicity of the active compound. *In silico* studies are generally undertaken at the early stage of drug development to predict *in vivo* effects of selected compounds. These are followed by *in vitro* studies that provide theoretical evidence of safety and efficacy. Finally, *in vivo* studies are undertaken in animals to verify *in vitro* observations.

1.3. PRECLINICAL STUDIES

1.3.1. *In silico* Studies

The word "*in silico*" in Latin refers to the mass use of silicon for semiconductor computer chips. *In silico* is also a term used to describe experimentation performed by a computer or computer simulation software (2). Computer software packages provide a convenient tool to screen a large number of drug candidates in a short time without the need for laboratory bench experimentation particularly in the early stage of drug development where hits are identified.

The shift towards *in silico* tools has recently gained attention by pharmaceutical industry as it can accelerate the drug development process and reduce the cost associated with bringing a drug to market. Traditionally, compounds were evaluated for their likelihood to be developed into drugs largely by trial and error approaches that included both *in vitro* and *in vivo* testing, followed by matching the pharmacological effect to the drug. Conversely, the *in silico* drug design approach is based on knowledge of a biological response or drug target and then tailoring a drug that will exert the desired effect (3). In addition to employing *in silico* tools in drug discovery and design, these tools can also be utilized after a lead has been developed to predict its *in vivo* effects.

In silico tools can provide insight about the nature of interactions between a drug (and xenobiotic) and the site of action. Further, these tools can be used to predict physicochemical

properties (e.g.: solubility, partition coefficient), and biopharmaceutical properties (e.g. ability to permeate across biological barriers). Additionally, in silico tools can be used to predict the fate of drugs in the body including absorption, distribution, metabolism, excretion (ADME) as well as toxicity. A comprehensive list of computer-aided drug design (CADD) tools is documented by the Swiss Institute of Bioinformatics (SIB) online website (4) as shown in table 1.

1.3.2. *In vitro* Studies

The term "*in vitro*" in Latin means in glass, referring to experiments carried out in a test tube or using components of living organism that have been isolated from their normal biological surrounding such as cells or microorganisms. During the drug development process, in vitro studies are carried out to provide theoretical evidence such as proof of pharmacological activity, efficacy, toxicity, drug release, and dissolution. *In vitro* studies are of particular importance in providing mechanistic information about drug behaviour *in vivo* (5).

1.3.3. *In vivo* Studies

The term "*in vivo*" in Latin means "within the living" referring to experiment carried out using a whole living organism (e.g.: animal, human) rather than tissues. *In vivo* studies are undertaken to verify in vitro observations. Initially *in vivo* experiments are conducted in animal models to study pharmacokinetics, toxicology, biomarkers and also and also provides a proof of concept.

1.3.4. Translation to Humans

After determining safety and efficacy of investigational compounds by *in vitro* and *in vivo* studies (pre-clinical phase), clinical trials in healthy humans can be undertaken once approved by regulatory authorities.

Table 1.1. A comprehensive list of computer-aided drug design (CADD) software, databases and web services as delineated by the Swiss Institute of Bioinformatics (4).

Application field	**Computer-aided drug design tool**
Databases	ZincDatabase, Zinc15Database, ChEMBL, JChemforExcel, ProteinDataBank(PDB), BindingMOAD(MotherOfAllDatabase), PDBbind, STITCH, SMPDB
Chemical structure representations	ChemDraw, MarvinSketch, ACD/ChemSketch, jsMolEditor, Marvinmoleculeeditorandviewer, ChemWriter, UCSFChimera, Pymol, OpenStructure, DaylightSMILES, InChI, SDFformat, OpenBabel, OMEGA, TorsionAnalyzer, PoseView, DSVisualizer, BINANA, E-Babel, ChemicalIdentifierResolver, VEGAWE, ChemMobi, ChemSpotlight
Molecular Modeling	CHARMM, GROMACS, Amber, SwissParam, CHARMM-GUI, CHARMMing.org, SwissSideChain
Homology Modeling	Modeller, I-TASSER, LOMETS, SWISS-MODEL, SWISS-MODELRepository, Robetta
Binding site prediction	MED-SuMo, CAVER, FINDSITE, sc-PDB, Pocketome, PocketAnnotatedatabase, 3DLigandSite, metaPocket, PocketAnnotate
Docking	Autodock, DOCK, GOLD, SwissDock, DockingServer, 1-ClickDocking
Screening	Pharmer, Catalyst, PharmaGist, SwissSimilarity, Blaster, AnchorQuery
Target prediction	MolScore-Antivirals, MolScore-Antibiotics, SwissTargetPrediction, SEA, ChemProt
Ligand design	GANDI, LUDI, AutoT&T2, SwissBioisostere, VAMMPIRE, sc-PDB-Frag, e-LEA3D, eDesign, iScreen
Binding free energy estimation	Hyde, X-score, NNScore, DSXONLINE, BAPPLserver, BAPPL-Zserver
QSAR	cQSAR, clogP, ClogP/CMR, MOLEdb, ChemDB/Datasets, DatasetsfromtheMilanoChemometricsandQSARResearchGroup, OCHEM, E-Dragon, PatternMatchCounter
ADME Toxicity	VolSurf, GastroPlus, MedChemStudio, ALOGPS, OSIRISPropertyExplorer, SwissADME, Metrabase, PACT-F, TOXNET

1.5. PRODRUG APPROACH TO OPIMTIMIZE DRUG DELIVERY

1.5.1. Prodrugs

The term “prodrug” was first introduced in 1985 by Adrien Albert (18) to describe “biologically inert derivatives of drug molecules that undergo an enzymatic and/or chemical conversion *in vivo* to release the pharmacologically active parent drug” (19). Prodrugs are compounds that undergo biotransformation *in vivo* before exerting pharmacological activity. Nevertheless, some of the drugs that fit in the criteria of a prodrug were actually developed before the term “prodrug” was officially introduced. Acetanilide (hydroxylated to the active component acetaminophen *in vivo*) was introduced to medical practice in 1867 by Chahn and Hepp (20). Another example is Aspirin. Aspirin (acetyl salicylic acid hydrolyzed to the active component salicylic acid *in vivo*) was synthesized by Felix Hoffman (Bayer) in 1897 and introduced into medicine by Dreser in 1899 (21).

The prodrug approach may be considered when a drug exhibits a potent pharmacological effect but also causes some undesirable effects. Over the years there has been an increase in the number of prodrugs in the market. It is estimated that 10% of the drugs in the market are prodrugs (20). The goal of designing prodrugs is to optimize the desired pharmacological activity of a drug while mitigating its undesirable effects/ properties that may halt its development into a clinical medication.

The prodrug approach has been successfully applied to overcome drug formulation or delivery barriers related to physicochemical, biopharmaceutical, pharmacokinetic or pharmacological effects (22,23). For example, the prodrug approach could mitigate poor water solubility, low lipophilicity, and chemical stability, which are barriers related to physicochemical properties of the drug (23). Additionally, it can be used to mitigate biopharmaceutical barriers

such as limited ability of a drug to cross biological membranes and pharmacokinetic barriers including poor oral absorption, first pass metabolism, and poor oral bioavailability. Pharmacological barriers such as toxicity or irritation caused by the parent drug could also be mitigated using a pro-drug approach. An ideal prodrug is designed to cross the limiting barrier, release the pharmacological entity via either enzymatic or chemical cleavage at the desirable cite of action, followed by elimination of the pro-moiety/backbone.

1.5.2. Classification of Prodrugs

There are several ways to classify prodrugs. In general prodrugs can be classified based on their mechanism of activation into two main types; carrier linked prodrugs and bioprecursors (20). In carrier-linked prodrugs the active drug is temporary linked to a carrier (also known as a promoiety) via a bioreversible covalent linkage. The carrier-linked prodrug undergoes biotransformation *in vivo*, releasing the parent drug and the carrier (20). A bioprecursor does not contain a carrier or pro-moiety but still undergoes biotransformation (e.g., oxidation, reduction) *in vivo* resulting in a new pharmacologically active compound (22). Sulindac is an example of a bioprecursor where sulindac sulphoxide, the prodrug, is about 100-times more water-soluble than the pharmacologically active sulphide (20).

Prodrugs can also be classified according to their therapeutic categories (e.g., anticancer, antiviral prodrugs), chemical linkages attached to the active drug (e.g., esteric prodrugs, glycosidic prodrugs), functional category to circumvent deficiencies (e.g., prodrugs to improve site specificity, prodrugs to by-pass high first-pass effect), or depending on the site of activation (e.g., activated intracellularly, activated extracellularly) (23).

1.5.3 General Consideration for Derivatization

As the prodrug approach is based on chemical structure modification of a parent drug into a new compound, the derivatization process may alter physicochemical and biopharmaceutical properties, pharmacokinetics and pharmacological activity, and safety of the parent drug. Thus, to examine the feasibility for prodrug design, there are general considerations related to the parent drug and the pro-moiety to take into account. An ideal parent drug would contain functional groups amenable for prodrug design, while an ideal pro-moiety/carrier would be safe and rapidly eliminated from the body (19,23). In addition, the pro-moiety/carrier should be selected based on the dose, condition, and the duration of therapy (19). Furthermore, both the parent drug and the pro-moiety/carrier should be evaluated for potential degradation by products, safety, and biopharmaceutical properties (19).

1.5.4. Functional Groups Amenable to Prodrug Design

Some of the most common functional groups that are amenable to prodrug design include carboxylic, hydroxyl, amine, phosphate/phosphonate and carbonyl groups (Figure 1.1). Prodrugs are typically designed via the modification of those groups include esters, carbonates, carbamates, amides, phosphates and oximes (22,23).

Ester prodrugs are the most common prodrugs constituting ~ 49% of all prodrugs in the market (24). They are activated by enzymatic hydrolysis *in vivo* as the ester bond is cleaved by the action of esterases in blood, liver, and other organs. Ester prodrugs are mainly used to enhance lipophilicity of water soluble drugs by masking charged functional groups (carboxylic acid, phosphates) thus increasing passive membrane permeability (25).

Phosphate esters are typically stable and are converted to the parent compound by the action of phosphatases in the intestine and liver. They are typically designed to increase water solubility of poorly water soluble drugs to allow parenteral or oral administration (26).

Carbonates and carbamates are similar to esters in that they are both derivatives of carboxylic acids. Carbonates are derivatives of carboxylic acids and alcohols, while carbamates are derivatives of carboxylic acid and amine. They are activated *in vivo* by the action of esterases and are enzymatically more stable than amides (27).

Amides are derivatives of amine and carboxyl functional groups and are hydrolyzed *in vivo* carboxylesterases, peptidases or proteases (27,28). They are often used to enhance oral absorption by utilizing intestinal uptake transporters and are less commonly used in pro-drug design due to their relatively high enzymatic hydrolysis (29).

Oximes are derivatives of ketones (ketoximes), amidines (amidoximes) and guanidines (guanidoximes) and are metabolized by cytochrome P450 (CYP450) enzymes *in vivo* (30,31). They can be used to enhance the membrane permeability and absorption of a parent drug (32).

1.5.5. Limitations of the Prodrug Approach

As with any drug optimization strategy, the prodrug approach has limitations. The prodrug itself may exhibit pharmacological activity that may interfere with normal physiology, result in drug interactions, or may consume a vital endogenous component during metabolic process such as glutathione. It is also possible that a toxic metabolite or a degradation by product may be formed from the parent drug or the carrier moiety (22,23).

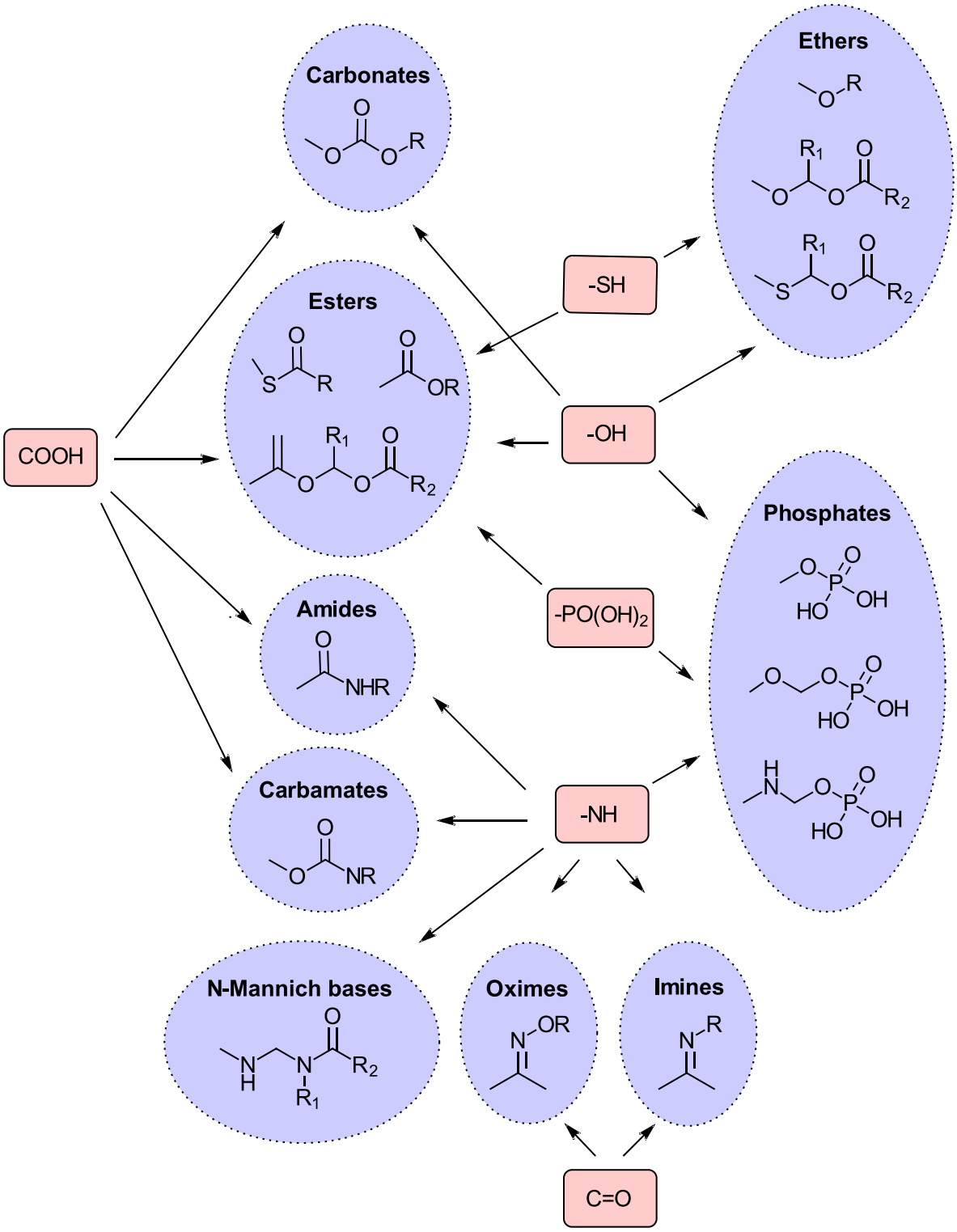

Figure 1.1. Functional groups amenable to prodrug design. Recreated from reference (22).

1.6. PRODRUG APPROACH TO IMPROVE DRUG DELIVERY OF SELECTED XENOBIOTICS

Based on the general consideration for derivatization and the presence of amenable functional groups in the parent drug, the prodrug design could be a useful strategy to mitigate therapeutic barriers and optimize drug delivery. DoxQ and MyoNovin® are examples of two investigational compounds, which were developed utilizing a prodrug approach. Both compounds were developed to deliver the pharmacologically active entity to target tissues by modifying the chemical structure of an existing drug and using a carrier that has affinity to specific tissues. In the case of DoxQ, the parent drug doxorubicin was conjugated to the lymphatic carrier quercetin via a linker to improve intestinal lymphatic drug delivery. While, in the case of MyoNovin® the active chemical entity nitric oxide (NO) is derivatized into two nitro groups (ONO_2), which are attached to the skeletal muscle carrier guaifenesin.

1.7. PRODRUG APPROACH TO IMPROVE INTESTINAL LYMPHATIC DELIVERY

1.7.1. Background

Despite the clinical effectiveness of anti-cancer medications, there are still therapeutic barriers that limit their use such as: systemic toxicities, poor oral bioavailability, and metastatic spread of cancers via lymph nodes. Hence, efforts to improve the safety and efficacy of anti-cancer drugs are needed for better therapeutic outcomes. By enhancing the localization of such drugs in the lymphatics, it may be possible to limit the metastatic spread of cancers and systemic toxicities, treat lymphomas with better efficacy, and improve the bioavailability of drugs that undergo extensive first pass effect (33,34,35). To better understand how DoxQ was developed and how it may potentially enhance the intestinal lymphatic delivery of doxorubicin, the

anatomical characteristics of the lymphatic system function in normal and pathological state are described with emphasis on lymphatic drug delivery.

1.7.2. Overview of the Lymphatic System

The lymphatic system is part of the circulatory system and is composed of a network of lymphatic vessels and organs. The lymph organs include lymph nodes, tonsils, Peyer's patches, spleen and thymus (36). Lymph is a protein rich exudate that fills lymphatic vessels and carries excess fluid, white blood cells, proteins, fats and other substances from tissue surroundings back to the blood for circulation, thus, serving as an intermediate between the tissues and the vasculature (36,37). One distinct difference between the lymphatic and cardiovascular system is that the lymphatic system is an opened ended system with no driving force, whereas the cardiovascular system is a closed system in which the heart acts as a driving force pumping blood to the tissues (36,37).

The major functions of the lymphatic system are tissue fluid homeostasis, transport of dietary lipids and fat soluble vitamins, and transport of white blood cells (immune regulation). It also carries antigen presenting cells from the interstitium of peripheral tissues to their adjacent lymph nodes where immune responses take place and plays a role in the metastasis of cancer to other tissues.

The lymphatic system is a one-way system where fluid and macromolecular molecules such as proteins are transported from the interstitial space to the blood circulation (38). When blood travels from the larger blood vessels to smaller capillaries, plasma fluid and proteins transverse into the interstitial space that surrounds tissues. The exudate is mainly reabsorbed through the venous capillaries; however, the excess fluid and proteins leaking out of the

vasculature into the interstitium can enter the lymphatics via the initial lymph vessels due to the permeability of their walls to macromolecules. Therefore, the lymphatics are essential in maintaining the osmotic pressure of the space surrounding the tissues. Cells such as white blood cells and metastatic cancer cells may also enter lymphatics via the porous walls of the lymphatic capillaries (38).

1.7.3. Functions of the Lymphatic System in Normal and Disease State

Under normal physiological conditions the lymph carries fluids, macromolecules, and cells from the interstitium through initial lymph capillaries which collect into larger collecting pre-nodal (afferent) lymph vessels through lymph nodes and exit via post-nodal (efferent) lymph vessels. The lymph then flows into collecting lymphatic ducts before entering the venous blood at the junction of the subclavian and the left jugular veins (39). The lymphatic vessels contain unilateral valves and are surrounded by smooth muscles, which facilitate uni-directional flow of the lymph and prevent its back flow since the lymphatic system does not have a driving force to pump lymph like the heart in the cardiovascular system (38,39).

In disease states there are morphological changes that occur leading to changes in the lymphatic system. For example, cancer tumors can spread from primary sites to other tissues often through the lymphatic capillaries to the sentinel lymph node. Tumor cells and macrophages move along the lymphatic vessels and release pro-inflammatory and lymphangiogenic factors resulting in enlargement of lymph vessels (lymphangiogenesis). This causes dilation of lymphatic vessels and an increase in the interstitial pressure, which alters lymphatic flow and may also modulate immunity (40). Likewise, in an inflammatory disease condition, inflammatory cells release pro-inflammatory and lymphangiogenic factors leading to lymphatic

hyperplasia. These changes affect the flow of lymphatic fluids and cellular components thereby modulating inflammation and immunity (41). The importance of understanding the role of lymphatic system in diseases such as cancer and inflammatory conditions makes it an interesting and important target for drug development and delivery and may also be a useful diagnostic tool for such diseases.

1.7.4. Drug Delivery to Lymphatics

In the past, the importance of the lymphatic system was centered on its physiological functions in fluid homeostasis and transport of lipids. Recently, the lymphatic system received more attention because of its important role in disease conditions, immune modulation, and metastasis of cancer. This led to recognizing the lymphatics as potential target for drug and vaccine development.

Targeting lymphatics is difficult due to its anatomical characteristics and low flow. Thus, novel therapeutic approaches to overcome these challenges in targeting lymphatics will have a great impact in the management of pathological conditions involving lymphatics such as metastatic cancer to lymph nodes.

There are several advantages of using lymphatic targeted delivery approaches such as: increasing drug exposure particularly after oral administration and increasing drug lymphatic concentration compared to systemic blood concentration (34,39). When a drug is administered orally it is mainly absorbed in the intestine to the circulation through the hepatic portal vein. A small portion of the drug may be absorbed into the lymphatics through the mesenteric lymph duct (34). Thus, drugs that enter lymphatics by-pass entry to the liver and the first pass effect resulting in enhanced oral bioavailability. Additionally, targeting lymphatics may enhance the

therapeutic efficacy by enhancing the localization of the drug in the lymphatics and thus minimizing toxicities to other tissues.

Recent advances in understanding the physiology of the lymphatic system as well as its importance in various pathological conditions, opened new perspectives in designing drugs and drug delivery systems that mimic the endogenous lymphatic transport pathway (34). Drug delivery systems such as liposomes, polymeric micelles, nanoparticles, and emulsification were used to target the lymphatic system (42,43). Other approaches to target lymphatics include using a long-fatty acid chain or a triglyceride moiety as a carrier to the lymphatics. In addition, natural carriers such as dextran, hyaluronic acid, and albumin have been reported as lymphatic drug delivery systems (42). Furthermore, some drugs possess a natural tendency to be absorbed via intestinal lymphatics, which could be useful for lymphatic delivery (43-52).

1.7.5. Development of DoxQ as an Example of Lymphatic Drug Delivery Approach

Doxorubicin, also called Adriamycin, is an anthracycline antibiotic with anti-cancer activity (Figure 1.2) and commonly used to treat a wide variety of cancers such as: lymphomas, breast, and ovarian cancers (53). Doxorbicin is a topoisomerase II inhibitor, which exerts its anti-cancer activity by interfering with deoxyribonucleic acid (DNA) synthesis. It intercalates with the two strands of DNA and inhibits the activity of topoisomerase and DNA synthesis (54-56).

Table 1.2. Examples of drugs absorbed via intestinal lymphatic pathway.

Drug	Chemical structure	Method/procedure	Animals	Reference
Vitamin D3	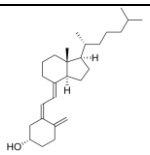	Mesenteric lymph cannulation Chylomicron flow blocking rat by cycloheximide (3mg mg/kg IP)	Male Wister rats 300-325g	(43)
Darunavir	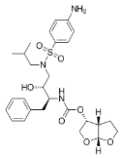	Lymph duct cannulation Chylomicron flow blocking rat by cycloheximide (3mg mg/kg IP)	Male Wister rats 180-250g	(44)
Nimodipine	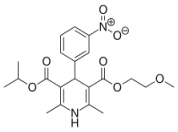	Mesenteric lymph duct cannulated SD rats Chylomicron flow blocking rat by cycloheximide (3mg mg/kg IP)	Male SD rats 300-350g Male SD rats 220-250g	(45)
Docetaxel	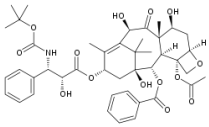	Chylomicron flow blocking rat by cycloheximide (3mg mg/kg IP)	Male SD rats 300-325 g	(46)
Sirolimus	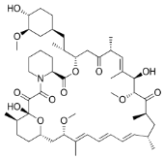	Chylomicron flow blocking rat by cycloheximide (3mg mg/kg IP)	Male SD rats 190-230 g	(47)
Halofantrine	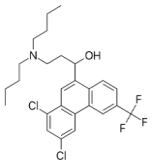	Chylomicron flow blocking rat by cycloheximide (3mg mg/kg IP)	Male SD rats 270-310 g	(48)
Candesartan cilexetil	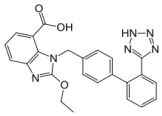	Chylomicron flow blocking rat by cycloheximide (3mg mg/kg IP)	Male SD rats 200-250 g	(49)
Praziquantel	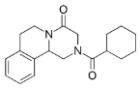	Chylomicron flow blocking rat by cycloheximide (3mg mg/kg IP)	Charles Foster strain albino rats 220-270 g	(50)
Efavirenz	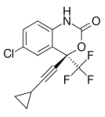	Chylomicron flow blocking rat by cycloheximide (3mg mg/kg IP)	Male SD rats 220-270 g	(51)
Naringin	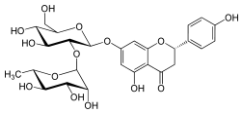	Lymph duct cannulation Lymph duct cannulation	Male SD 300 g	(52)

Doxorubicin is a substrate of the P-glycoprotein (P-gp) transporter and Cytochrome 3A4 (CYP 3A4) (57-59). Both P-gp and CYP metabolic enzymes are major contributors in first pass metabolism, both limiting its intestinal absorption when administered orally and contributing to its poor oral bioavailability. Thus, doxorubicin formulations are only available for parenteral administration. The clinical use of doxorubicin is also limited by its cardiac and renal toxicities, which are likely caused by oxidative stress (60). Therefore, efforts to mitigate its toxicities would likely improve its safety, while mitigating its poor oral bioavailability may provide a novel way to administer doxorubicin orally.

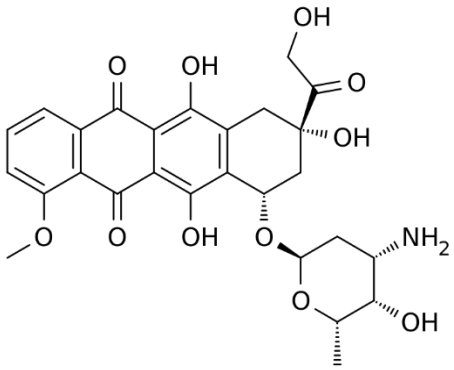

Figure 1.2. Chemical structures of doxorubicin.

To overcome the limitation associated with doxorubicin therapy, our group investigated natural carriers for lymphatic drug delivery that could possibly shunt oral doxorubicin to the intestinal lymphatic absorption pathway as opposed to the normal absorption pathway via the hepatic portal vein, which plays a major role in doxorubicin's poor bioavailability. As our group has been extensively studying flavonoids, which are polyphenolic compounds consumed in plant based diet with various health benefits. Among these flavonoids quercetin was recognized to be naturally transported via intestinal lymphatics (61-63) and its chemical structural is similar to

that of cholesterol (Figure 1.3). The "cholesterol like" structure of quercetin was speculated to facilitate its intestinal lymphatic absorption at least partially and could be a potential lymphatic carrier for drug delivery. Quercetin also possess anti-oxidant, anti-cancer, and anti-inflammatory properties (64-66), which could have protective effects against chemotherapeutic induced toxicities (67) as well as disease prevention.

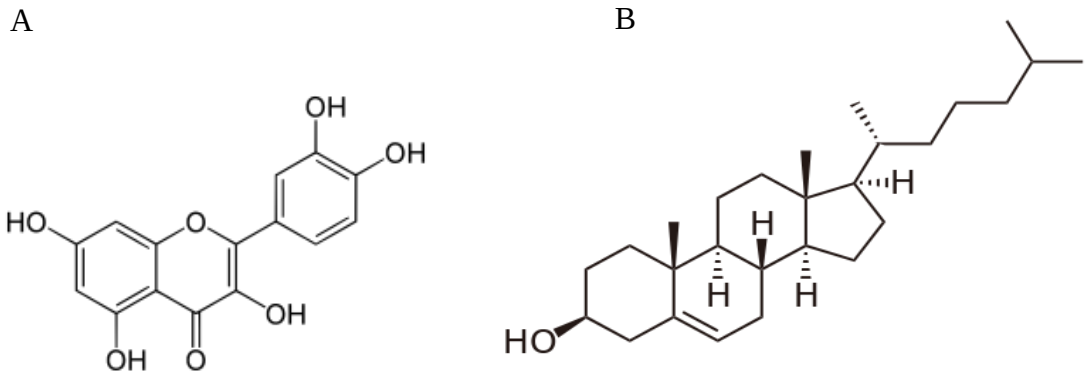

Figure 1.3. Chemical structures of (A) quercetin and (B) cholesterol.

Studies have shown that quercetin promoted the anti-cancer effects of doxorubicin in breast cancer cells by increasing their chemosensitivity to Dox (68) while protecting non-tumor breast cells and cardiomyocytes treated with Dox (69). Similarly, quercetin potentiated the anti-tumor effect of Dox in liver cancer cells by selectively sensitizing liver cancer cells to Dox-induced cytotoxicity while protecting normal liver cells (70). Moreover, quercetin increased the bioavailability of doxorubicin by inhibiting P-gp and CYP3A4 (71) and attenuated doxorubicin-induced cardiotoxicity *in vitro* and *in vivo* by reducing oxidative stress (72). Given that most of

the studied described above (68-71) were conducted using cell lines (*in vitro)* the effects of quercetin on tumor vs non-tumor cells could be cell line specific.

The reported beneficial effects of quercetin and its natural affinity to concentrate in the lymphatics (61-63) have brought our attention to develop a doxorubicin-quercetin conjugate (DoxQ) and assess the utility of using quercetin as a lymphatic carrier. DoxQ was developed by conjugating quercetin to doxorubicin using the amino acid glycine as a linker (Figure 1.4) such that the peptide bond of the conjugate can be easily cleaved *in vivo* releasing doxorubicin and quercetin.

A pilot investigation demonstrated that oral administration of DoxQ enhanced the bioavailability of doxorubicin by more than 3-fold compared to after doxorubicin alone (unpublished observations Davies and Forrest Laboratories), likely through inhibiting the P-glycoprotein (P-gp) efflux pump and metabolism (71). To the best of my knowledge, there are no published studies whereby quercetin was used as carrier for lymphatic targeted delivery or as a strategy to improve oral bioavailability of pharmaceuticals.

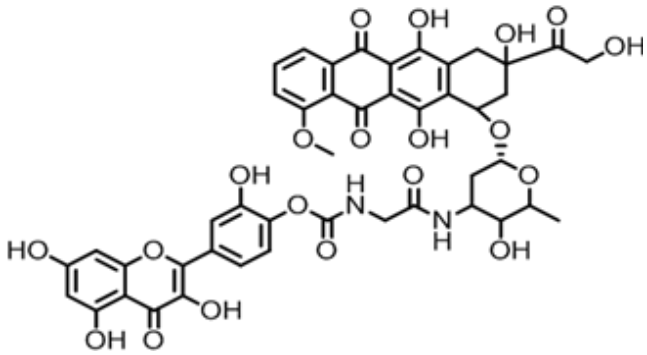

Figure 1.4. Chemical structure of DoxQ.

1.8. PRODRUG APPROACH TO IMPROVE DRUG DELIVEY TO SKELETAL MUSCLES

1.8.1. Background

Nitric oxide (NO) is a ubiquitous neurotransmitter that is involved in various physiological functions (73). NO is known to play a role in the process of vascular smooth muscles relaxation as well as several physiological roles in skeletal muscles. Recent studies revealed that nitric oxide is important in skeletal muscle regeneration, which does not occur under normal physiological conditions, and could be beneficial in the treatment of some skeletal muscle diseases. Given than nitric oxide is a gas with a short half-life (74), administration of nitric is not feasible and thus nitric oxide donors are clinically used to release NO *in vivo* for the treatment of various diseases. The administration of nitric oxide donors will likely affect many different organs and interrupt the normal physiology resulting in many undesirable effects. Therefore, using a skeletal muscle carrier to facilitate the delivery of NO to skeletal muscles would likely improve therapeutic efficacy. To better understand how MyoNovin® could enhance the delivery of NO to skeletal muscles, an overview of skeletal muscles structure and physiology, the process of muscle injury and repair, and the role of nitric oxide in skeletal muscle regeneration is described.

1.8.2. Overview of Skeletal Muscle Physiology

There are three main types of contractile cells in the human body: skeletal cells, smooth muscles, and cardiac muscles. They are classified according to their shape, presence of striations, number and location of nuclei, and whether they are under voluntary or involuntary control. Skeletal muscles are long, striated, with multiple nuclei, and under voluntary control. The

smooth muscles and cardiac muscles are both involuntary muscles. Cardiac muscles are striated and branched with a single central nucleus. Smooth muscles are spindle-shaped having no striations and one central nucleus and have no striations.

Skeletal muscles constitute a large proportion of the human body comprising 30-38% of the total body mass of women or men, respectively (75). Maintaining healthy strong muscles during normal aging is essential for a number of reasons. Firstly, skeletal muscles surround body skeleton and provide a physical protective barrier against bone fractures. Secondly, skeletal muscles frame the body and are the fundamental organs of movement, and thus would have a great impact on the quality of life of the elderly and their ability to perform daily activities such as walking, climbing stairs, and lifting objects. Thirdly, loss of muscle mass often leads to inactivity, which could increase the likelihood of developing pathological conditions such as obesity and diabetes.

Loss of skeletal muscle mass occurs as a natural process with aging. It may also result from malnutrition, inactivity as well as chronic conditions such as cancer, chronic kidney, and chronic heart failure. Conditions that affect muscle loss can be classified according to their etiology as sarcopenia, cachexia, or atrophy.

Sarcopenia is a term used to describe muscle loss that occurs with aging and is often associated with bone loss, increasing the chances of developing bone fractures (76). Cachexia refers to loss of muscle mass that is accompanied by a chronic disease such as cancer, chronic kidney, and chronic heart failure has a metabolic etiology (76). Atrophy refers to loss of muscle mass due to inactivity as in the case of bed-ridden patients (76) and may occur independent of ageing or other diseases.

1.8.3. Skeletal Muscle Development and Structure

Skeletal muscles are developed during embryogenesis from immature cells called myoblasts. Myoblasts fuse together and form multi-nucleated muscle fibres. Because skeletal muscles are multi-nucleated, they cannot undergo mitosis. Thus, the number of skeletal muscle fibres does not increase as the human body grows with age. However, the number of filaments within a muscle fibre can increase resulting in an enlargement in the size of muscle fibre (hypertrophy) and stronger muscles. Growth hormones and testosterone play a major role in the enlargement of muscle cells with age. Following birth, skeletal muscles are fully developed (77).

Each skeletal muscle is composed of layers of connective tissue and contractile components (Figure 1.5) (77). There are three layers of connective tissues in the muscle, they are: epimysium, perimysium, and endomysium. The whole muscle is surrounded from the outside by the first layer of connective tissue called epimysium. The skeletal muscle is composed of bundles of muscle fibres called fascicles that holds the individual myofibrils. Each fascicle is wrapped by a second layer of connective tissue called the perimysium. Within the fascicle, a third layer of connective tissue called the endomysium surrounds each muscle fibre. The three layers of connective tissue provide strength and support to the entire muscle and connects the edge of the muscle to tendons.

The plasma membrane of the muscle fibre is called sarcolemma. Within each muscle fibre the cytoplasm is called cytosol and a special type of smooth endoplasmic reticulum is called sarcoplasmic reticulum. Each muscle fibre contains bundles of contractile filaments called myofibrils (77), which play a key role in the process of muscle contraction and relaxation. The muscle fibre can contract or relax when it receives neuronal signals from the central nervous system through the neuron to the neuromuscular junction. Each muscle fibre is composed of

many cylindrical myofibrils that split into individual units called sarcomeres. The sarcomeres are composed of thick (myosin) and thin (actin) filaments, which contribute to the striated appearance of the muscle. The thick myosin filaments are connected to the edge of the sarcomere

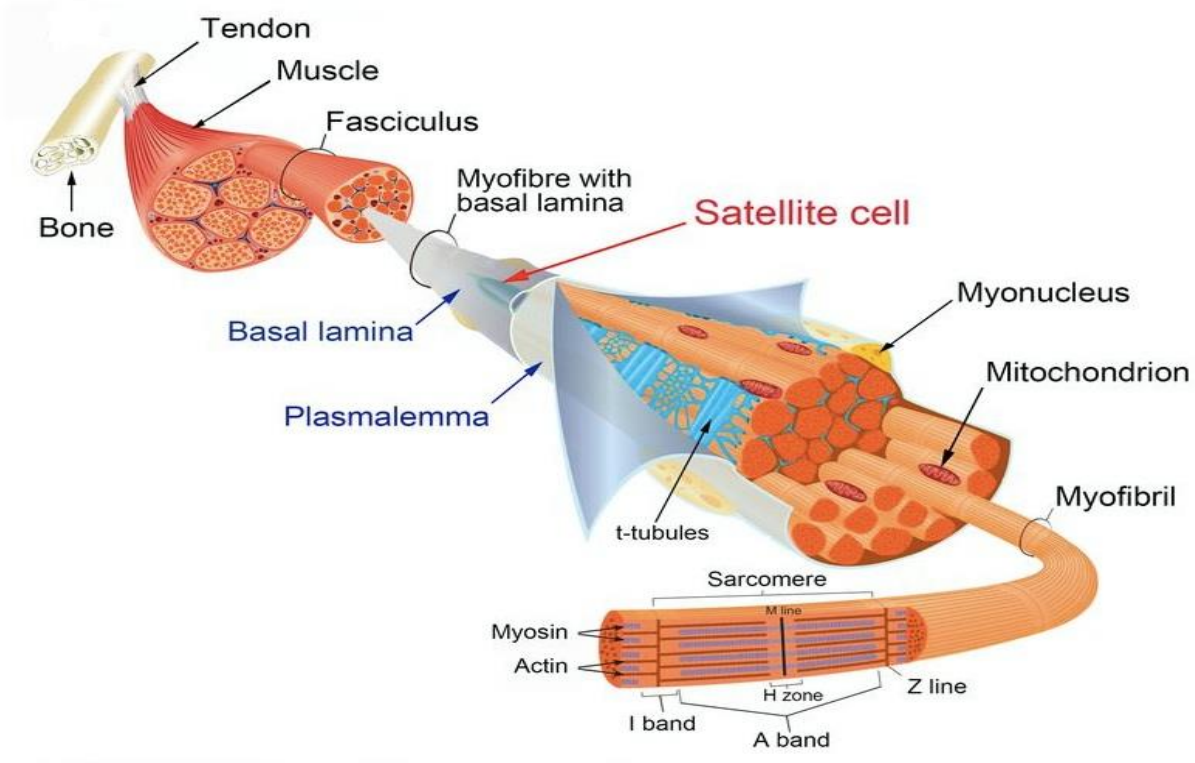

Figure 1.5. The skeletal muscle structure. Adapted from reference (77) with modification. Permission obtained.

on the z-line. The sliding movement of myosin and actin contribute to muscle contraction. The myosin connects to actin via cross-bridges pulling the actin towards the myosin allowing the edge of the sarcomere to be pulled towards the center of the sarcomere resulting in shortening of the sarcomere and muscle contraction. This process requires energy in the form of ATP (hydrolyzed to ADP and phosphate), which triggers the myosin to connect to actin pulling it toward the center, leading to the shortening of the sarcomere and overall muscle fibre. The ADP and phosphate are then released allowing a new ATP molecule to bind to myosin and relaxing or

contracting the sarcomere depending on the signals received from the central nervous system. The rich blood and nerve supply to skeletal muscles enables it to perform its physiological functions. Blood capillaries facilitate adequate delivery of nutrients to the muscles, while neurons contribute to signal transduction between skeletal muscles with the central nervous system.

At the outmost layer the skeletal muscle fibre between the sarcolemma and the basal lamina a group of muscle precursor cells called satellite cells (also called myosatellite cells) reside (78). These cells were discovered in the 1960s and named by Mauro based on their peripheral location on the muscle fibre (79,80). They are unique because of their quiescent nature under normal physiological conditions but can be activated in response to a trigger such as muscle injury. The presence of satellite cells plays a major role in the repair and regeneration of injured muscles. Because satellite cells are single nucleated cells, they can undergo mitosis as opposed to the skeletal muscle fibre, which is multi-nucleated. Therefore, when muscle injury occurs, satellite cells get activated and can then proliferate and differentiate into skeletal muscles to repair the injured muscle.

1.8.4. Skeletal Muscle Injury and Repair

Skeletal muscles have a robust ability to adapt to injury and mechanical stress. Muscles respond to injuries by activating cellular mechanisms that result in muscle repair and regeneration (81). Skeletal muscles are capable of repairing minor injuries such as tears that are not accompanied by a significant loss of muscle result and usually the damaged tissue is restored (82). However, if the extent and magnitude of the damage is beyond the capacity of the muscle, i.e. when more than 20% of the muscle tissue is lost, restoration of the damaged skeletal muscle

tissue may not be fully accomplished. The damaged muscle tissue may be replaced by a scar tissue that fills the gap between functional muscle fibers and may ultimately affect the contractile function of the muscle (82).

During the normal aging process the ability of skeletal muscles to regenerate and restore the lost muscle tissue diminishes with time. If the loss in muscle tissue is progressive and extensive as in the case of sarcopenia, muscles will not be capable of regenerating to restore the large loss in the muscular tissue. Therefore, a thorough understanding of the cellular processes involved in muscle repair will help in identifying molecular targets for drug delivery that may be useful in the treatment of conditions where muscle regeneration is needed.

When skeletal muscle injury occurs, three main phases that take place during skeletal muscle repair; destruction/inflammatory phase, repair phase, and remodelling phase (82). The destruction phase is characterized by a rupture of the muscle fibre exposing the intracellular components to the extracellular environment, subsequently releasing inflammatory mediators. The inflammatory mediators then attract neutrophils and macrophages at the site of injury. This is followed by the repair phase where macrophages migrate to phagocytose cell debris, cytoplasm, nucleus, and other cellular organelles that leak out of the injured muscle. The macrophages also attract satellite cells to migrate towards the site of injury and facilitate the repair of injured myofibre. Activated satellite cells then enter the interstitium and proliferate. Some of the activated satellite will exit the cell cycle and go back to their quiescent state, while others will begin to differentiate. As part of the differentiation process, satellite cells can either fuse with the damaged site of the myofibre or align and fuse together to form a new muscle fibre depending on the extent of muscle damage. At a later stage of differentiation, the nucleus of the satellite cell aligns longitudinally with nuclei of the regenerated myofibre forming a central

nuclei, which is a distinctive feature of a myofibre undergoing differentiation (83,84). At the final stage of differentiation the newly fused satellite cells migrate towards the outer surface of the myofibre and become quiescent (82,84). While a new myofibre is being formed, formation of a scar tissue may also take place connecting the remaining functional myofibres together and preserving signal transduction within the muscle (82). In the case of sever injury with extensive loss of muscle tissue, a dense scar tissue will form, splitting the original myofibre into two myofibres (82). After full differentiation, remodelling of the myofibre and scar tissue and restoration of muscle function takes place, which is the last phase of muscle repair. In this phase, the newly formed myofibre mature and attach to the extracellular matrix and satellite myofibres are also formed (82).

1.8.5. Role of Nitric Oxide in Muscle Regeneration

NO is an essential physiological mediator and plays a role in cellular signalling, vascular smooth muscle relaxation, and physiological functions in skeletal muscles (85). In 2000 Anderson reported that nitric oxide activates satellite cells in skeletal muscles to enter the cell cycle (86). The activation of satellite cells thus contributes to their repair and growth following injury or disease (87,88).

Anderson et al reported that sarcolemmal induced injury triggers satellite cell activation through a bolus release of nitric oxide (85). When the muscle fibre is undamaged with normal contractile and relaxation function, satellite cells are quiescent and contain a few organelles. Satellite cells that reside between the external lamina and sarcolemma of the muscle fibre are subject to pulsatile release of nitric oxide that is synthesized from nitric oxide synthase (NOS) and diffuses normally out of the muscle fibre to exert its physiological effects. However, if the

sarcolemma of the muscle fibre is injured, the muscle fibre contracts resulting in intense shear between the plasmalemma and the external lamina. The shear provokes bolus release of nitric oxide, which activates satellite cells. Once the satellite cells are activated, the organelles within start to enlarge in size and the hepatocyte growth factor (HGF) from the damaged fibre becomes activated and moves towards the c-met receptor on satellite cells. This results in hypercontraction of fibrils within the damaged fibre and retraction of the damaged segments within the external lamina maintain shear and release of nitric oxide can activate adjacent satellite cells from undamaged fibres. Subsequently, the HGF binds to the c-met receptor resulting in retraction of segments within the muscle fibre and detachment of satellite cells (86).

Tidball reported that alteration in the calcium ion concentration during muscle injury could activate satellite cells (81). When the muscle fibre is injured, the muscle membrane becomes leaky increasing the influx of calcium ions. The increase in intracellular calcium ion concentration leads to an increase in the activation of neuronal NOS (nNOS) and elevation in NO release, which triggers metalloproteinases (MMP) activation extracellularly. MPP contributes to the cleavage of HSP core protein and results in the release of heparin sulfate proteoglycans (HSP), HGF and fibroblast growth factor (FGF2), which activate satellite cells to perform its regenerative function (81).

1.8.6. Effects of Nitric Oxide Donors on Skeletal Muscles and Development of MyoNovin®

As nitric oxide was shown to activate satellite cells to enter cell cycle, Wang et al examined the effects of administrating a nitric oxide donor (isosorbide dinitrate) and a muscle relaxant (methocarbamol) on skeletal muscles in mice. Administration of isosorbide dinitrate (nitric oxide donor) orally and transdermally in normal adult mice showed an increased in DNA

synthesis of skeletal muscles after 24 hours of a single transdermal or oral dose suggesting that the release of NO could have activated satellite cells to enter the cell cycle in adult normal mice (89). When methocarbamol was administered an increase in DNA synthesis was also observed and this effect was additive when both methocarbamol and isosorbide dinitrate were administered together to normal mice (89). This finding led to the development of MyoNovin®.

MyoNovin® (Figure 1.6) was synthesized by attaching two nitro groups to guaifenesin, the active metabolite of the commercially available muscle relaxant methocarbamol, where guaifenesin acts a carrier to deliver nitic oxide to skeletal muscles (89). In the study by Wang et al the authors also examined the effects of MyoNovin® on the activation of satellite cells (89). When MyoNovin® was transdermally or orally administered to normal adult an increase in DNA synthesis, after 24 h of administration, in muscles was observed indicating that MyoNovin® stimulated the proliferation of satellite cells (89).

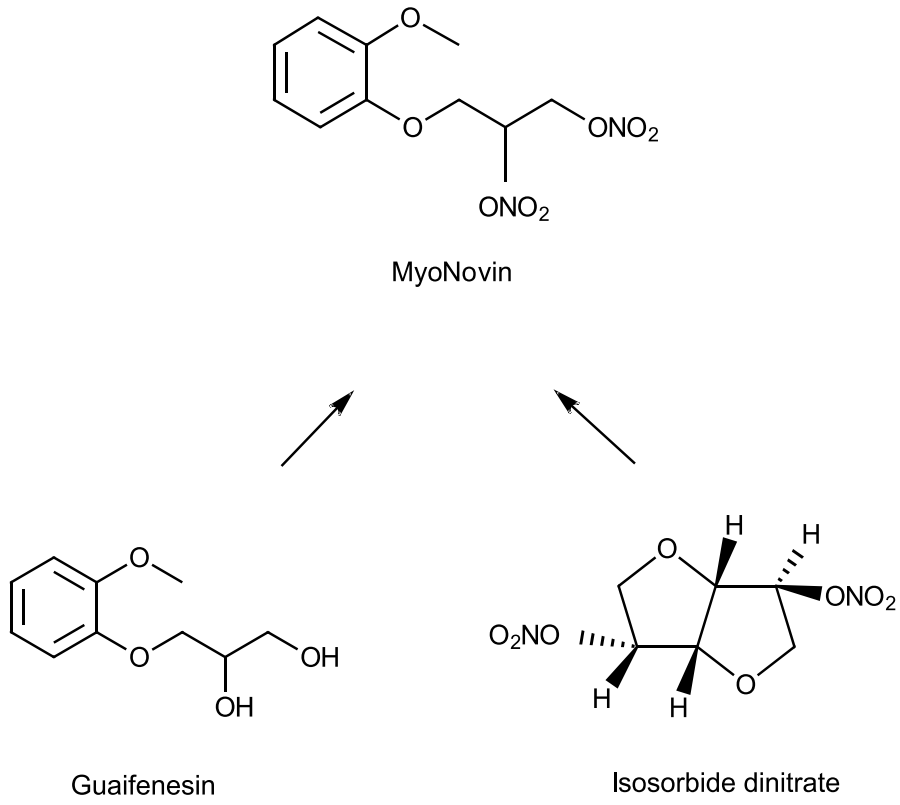

Figure 1.6. The chemical structures of MyoNovin®, guaifenesin, and isosorbide dinitrate.

1.8.7. Other Effects of Nitric Oxide Donors on Skeletal Muscles

One way to trigger the activation of satellite cells (mechanically) is exercise, which can cause skeletal muscles to regenerate. However, in aged skeletal muscles, satellite cells may not respond to activation by exercise. Liteir et al (90) reported that skeletal muscle growth as a result of induction by exercise is muscle specific and age dependent. In their study, old mice (18 months old) were refractory to hypertrophy after three weeks of voluntary exercise, while younger mice at the age of 8 months were responsive to exercise as observed by enlargement of the quadriceps muscle (90).

Letier et al later examined the effect of administering a nitric oxide donor to aged mice that were refractory to hypertrophy by exercise (91). The study compared the effects of using

isosorbide dinitrate or exercise alone or together in aged mice (18.5-19 months old), when they started to show signs of sarcopenia. The result of this study showed a significant increase in the mass of the quadriceps muscle when isosorbide dinitrate was used in combination with exercise indicating hypertrophy. The study also revealed an increase in DNA synthesis of the quadriceps as well as an increase in the diameter of muscle fibre in the same muscle (91). The findings of this study suggest that the administration of a nitric oxide donor can reverse the reduced capacity of aged muscles to grow following exercise.

1.9. SUMMARY

In conclusion, DoxQ and MyoNovin® are examples of novel drug delivery systems designed using a pro-drug approach to improve the delivery of the active entity to lymphatics and skeletal muscles respectively. By enhancing the localization of the drug where it's needed, the efficacy and safety will likely improve.

The pro-drug approach is based on chemical derivatization of a parent compound resulting in the formation of a new compound. As a result, the pharmacological effects of the new compound and its biodistribution will change. Therefore, for further pharmaceutical development of DoxQ and pre-clinical studies (*in silico, in vitro, in vivo*) are necessary to characterize the new compound. These studies will provide insight into its efficacy, safety, and feasibility for drug development.

1.10. REFERENCES

1. Terstappen GC, Reggiani A. In silico research in drug discovery. Trends Pharmacol Sci. 2001;22(1):23-6.

2. Ekins S, Mestres J, Testa B. In silico pharmacology for drug discovery: methods for virtual ligand screening and profiling. Br J Pharmacol. 2007;152(1):9-20.
3. Rao VR, and Srinivas K. Modern drug discovery process: An in silico approach. Journal of Bioinformatics and Sequence Analysis 3.2011; 3(5): 89-94.
4. Swiss Institute of Bioinformatics website. (www.click2drug.org).
5. Pelkonen O, Turpeinen M, Raunio H. In vivo-in vitro-in silico pharmacokinetic modelling in drug development: current status and future directions. Clin Pharmacokinet. 2011;50(8):483-91.
6. Lu ZR, Qiao P. Drug Delivery in Cancer Therapy, Quo Vadis? Mol Pharm. 2018. https://pubs.acs.org/doi/10.1021/acs.molpharmaceut.8b00037.
7. Anselmo AC, Mitragotri S. An overview of clinical and commercial impact of drug delivery systems. J Control Release. 2014; 28(190):15-28.
8. Wen H, Jung H, Li X. Drug Delivery Approaches in Addressing Clinical Pharmacology-Related Issues: Opportunities and Challenges. AAPS J. 2015;17(6):1327-40.
9. Fasinu P, Pillay V, Ndesendo VM, du Toit LC, Choonara YE. Diverse approaches for the enhancement of oral drug bioavailability. Biopharm Drug Dispos. 2011;32(4):185-209.
10. Nazir, S, Hussain T, Ayub A, Rashid U, MacRobert AJ. Nanomaterials in combating cancer: Therapeutic applications and developments. Nanomedicine. 2014; 10 (1), 19−34.
11. Abellan-Pose R, Csaba N, Alonso MJ. Lymphatic Targeting of Nanosystems for Anticancer Drug Therapy. Curr Pharm Des. 2016;22(9):1194-209.
12. Schrama D, Reisfeld RA, Becker JC. Antibody targeted drugs as cancer therapeutics. Nat Rev Drug Discov. 2006;5(2):147-59.

13. Adams GP, Weiner LM. Monoclonal antibody therapy of cancer. Nat Biotechnol. 2005;23(9):1147-57.
14. Scott AM, Allison JP, Wolchok JD. Monoclonal antibodies in cancer therapy. Cancer Immun. 2012;12:14.
15. Han HK, Amidon GL. Targeted prodrug design to optimize drug delivery. AAPS PharmSci. 2000;2(1):E6.
16. Rautio J, Kumpulainen H, Heimbach T, Oliyai R, Oh D, Järvinen T, Savolainen J: Prodrugs: design and clinical applications. Nat Rev Drug Discov. 2008; 7, 255–70.
17. Beaumont K, Webster R, Gardner I, Dack K. Design of ester prodrugs to enhance oral absorption of poorly permeable compounds: challenges to the discovery scientist. Curr Drug Metab. 2003;4(6):461-85.
18. Albert A. Chemical Aspects of Selective Toxicity. Nature. 1958.;182(4633):421-2.
19. Williams D A, & Lemke TL Foye's principles of medicinal chemistry 7th ed. 2013. Philadelphia: Lippincott Williams & Wilkins.
20. Zawilska JB1, Wojcieszak J, Olejniczak AB. Prodrugs: a challenge for the drug development. Pharmacol Rep. 2013;65(1):1-14.
21. Sneader W. The discovery of aspirin: a reappraisal. BMJ. 2000; 321(7276): 1591–94.
22. Rautio J, Kumpulainen H, Heimbach T, Oliyai R, Oh D, Järvinen T, Savolainen J.Prodrugs: design and clinical applications. Nat Rev Drug Discov. 2008;7(3):255-70.
23. Shirke S, Shewale S, Satpute M. Prodrug Design: An Overview. IJPCBS. 2015; 5(1): 232-41.
24. Ettmayer, P., Amidon, G. L., Clement, B. & Testa, B. Lessons learned from marketed and investigational prodrugs. J. Med. Chem. 2004; 47: 2393–404.

25. Beaumont, K., Webster, R., Gardner, I. & Dack, K. Design of ester prodrugs to enhance oral absorptionof poorly permeable compounds: challenges to the discovery scientist. Curr. Drug Metab. 2003; 4: 461–85.
26. Heimbach, T. et al. Enzyme-mediated precipitation of parent drugs from their phosphate prodrugs. Int. J.Pharm. 2003; 261:81–92.
27. Potter, P. M. & Wadkins, R. M. Carboxylesterases - detoxifying enzymes and targets for drug therapy. Curr. Med. Chem. 2006; 13: 1045–54.
28. Yang, C. Y., Dantzig, A. H. & Pidgeon, C. Intestinal peptide transport systems and oral drug availability.Pharm. Res. 1999; 16: 1331–43.
29. Steffansen, B. et al. Intestinal solute carriers: an overview of trends and strategies for improving oral drug absorption. Eur. J. Pharm. Sci. 2004; 21:3–16.
30. Jousserandot, A. et al. Microsomal cytochrome P450 dependent oxidation of N-hydroxyguanidines, amidoximes, and ketoximes: mechanism of the oxidative cleavage of their C=N (OH) bond with formation of nitrogen oxides. Biochemistry.1988; 37: 17179–91.
31. Kumpulainen, H. et al. Evaluation of hydroxyimine as cytochrome P450-selective prodrug structure. J. Med.Chem. 2006; 49: 1207–11.
32. Clement, B. Reduction of N-hydroxylated compounds: amidoximes (N-hydroxyamidines) as pro-drugs ofamidines. Drug Metab. 2002; 34: 565–79.
33. Yáñez JA, Wang SW, Knemeyer IW, Wirth MA, Alton KB. Intestinal lymphatic transport for drug delivery. Adv Drug Deliv Rev. 2011;63(10-11):923-42.
34. Trevaskis NL, Charman WN, Porter CJ. Lipid-based delivery systems and intestinal lymphatic drug transport: a mechanistic update. Adv Drug Deliv Rev. 2008; 17;60(6):702-16.

35. Abellan-Pose R, Csaba N, Alonso MJ. Lymphatic Targeting of Nanosystems for Anticancer Drug Therapy. Curr Pharm Des. 2016;22(9):1194-209.
36. Cueni LN, Detmar M. New insights into the molecular control of the lymphatic vascular system and its role in disease. J Invest Dermatol. 2006;126(10):2167-77.
37. Singh I, Swami R, Khan W, Sistla R. Lymphatic system: a prospective area for advanced targeting of particulate drug carriers. Expert Opin Drug Deliv. 2014;11(2):211-29.
38. Swartz MA. The physiology of the lymphatic system. Adv Drug Deliv Rev. 2001; 23;50(1-2):3-20.
39. Trevaskis NL, Kaminskas LM, Porter CJ. From sewer to saviour - targeting the lymphatic system to promote drug exposure and activity. Nat Rev Drug Discov. 2015;14(11):781-803.
40. Swartz MA, Lund AW. Lymphatic and interstitial flow in the tumour microenvironment: linking mechanobiology with immunity. Nat Rev Cancer. 2012; 24;12(3):210-9.
41. Proulx ST, Luciani P, Dieterich LC, Karaman S, Leroux JC, Detmar M. Expansion of the lymphatic vasculature in cancer and inflammation: new opportunities for in vivo imaging and drug delivery. J Control Release. 2013; 172(2):550-7.
42. Singh I, Swami R, Khan W, Sistla R. Lymphatic system: a prospective area for advanced targeting of particulate drug carriers. Expert Opin Drug Deliv. 2014;11(2):211-29.
43. Dahan A, Hoffman A. Evaluation of a chylomicron flow blocking to investigate the intestinal lymphatic transport of lipophilic drugs. Eur J Pharm Sci. 2005;24(4):381-8.
44. Bhalekar MR, Upadhaya PG, Madgulkar AR, Kshirsagar SJ, Dube A, Bartakke US. In-vivo bioavailability and lymphatic uptake evaluation of lipid nanoparticulates of darunavir. Drug Deliv. 2016;23(7):2581-86.

45. Fu Q, Sun J, Ai X, Zhang P, Li M, Wang Y, Liu X, Sun Y, Sui X, Sun L, Han X, Zhu M, Zhang Y, Wang S, He Z. Nimodipine nanocrystals for oral bioavailability improvement: Role of mesenteric lymph transport in the oral absorption. Int J Pharm. 2013; 1;448(1):290-7.
46. Attili-Qadri S, Karra N, Nemirovski A, Schwob O, Talmon Y, Nassar T, Benita S. Oral delivery system prolongs blood circulation of docetaxel nanocapsules via lymphatic absorption. Proc Natl Acad Sci U S A. 2013;110(43):17498-503.
47. Sun M, Zhai X, Xue K, Hu L, Yang X, Li G, Si L. Intestinal absorption and intestinal lymphatic transport of sirolimus from self-microemulsifying drug delivery systems assessed using the single-passintestinal perfusion (SPIP) technique and a chylomicron flow blocking approach: Linear correlation with oral bioavailabilities in rats. Eur J Pharm Sci. 2011; 14;43(3):132-40.
48. Lind ML, Jacobsen J, Holm R, Müllertz A. Intestinal lymphatic transport of halofantrine in rats assessed using a chylomicron flow blocking approach:The influence of polysorbate 60 and 80. Eur J Pharm Sci. 2008; 2;35(3):211-8.
49. Gao F, Zhang Z, Bu H, Huang Y, Gao Z, Shen J, Zhao C, Li Y. Nanoemulsion improves the oral absorption of candesartan cilexetil in rats:Performance and mechanism. J Control Release. 2011; 20;149(2):168-74.
50. Mishra A, Vuddanda PR, Singh S. Intestinal Lymphatic Delivery of Praziquantel by Solid Lipid Nanoparticles: Formulation Design, In Vitro and In Vivo Studies. Journal of Nanotechnology. 2014; 2014: 12 pages. (Article ID 351693).
51. Makwana V, Jain R, Patel K, Nivsarkar M, Joshi A. Solid lipid nanoparticles (SLN) of Efavirenz as lymph targeting drug delivery system: Elucidation of mechanism of uptake using chylomicron flow blocking approach. Int J Pharm. 2015; 495(1):439-46.

52. Tsai YJ1, Tsai TH. Mesenteric lymphatic absorption and the pharmacokinetics of naringin and naringenin in the rat. J Agric Food Chem. 2012;60(51):12435-42.
53. Thorn CF, Oshiro C, Marsh S, Hernandez-Boussard T, McLeod H, Klein TE, Altman RB. Doxorubicin pathways: pharmacodynamics and adverse effects. Pharmacogenet Genomics 2011;21(7):440-6.
54. Swift LP, Rephaeli A, Nudelman A, Phillips DR, Cutts SM. Doxorubicin-DNA adducts induce a non-topoisomerase II-mediated form of cell death. Cancer Res. 2006; 1;66(9):4863-71.
55. Agudelo D, Bourassa P, Bérubé G, Tajmir-Riahi HA. Intercalation of antitumor drug doxorubicin and its analogue by DNA duplex: structural features and biological implications. Int J Biol Macromol. 2014;66:144-50.
56. Nitiss JL. Targeting DNA topoisomerase II in cancer chemotherapy. Nat Rev Cancer. 2009;9(5):338-50.
57. Gustafson DL, Merz AL, and Long ME. Pharmacokinetics of combined doxorubicin and paclitaxel in mice. Cancer Lett. 2005;220:161-69.
58. Lee HJ, Lee MG. Effects of dexamethasone on the pharmacokinetics of adriamycin after intravenous administration to rats. Res. Commun. Mol. Pathol. Pharmacol. 1999;105:87-96.
59. Kim JE, Cho HJ, Kim JS, Shim CK, S.J. Chung, Oak MH, Yoon IS, Kim DD. The limited intestinal absorption via paracellular pathway is responsible for the low oral bioavailability of doxorubicin. Xenobiotica; the fate of foreign compounds in biological systems. 2013; 43:579-91.
60. Olson, R.D.; Mushlin, P.S. Doxorubicin cardiotoxicity: Analysis of prevailing hypotheses. FASEB J. 1990; 4: 3076–86.

61. Chen IL, Tsai YJ, Huang CM, Tsai TH. Lymphatic absorption of quercetin and rutin in rat and their pharmacokinetics in systemic plasma. J Agric Food Chem. 2010; 58(1):546-51.
62. Murota K, Terao J. Quercetin appears in the lymph of unanesthetized rats as its phase II metabolites after administered into the stomach. FEBS Lett. 2005; 579(24):5343-6.
63. Murota K, Cermak R, Terao J, Wolffram S. Influence of fatty acid patterns on the intestinal absorption pathway of quercetin in thoracic lymph duct-cannulated rats. Br J Nutr. 2013;109(12):2147-53.
64. Russo M, Spagnuolo C, Tedesco I, Bilotto S, Russo GL. The flavonoid quercetin in disease prevention and therapy: facts and fancies. Biochem Pharmacol. 2012; 1;83(1):6-15.
65. Spagnuolo C, Russo M, Bilotto S, Tedesco I, Laratta B, Russo GL. Dietary polyphenols in cancer prevention: the example of the flavonoid quercetin in leukemia. Ann N Y Acad Sci. 2012;1259:95-103.
66. Rani N, Velan LP, Vijaykumar S, Arunachalam A. An insight into the potentially old-wonder molecule-quercetin: the perspectives in foresee. Chin J Integr Med. 2015; 2015:1-16.
67. Cote B, Carlson LJ, Rao DA, Alani AW. Combinatorial resveratrol and quercetin polymeric micelles mitigate doxorubicin induced cardiotoxicity in vitro and in vivo. J Control Release. 2015; 6(213):128-133.
68. Li SZ, Li K, Zhang JH, Dong Z. The effect of quercetin on doxorubicin cytotoxicity in human breast cancer cells. Anticancer Agents Med Chem. 2013;13(2):352-5.
69. Li S, Yuan S, Zhao Q, Wang B, Wang X, Li K. Quercetin enhances chemotherapeutic effect of doxorubicin against human breast cancer cells while reducing toxic side effects of it. Biomed Pharmacother. 2018;100:441-47.

70. Wang G, Zhang J, Liu L, Sharma S, Dong Q. Quercetin potentiates doxorubicin mediated antitumor effects against liver cancer through p53/Bcl-xl. PLoS One. 2012;7(12):e51764.
71. Choi JS, Piao YJ, Kang KW. Effects of quercetin on the bioavailability of doxorubicin in rats: role of CYP3A4 and P-gp inhibition by quercetin. Arch Pharm Res. 2011;34(4):607-13.
72. Dong Q, Chen L, Lu Q, Sharma S, Li L, Morimoto S, Wang G. Quercetin attenuates doxorubicin cardiotoxicity by modulating Bmi-1 expression. Br J Pharmacol. 2014;171(19):4440-54.
73. Moncada S, Higgs A. The L-arginine-nitric oxide pathway. N Engl J Med. 1993; 30;329(27):2002-12.
74. Thomas DD, Liu X, Kantrow SP, Lancaster JR Jr. The biological lifetime of nitric oxide: implications for the perivascular dynamics of NO and O2. Proc Natl Acad Sci U S A: 2001; 2;98(1):355-60.
75. Janssen I, Heymsfield SB, Wang ZM, Ross R. Skeletal muscle mass and distribution in 468 men and women aged 18-88 yr. J Appl Physiol (1985): 2000; 89(1):81-8.
76. Evans WJ. Skeletal muscle loss: cachexia, sarcopenia, and inactivity. Am J Clin Nutr. 2010; 91(4):1123S-1127S.
77. Tajbakhsh S. Skeletal muscle stem cells in developmental versus regenerative myogenesis. J Intern Med. 2009; 266(4):372-89.
78. Muir AR, Kanji AH, Allbrook D. The structure of the satellite cells in skeletal muscle. J Anat. 1965;99(Pt 3):435-44.
79. Mauro A. Satellite cell of skeletal muscle fibers. J Biophys Biochem Cytol. 1961;9:493-5.
80. Katz FRS. The termination of the afferent nerve fiber in the muscle spindle of the frog. Philos Trans R Soc Lond B Biol Sci. 1961;243: 21–225.

81. Tidball JG. Mechanisms of muscle injury, repair, and regeneration. Compr Physiol. 2011;1(4):2029-62.
82. Turner NJ, Badylak SF. Regeneration of skeletal muscle. Cell Tissue Res. 2012;347(3):759-74.
83. Tidball JG. Inflammatory processes in muscle injury and repair. Am J Physiol Regul Integr Comp Physiol. 2005;288(2):R345-53.
84. Hawke TJ, Garry DJ. Myogenic satellite cells: Physiology to molecular biology. J Appl Physiol. 2001;91: 534-51.
85. Reid MB. Role of nitric oxide in skeletal muscle: synthesis, distribution and functional importance. Acta Physiol Scand. 1998.;162(3):401-9.
86. Anderson JE. Molecular Biology of Cell. 2000;11:1859-74.
87. Mauro A. Satellite cell of skeletal muscle fibers. J Biophys Biochem Cytol. 1961;9:493-5.
88. Moss FP, Leblond CP. Satellite cells as the source of nuclei in muscles of growing rats. Anat Rec. 1971;170(4):421-35.
89. Wang G, Burczynski FJ, Hasinoff BB, Zhang K, Lu Q, Anderson JE. Development of A Nitric Oxide Releasing Analogue of the Muscle Relaxant Guaifenesin for Skeletal Muscle Satellite Cell Myogenesis. Mol Pharm. 2009;6(3):895-904.
90. Leiter JR, Peeler J, Anderson JE. Exercise induced muscle growth is muscle-specific and age dependent. Muscle nerve. 2011;43: 828-38.
91. Leiter JR, Upadhaya R, Anderson JE. Nitric oxide and voluntary exercise together promote quadriceps hypertrophy and increase vascular density in female 18-mo-old mice. Am J Physiol Cell Physiol. 2012;302: C1306–C1315.

CHAPTER 2

RATIONALE, HYPOTHESIS, AND OBJECTIVES

2.1. DOXQ

2.1.1. Rationale

The use of the anticancer drug doxorubicin is limited by its cardiac toxicity, which is caused by formation of highly reactive oxygen species leading to myocardial toxicity. It also has poor bioavailability and therefore can only be given parenterally. The intravenous administration of doxorubicin results in a high initial maximum drug concentrations in the systemic circulation, as well as high tissue concentrations further increasing susceptibility of cardiac and renal toxicities. Given antioxidant properties of quercetin, IV DoxQ may have potential protective effects on the heart and kidneys by scavenging reactive oxygen species generated from doxorubicin. Additionally, quercetin may alter the distribution of doxorubicin resulting in lower systemic side-effects and possibly increased localization into lymphatics. Therefore, an IV formulation of DoxQ could provide a sustained release of doxorubicin and reduce its systemic toxicities.

The poor bioavailability of doxorubicin is mainly due to it poor intestinal absorption and extensive first pass metabolism. Thus, oral DoxQ could reduce effects on efflux transporters and metabolic enzymes and also shunt doxorubicin towards intestinal lymphatics as opposed to the intestinal hepatic absorption pathway due to the presence of quercetin. As a result, the absorption of doxorubicin after oral DoxQ will likely improve the systemic exposure of doxorubicin. An oral formulation of DoxQ could be beneficial for the treatment of lymphomas and metastatic cancers, provide a convenient route of administration for patients, and could reduce the dose required to achieve effective drug concentrations by increasing localization in lymphatics and increasing the overall systemic exposure.

2.1.2. Hypothesis

We hypothesize that the cholesterol like structure of quercetin in DoxQ may preferentially be absorbed in the lymphatics rather than the gastrointestinal vasculature following oral administration, thus providing a novel therapeutic approach to target lymphatics and bypass hepatic metabolism. The release of quercetin from DoxQ will likely have a beneficial effect and limit the cardiac and renal side-effects of doxorubicin. In addition, the synthesis and change in physiochemical properties of DoxQ may alter pharmacokinetics, metabolism and release of quercetin from DoxQ or DoxQ intact may also have effects on CYP3A4 and P-gp, which could further augment the disposition and bioavailability of doxorubicin *in vivo*.

2.1.3. Project Objectives

1. To synthesize and purify DoxQ
2. To examine the physiochemical properties of DoxQ in comparison to doxorubicin and quercetin using computer software packages.
3. In vitro studies of DoxQ in comparison to doxorubicin, quercetin, and a mixture of doxorubicin plus quercetin mixture i.e. anti-oxidant activity, CYP3A4 inhibition, P-gp inhibition etc.
4. To examine the safety of DoxQ in comparison to doxorubicin on cardiomyocytes and elucidate the mechanism involved in cardiac protection or toxicity.
5. To develop an analytical assay to quantitate doxorubicin's concentrations in biological matrices (rat lymph, serum, urine).
6. To delineate the pharmacokinetics and toxicokinetics of doxorubicin in blood and urine after oral and intravenous administration of DoxQ and Dox in a rat model.

7. Examine the feasibility of drug delivery after oral and intravenous administration.
8. To examine the intestinal lymphatic absorption of doxorubicin after oral administration of DoxQ or Dox-HCl in rats.

2.2. MYONOVIN®

2.2.1. Rationale

MyoNovin® represents a new class of nitric oxide donors, where the guaifenesin backbone acts as carrier to facilitate transport of nitric oxide to skeletal muscles. MyoNovin® could be used to restore loss of skeletal muscles in various conditions such as: muscle injury and muscle atrophy especially because there are no viable pharmacological treatment to treat such conditions. The presence of guaifenesin in MyoNovin® is anticipated to limit the systemic effects of nitric oxide associated with conventional nitric oxide donors, thus improving the overall therapeutic efficacy and safety.

2.2.2. Hypothesis

We hypothesize that the change in chemical structure of guaifenesin into MyoNovin® will alter its physicochemical and biopharmaceutical properties, pharmacological activity and its disposition in biological fluids. The release of NO from MyoNovin® may have an effect on CYP3A4, antioxidant activity as well as cardiac and renal tissues.

2.2.3. Project Objectives

1. To synthesize and purify MyoNovin®.

2. To examine the physiochemical and biopharmaceutical properties of MyoNovin® in comparison to guaifenesin using computer software packages.
3. In vitro studies of MyoNovin®: CYP3A4 inhibition and antioxidant activity.
4. To examine the cardiac safety of MyoNovin® using human cardiomyocytes.
5. To develop an analytical assay to quantitate MyoNovin® concentrations in biological matrices (rat blood and urine).
6. To delineate the pharmacokinetics and toxicokinetics of MyoNovin® in blood and urine after intravenous administration in a rat model.
7. Examine the feasibility of drug delivery for oral, transdermal, and intravenous administration.

CHAPTER 3

MECHANISTICALLY ELUCIDATING THE IN VITRO SAFETY AND EFFICACY OF A NOVEL DOXORUBICIN DERIVATIVE*

A version of this chapter has been published:

Alrushaid S, Zhao Y, Sayre CL, Maayah ZH, Forrest ML, Senadheera SN, Chaboyer K, Anderson HD, El-Kadi A, Davies NM . Mechanistically Elucidating the In-Vitro Safety and Efficacy of a Novel Doxorubicin Derivative. Drug Deliv Transl Res. 2017;7(4):582-97.

3.1. ABSTRACT

Purpose: Doxorubicin is an effective anticancer drug; however, it is cardiotoxic and has poor oral bioavailability. Quercetin is a plant based flavonoid with inhibitory effects on P-glycoprotein (P-gp) and CYP3A4, and also antioxidant properties. To mitigate these therapeutic barriers, DoxQ, a novel derivative of doxorubicin, was synthesized by conjugating quercetin to doxorubicin. The purpose of this study is to mechanistically elucidate the *in vitro* safety and efficacy of DoxQ. **Methods:** Drug release *in vitro* and cellular uptake by multi-drug resistant canine kidney cells (MDCK-MDR) were quantified by HPLC. Antioxidant activity, CYP3A4 inhibition, and P-gp inhibitory effects were examined using commercial assay kits. Drug potency was assessed utilizing triple negative murine breast cancer cells and the cardiotoxicity was assessed utilizing adult rat and human cardiomyocytes (RL-14). Levels of reactive oxygen species and gene expression of cardiotoxicity markers, oxidative stress markers, and CYP1B1 were determined in RL-14. **Results:** DoxQ was less cytotoxic to both rat and human cardiomyocytes and retained anticancer activity. Levels of ROS and markers of oxidative stress demonstrate lower oxidative damage induced by DoxQ compared to doxorubicin. DoxQ also inhibited the expression and catalytic activity of CYP1B1. Additionally, DoxQ inhibited CYP3A4 and demonstrated higher cellular uptake by MDCK-MDR cells than doxorubicin. **Conclusions:** DoxQ provides a novel therapeutic approach to mitigate cardiotoxicity and poor oral bioavailability of doxorubicin. The cardioprotective mechanism of DoxQ likely involves scavenging ROS and CYP1B1 inhibition, while the mechanism of improving poor oral bioavailability of doxorubicin is likely related to inhibiting CYP3A4 and P-gp.

3.2. INTRODUCTION

Doxorubicin, also called Adriamycin, is an anti-cancer drug used to treat lymphomas, breast, and ovarian cancers (1). The anti-cancer activity of doxorubicin is due to its intercalation between the two strands of DNA, inhibiting the activity of topoisomerase and DNA synthesis (2,3). Despite the clinical effectiveness of doxorubicin, its use is limited by off-target adverse effects particularly dose related cardiotoxicity which can be life threatening (4). Additionally, doxorubicin is a substrate of P-glycoprotein (P-gp) efflux pump (5) and cytochrome P450 metabolic enzymes (6) both of which contribute to its poor oral absorption and low oral bioavailability. For this reason, doxorubicin is only available as a parenteral treatment, which is administered intravenously as a hydrochloride salt formulation.

Over the years several attempts were undertaken to overcome these limitations including: drug delivery systems such as micelles (7), synthetic polymer conjugates (8), and antibody targeted carriers (9) with varied success. The currently available formulation of doxorubicin (Doxil^{TM}) is a pegylated liposomal formulation (10) that is administered intravenously and retains the risk of cardiotoxicity.

The potential therapeutic utility of polyphenols, including flavonoids, is being studied extensively (11). One flavonoid found in plant-based food with potential health benefits is quercetin. Quercetin has been reported to have a role in disease prevention such as liver disease (12), pulmonary hypertension (13), and other cardiovascular diseases (14). Furthermore, quercetin exhibits anti-inflammatory (15), anti-cancer (16), and anti-oxidant effects (17,18).

Preliminary studies suggest that combining quercetin with doxorubicin may have beneficial effects. Quercetin enhanced the anti-tumor effect of doxorubicin in colorectal HT29 cancer cell line (19), MCF-7 breast cancer cell line (20), liver cancer cells (21), and K562 human

leukemia cell line (22). Quercetin also showed cardioprotection against cardiotoxicity induced by doxorubicin (23, 24). Additionally, quercetin could potentially minimize doxorubicin's loss during first pass metabolism and P-gp efflux by inhibiting CYP3A4 and P-gp and thus enhance its oral bioavailability (25). Furthermore, quercetin has a natural tendency to be transported to the lymphatics after intraduodenal administration in rat studies as its concentrations in the lymph were higher than plasma (26). This observation suggests that quercetin may be preferentially absorbed from the intestine into the lymphatics over the hepatic portal vein resulting in lower first pass effect and improved bioavailability. As bioavailability (F) = 1- extraction ratio (E), utilizing quercetin as a novel lymphatically targeted carrier for doxorubicin, could increase its systemic delivery (F) by increasing its localization and delivery in the lymphatics through a reduction in its first pass liver metabolism and extraction (E). Here, quercetin was conjugated to doxorubicin via a glycine linker to give DoxQ as a novel derivative and delivery system of doxorubicin. The doxorubicin-quercetin conjugate (DoxQ) may provide a natural lymphatically targeted delivery approach to improve lymphatic metastasis, and may also serve as a novel therapeutic delivery approach to improve the safety and tolerability of doxorubicin in patients both parenterally and orally.

In this study, the *in vitro* safety and efficacy of DoxQ are mechanistically characterized. The efficacy, metabolism and safety of DoxQ in comparison to doxorubicin are examined for the first time with a potential to enhance the bioavailability, safety and efficacy of the parent compound utilizing several *in-vitro* assays. Additionally, the effects of DoxQ on adult rat cardiomyocytes and human cardiomyocytes were tested in comparison to doxorubicin to assess its cardiotoxicity and suggest possible mechanisms involved in cardioprotection or

cardiotoxicity. The effects of the novel derivative were also examined in murine breast cancer cells to assess anti-cancer activity.

3. 3. MATERIALS AND METHODS

3.3.1. Materials

Doxorubicin and quercetin were obtained from Sigma Aldrich (Oakville, ON). Chemical solvents were from Fisher (Ottawa, ON). H-Gly-OtBu-HCl was from Bachem Americas Inc. (Torrance, CA). Bis (4-nitrophenyl) carbamate was from Alfa Aesar (Tewksbury, MA). Cayman anti-oxidant assay kit catalogue #709001 was purchased from Cayman Chemical (Ann Arbor, MC), cytochrome P450 kit catalogue # P2857 was from Life Technologies (Burlington, ON), and P-glycoprotein assay kit catalogue # V3601 was from Promega (Madison, WI). "High capacity cDNA Reverse Transcription kit for 200 or 1000 reactions" was obtained from Applied Biosystems (AB).

3.3.2. Chemical Synthesis

The chemical synthesis of DoxQ (doxorubicin and quercetin conjugate) is shown in Figure 3.1. All glassware was oven dried at 140˚C prior to use. Dry organic solvents (THF and DMF) were used. Reactions were performed at ambient temperature under dry argon.

Compound 1 (Quercetin-Gly-tBu)

Quercetin-Gly-tBu was synthesized according to Kim MK et al, 2009 (27) with some modifications. In a 100-mL round bottom flask (RBF) H-Gly-OtBu-HCl (1 g, 6 mmol) and Bis (4-nitrophenyl carbonate) (2 g, 6.6 mmol) were dissolved in 30 mL of dry tetrahydrofuran (THF) and 15 ml of dimethylformamide (DMF) with stirring. Two (2) mL of diisopropylethylamine

(DIPEA) were then added to the RBF to initiate the reaction. The reaction was maintained at ambient temperature for 24 h. The following day, quercetin (1.82 g, 1.82 mmol) was added gradually over 10 min with stirring. The reaction was maintained for an additional 24 h. The product was transferred to a clean 250 mL RBF and concentrated under reduced pressure. The crude product was further dried overnight under high vacuum. The dried yellowish crude product was purified over the silica gel using dichloromethane (DCM)/acetone solvent system (gradient solvent system: initially 10/90, then 15/85 and finally 20/80). The fractions were analyzed by TLC (1/10, acetone/DCM). The fractions of interest were combined and concentrated under reduced pressure to afford the compound 1 as yellow solid (2 g). ^{1}H-NMR (Acetone-d_6, 400 MHz): δ = 12.06 (s, 1H), 9.23(bs, 1H), 7.99 (d, *J* = 2.2 Hz, 1H), 7.96 (dd, *J* = 8.6, 2.1 Hz, 1H), 7.06 (d, *J* = 8.7 Hz, 1H), 6.99 (t, *J* = 6.6 Hz, 1H), 6.46 (t, *J* = 2.1 Hz, 1H), 6.21 (t, *J* = 2.1 Hz, 1H), 3.86 (d, *J* = 6.0 Hz, 2H), 1.43 (s, 9H); ESI (m/z); Calculated for $C_{22}H_{20}NO_{10}$ $(M-H)^-$: 458.1087; Found: 458.0047.

Compound 2 (Quercetin-Gly-COOH)

Compound 1 (2 g) was dissolved in 10 mL of DCM and cooled on ice, then 40 mL of trifluoroacetic acid (TFA) were added gradually with stirring. An additional 10 mL of DCM was added to rinse the walls of the RBF and the reaction mixture was stirred for 4 h. The resulted yellow precipitate was filtered under vacuum using a ceramic Buchner funnel fitted with a filter paper. The precipitate was washed with DCM and ice cold acetone then oven dried to afford compound 2 as a yellow solid (~1g) which was used for the next step without further purification. ^{1}H-NMR ^{1}H-NMR (DMSO-d_6, 400 MHz): δ = 12.69 (bs, 1H), 12.44 (s, 1H), 10.81(bs, 1H), 10.38 (bs, 1H), 9.56 (s, 1H), 8.02 (t, *J* = 6.8 Hz, 1H), 7.91 (dd, *J* = 8.6, 2.3 Hz,

1H), 7.88 (d, *J* = 2.2 Hz, 1H), 7.06 (d, *J* = 8.6 Hz, 1H), 6.47 (d, *J* = 2.0 Hz, 1H), 6.21 (d, *J* = 2.0 Hz, 1H), 3.77 (d, *J* = 6.1 Hz, 2H); ESI (m/z) Calculated for $C_{18}H_{12}NO_{10}$ $(M-H)^-$: 402.0461; Found: 402.0419.

Compound 3 (Quercetin-Gly-Dox)

Doxorubicin HCl (500 mg, 0.86 mol), compound 2 (900 mg, 2.15 mol), 1-[Bis(dimethylamino)methylene]-1H-1,2,3-triazolo[4,5-b]pyridinium 3-oxid hexafluorophosphate (HATU) (655 mg, 1.72 mol) were dissolved in 100 mL of dry DMF with stirring. DIPEA (1.3 mL, 6.9 mmol) was added last. The reaction was maintained at ambient temperature with stirring over 48 h in the dark.

The reaction mixture was concentrated under reduced pressure in the dark. The crude product was purified by recrystallization using acetonitrile and methanol as follows: crude product was dissolved in minimum amount of acetonitrile:methonol (4:1, 10 mL) with the help of sonication and heating (~ 50-60 ^{0}C). Resulted solution was allowed to cool down to facilitate the crystallization and the RBF was stored overnight at 4 0C in refrigerator to facilitate crystallization/precipitation of the product. The dark red product with the solution was transferred into 50-mL centrifugation tube and centrifuged at 4000 g for 20 minutes. Supernatant was decanted. The centrifugation was repeated 4 times with ice cold acetonitrile:methanol (4:1, 5 mL x 4). The supernatant was carefully pipetted/decanted. After the final round of centrifugation, a clear solution of supernatant was observed. The resulted dark red solid residue was collected and dried to afford the final compound 3 (DoxQ, ~500 mg; ^{1}H-NMR (DMSO-d_6, 400 MHz): δ = 8.32 (s, 1H), 7.94 (t, *J* = 6.4 Hz, 1H), 7.90 (d, *J* = 1.2 Hz, 1H), 7.88 (s, 1H), 7.79 (s, 1H), 7.71 (s, 1H), 7.15 (d, *J* = 8.4 Hz, 1H), 7.06 (d, *J* = 8.4 Hz, 1H), 6.46 (s, 1H), 6.19 (s, 1H),

5.50 (s, 1H), 5.23 (s, 1H), 4.97 (s, 1H), 4.87 (s, 2H), 4.57 (s, 1H), 4.16 (s, 1H), 4.00-3.89 (m, 3H), 3.07 (s, 3H), 3.00 (s, 1H), 2.92 (s, 3H), 2.78 (d, *J* = 9.6 Hz, 1H), 2.68 (d, *J* = 6.4 Hz, 1H), 2.21-2.11 (m, 2H), 3.32 (s, 3H), 2.99-2.89 (m, 2H), 2.84-2.56 (m, 1H), 2.37-2.21 (m, 3H), 1.51-1.41 (m, 1H), 1.24 (s, 1H), 1.13 (d, *J* = 7.6 Hz, 3H); ESI (m/z) Calculated for $C_{18}H_{12}NO_{10}$ $(M+Na)^+$ calculated value; Found: 951.2089.

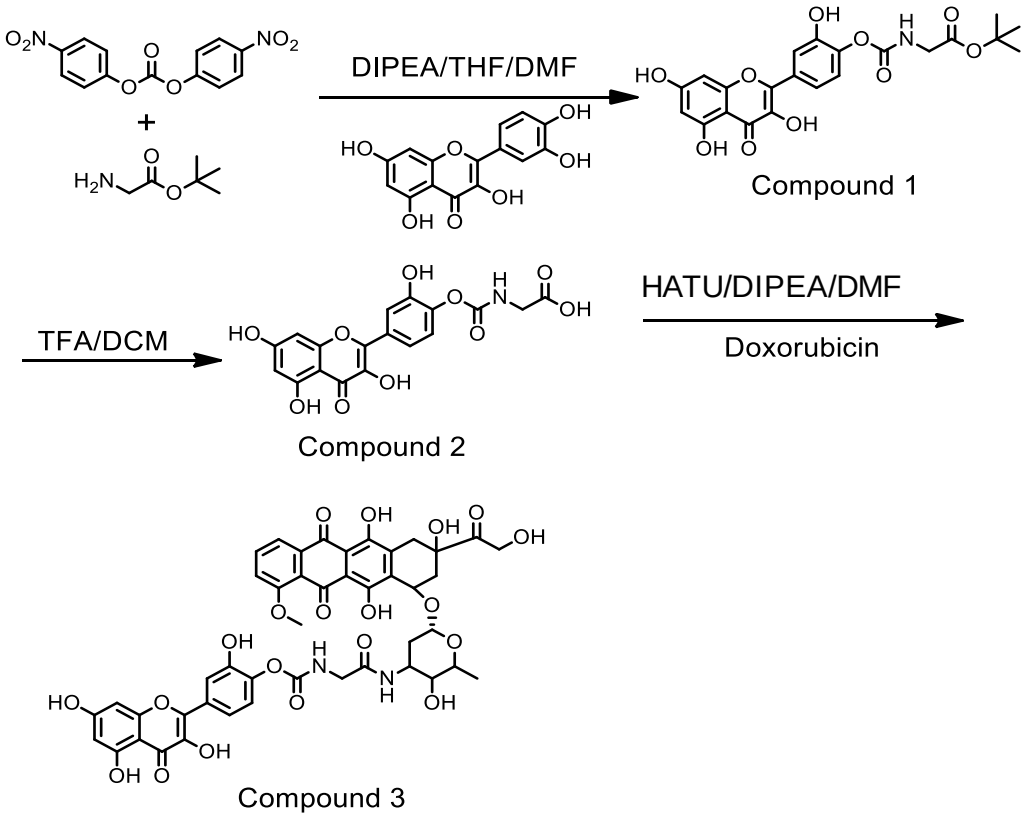

Figure. 3.1. A schematic diagram of DoxQ synthesis.

3.3.4. In Vitro Drug Release Studies

DoxQ release was examined in phosphate buffer saline (PBS) supplemented with 10% fetal bovine serum (FBS) at 37˚C. Aliquots (100 µl) from the sample were collected at pre-

determined time intervals and analyzed by HPLC coupled with fluorescence detector (ex/em 480/590).

3.3.5. Cellular Uptake by MDCK-MDR

Madin-Darby Canine Kidney- Multidrug Resistance (MDCK-MDR) were maintained in high glucose Dulbecco's modified eagle medium (DMEM) with 1× L-Glutamine and sodium pyruvate that was supplemented with 10 % FBS, 1× non-essential amino acid and 1× penicillin-streptomycin. Cells were seeded onto poly L-lysine pre-coated glass coverslips (BD, Franklin Lakes, NJ) in a 12-well culture plate at a density of 5000 cells/well.

After 12 h, cells were treated with 50 nM free doxorubicin, a mixture of doxorubicin and quercetin, or DoxQ alone with 3 µg/mL 4',6-diamidino-2-phenylindole (DAPI) at 15 min prior to cell imaging. After treatment, cells were washed three times with PBS. Live cells were rapidly imaged on a Nikon Eclipse 80i epifluorescence microscope (Melville, NY) with a 20 × 0.75 NA objective and a Hamamatsu ORCA ER digital camera (Houston, TX). The GFP filter set (Nikon, NY) was used to image the fluorescence signal from doxorubicin. All images were taken with identical instrument settings and scaled equally so that fluorescence intensity could be compared between independent images and quantified accurately.

Cellular uptake and accumulation of doxorubicin in MDCK-MDR cells was quantified using HPLC. Cells were seeded in 12-well plates at a density of 10,000 cells/well. After the cells attached to the surface, 1 µM of doxorubicin, a mixture of doxorubicin and quercetin, or DoxQ was added. After 6 h of treatment, the supernatant was collected and analyzed. Fluorescence signals were analyzed by ImageJ. Cellular uptake of Dox was by quantified by HPLC.

3.3.6. Effects on Murine Breast Cancer Cells

A triple negative murine breast cancer line was maintained in Dulbecco's modified eagle medium supplemented with 10 % fetal bovine serum (Hyclone Laboratory Inc., Logan, Utah). Cells were plated in white 96-well flat-bottomed plates at the concentration of 5,000 cells/well in 90 µL of growth medium. After 12 h, the parent compound doxorubicin, quercetin, and a mixture of doxorubicin and quercetin solution were added at different concentrations. Hanks' solution and 10 % trichloroacetic acid (TCA) were used as negative and positive control, respectively. The medium was refreshed 8 h after treatment. After 72 h post-treatment, resazurin blue (5 µM) was added and the resorufin product was measured with a fluorophotometer using an excitation wavelength of 550 nm and an emission wavelength of 590 nm.

3.3.7. Antioxidant Activity

The antioxidant activity of Dox-Q, doxorubicin, quercetin, or a mixture of doxorubicin and quercetin was examined using the anti-oxidant kit from Cayman Chemical. The assay is based on the ability of the antioxidant in the sample to inhibit the oxidation of ABTS® (2,2'-azino-di-[3-ethylbenzthiazoline sulphonate]) to $ABTS^{\circledR \cdot +}$ by metmyoglobin. The amount of ABTS produced is measured by absorbance at 750nm. Antioxidants will supress absorbance at 750 nm and the suppression is proportional to concentration. The antioxidant capacity is compared to a water soluble vitamin E (α-tocopherol) analog called Trolox® (6-hydroxy,2,5,7,8-tetramethylchroman-2-carboxylic acid), which is commonly used as a standard for antioxidant activity. In this assay, stock solutions of Dox-Q, doxorubicin, quercetin were freshly prepared on the day of the experiment in DMSO then further diluted in DMSO to achieve 1, 10, 50 and 100 mM. In a 96-well plate, 10 µl of test samples were added to each well followed by 10 µl of

metmyoglobin and 150 µl of chromagen. Afterwards, 40 µl of hydrogen peroxide working solution was added to each well within 1 min. Four replicates at each concentration were performed. The 96-well plate was covered, and contents were mixed by placing the plate on a shaker at room temperature for 5 min. The absorbance was measured at 750 nm using a Synergy HT multi-well plate reader and Gen5™ software for data analysis (Biotek Instruments Inc., Winooski, VT, USA). The result of the assay was expressed as molar Trolox® equivalents. More information about the assay can be found in the technical bulletin of the assay kit.

3.3.8. Effects on CYP3A4 Activity

The inhibitory effects of CYP3A4 by Dox-Q, doxorubicin, quercetin or a mixture of doxorubicin and quercetin were examined using CYP Vivid kits from Life Technologies following the manufacturer's instructions. Stock solutions of Dox-Q, doxorubicin, quercetin, and the positive control were prepared on the day of the experiment in DMSO then further diluted with the assay buffer to achieve a final concentration of 0.01, 0.1, 1, 10, 50, and 100 µM/well. The assay was performed using a black clear bottom 96-well plates in quadruplicates. To run the assay 40 µl of the test compounds or the positive control, 50 µl of a master pre-mix of CYP450 BACULOSOMES® (microsomes of insect origin expressing a single human CYP 450) and the regeneration system were combined in each well and incubated for 20 min at room temperature (23 ± 1℃). The reaction was initiated by adding 10 µl a mixture of the Vivid® fluorescent substrate and $NADP^+$. The fluorescence was measured immediately after the initiation of the reaction at excitation/emission wavelengths of 485 and 520 nm using a Synergy HT multi-well plate reader (Biotek Instruments Inc., Winooski, VT, USA). The inhibitory effects of the investigational compounds were compared to ketoconazole (10 µM) as a positive inhibitor of

CYP3A4 and the result was expressed as % inhibition. The concentration of the positive control ketoconazole was chosen as suggested by the kit user guidelines. More information about the assay can be found in the technical bulletin of the assay kit.

3.3.9. Effects on P-glycoprotein Activity

The PgP-Glo kit from Promega was utilized to determine if DoxQ exhibits inhibitory effects on P-gp or not. The assay detects the effects of compounds on recombinant human P-gp in a cell membrane fraction by measuring ATPase activity. The effect of the investigational compound on P-gp ATPase activity is compared to samples treated with sodium orthovanadate (Na_3VO_4), a selective inhibitor of P-gp. The samples treated with Na_3VO_4 have no effect on P-gp ATPase activity. The difference in the luminescence signal between samples treated with Na_3VO_4 and untreated represents the basal ATPase activity (ΔRLU_{basal}). The difference in the luminescence signal between samples treated with Na_3VO_4 and samples treated with investigational compounds represents the ATPase activity in presence of test compound ($\Delta RLU_{compound}$). The change in the basal ATPase activity can be compared to the change in the ATPase activity of the test compound to rank the compound as a stimulator, inhibitor, or has no effect on ATPase activity as described below:

$\Delta RLU_{compound} > \Delta RLU_{basal}$, compound is a stimulator of P-gp ATPase activity

$\Delta RLU_{compound} = \Delta RLU_{basal}$, compound has no effect on P-gp ATPase activity

$\Delta RLU_{compound} < \Delta RLU_{basal}$, compound is an inhibitor of P-gp ATPase activity

The result was expressed as fold change in P-gp ATPase activity of test compounds relative to the basal activity. More information about the assay can be found in the technical bulletin of the assay kit.

3.3.10. Effects on Adult Rat Cardiomyocytes

Animals were in full compliance with the Canadian Council on Animal Care, and animal ethics approval was granted by the University of Manitoba Animal Care Committee. Ventricular cardiomyocytes were isolated from adult rats and maintained in culture. The effect of the novel drug derivative on cell viability was examined in comparison to doxorubicin by trypan blue assay.

Adult cardiac myocytes were isolated from 6-7-week old rats transferred on to 24 well plates containing 500 μL of media. Cells were incubated for 2 hours in media.

Cells were exposed to 1, 5, or 10 μM treatments of doxorubicin, DoxQ or control, 3% PEG in DMSO. Stock solutions of the appropriate concentration were directly added to the wells with a micropipette. Treatments were performed in duplicate with each experiment. Three sets of experimental replicates were performed. All treatments proceeded under sterile conditions in a biosafety cabinet. Following the treatments the cells were then incubated at 37°C for 18 h.

Upon 18 hours of incubation 250 μL of media was removed from each well and replaced with 250 μL of trypan blue dye, which selectively dyes dead cells. The wells were then visualized under a bright-field microscope and six sets of pictures were taken at random for each treatment.

Live and dead cells were manually counted. Dead cells were identified to be of a rounded morphology and visibly darker due to the staining with trypan blue. The ratio of dead to total cell count was then calculated.

3.3.11. Effect of Doxorubicin and DoxQ on Cell Viability of RL-14 cells

Human cardiomyocytes RL-14 (American Type Cell Culture Patent Deposit Designation PTA-1499 Manassas, VA) were grown in DMEM/F-12 with phenol red supplemented with 12.5% Fetal Bovine Serum, 20 μM L-glutamate, 100 IU penicillin G and 100 μg/mL streptomycin. Cells were grown in 75 cm^2 tissue culture flasks at 37°C in a humidified incubator with 5% CO_2.

The cells were seeded in 12-well culture plates with DMEM/F-12 then washed with PBS. Cells were then replenished with serum free media and treated with the compounds of interest for 24 h.

The effects of DoxQ on the RL-14 viability were determined utilizing MTT assay. The assay measures the capacity of cells to convert MTT to coloured formazan crystals as described previously (28, 29).

3.3.12. Determination of Reactive Oxygen Species Levels by Dichlorofluorescein (DCF) Assay

RL-14 cells grown to 90% confluence in 96-well cell culture plates were treated for 24 h with test compounds. Thereafter, cells were washed with PBS before incubation for 30 min in fresh media containing 10 μM dichlorofluorescein (DCF). Fluorescence measurements at excitation/emission (545/575 nm) of the wells were recorded using the Bio-Tek Synergy H1Hybrid Multi-Mode Microplate Readers (Bio-Tek Instruments, Winooski, VT, USA).

3.3.13. Quantification of mRNA Expression by Quantitative Real-Time Polymerase Chain Reaction (RT-PCR)

Total RNA from treated cells was isolated using TRIzol reagent (Invitrogen®) according to the manufacturer's instructions and quantified by measuring the absorbance at 260 nm. RNA purity was determined by measuring the 260/280 ratio (>1.8). Thereafter, first strand complementary DNA (cDNA) synthesis was performed using the High-Capacity cDNA reverse transcription kit (Applied Biosystems), according to the manufacturer's instructions as described previously (30). Briefly, 1.5 µg of total RNA from each sample was added to a mixture of 2.0 µl of 10 × reverse transcriptase buffer, 0.8 µl of 25 × deoxynucleotide triphosphate (dNTP) mix (100 mM), 2.0 µl of 10 × reverse transcriptase random primers, 1.0 µl of MultiScribe reverse transcriptase, and 4.2 µl of nuclease-free water. The final reaction mixture was kept at 25 °C for 10 min, heated to 37 °C for 120 min, heated for 85 °C for 5 min, and finally cooled to 4 °C.

Quantitative analysis of specific mRNA expression was performed by (RT-PCR) by subjecting the resulting 1.5 µg cDNA to PCR amplification using 96-well optical reaction plates in the ABI Prism 7500 System (Applied Biosystems) (31). The 25-µl reaction mixture contained 0.1 µl of 10 µM forward primer and 0.1 µl of 10 µM reverse primer (40 nM final concentration of each primer), 12.5 µl of SYBR Green Universal Master mix, 11.05 µl of nuclease-free water, and 1.25 µl of cDNA sample. Human and rat primers sequences for brain natriuretic peptide (BNP), α-myosin heavy chain (α -MHC), β-myosin heavy chain (β-MHC), Glutathione S-transferase A1 – (GST-A1), HO-1, CYP1B1, and β-actin are illustrated in Table 3.1. These primers were purchased from Integrated DNA technologies (IDT, Coralville, IA). The ratio of β-MHC to α-MHC expression was quantitated by assessing relative cDNA levels of the genes

compared with β-actin expression from the same sample. The RT-PCR data was analyzed using the relative gene expression (i.e., ΔΔCT) method, as described and explained previously (32). Briefly, the fold change in the level of target genes between treated and untreated cells, corrected for the level of β-actin, was determined using the following equation: fold change = $2^{-\Delta(\Delta Ct)}$, where $\Delta Ct = Ct_{(target)} - Ct_{(\beta\text{-actin})}$ and $\Delta(\Delta Ct) = \Delta Ct_{(treated)} - \Delta Ct_{(untreated)}$.

Table 3.1. Primers sequences and Efficiency used for RT- PCR reactions.

Gene	Forward primer	Reverse primer	Slope	Amplification	Efficiency
α-MHC	CCAAACGAGTTC CGGCCT	TGCCCAAACCAAA GAGAATGA	-2.999	2.15	1.15
β-MHC	GAATGGCTTCTA GTCCCA	TCATCTTCTCACTA AGGGCT	-3.009	2.14	1.14
BNP	CAGAAGCTGCTG GAGCTGATAAG	TGTAGGGCCTTGGT CCTTTG	-3.33	1.99	0.995
CYP1B1	CAGAAGCTGGAG CTGATAAG	TGTAGGGCCTTGGT CCTTTG	-3.35	1.98	0.985
GST-A1	TTGATGTTCCAGC AAGTGCC	CACCAGCTTCATCC CATCAAT	-3.25	2.03	1.03
HO-1	ATGGCCTCCCTGT ACCACATC	TGTTGCGCTCAATC TCCTCCT	-3.01	2.14	1.14
β-actin	CCAGATCATGTTT GAGACCTTCAA	GTGGTACGACCAG AGGCATACA	-3.00	2.15	1.15

The Ct slope method was used to measure the efficiency of the RT-PCR reactions. This method involves generating a dilution series of the target template and determining the Ct value for each dilution. A plot of Ct versus log cDNA concentration range (with four concentrations points at 60, 6, 0.6, and 0.06 ng/μL) was made. Exponential amplification was calculated using the equation: $A = 10^{(-1/slope)}$. Efficiency was calculated using the equation: $Ex = 10^{(-1/slope)} - 1$.

3.3.14. Determination of CYP1B1 Enzymatic Activity

CYP1B1-dependent methoxyresorufin O-deethylase (MROD) and ethoxyresorufin O-deethylase (EROD) activity was performed on intact living RL-14 cells (33,34). After incubation of the cells with test compounds, 100 µl of 2 µM methoxyresorufin or ethoxyresorufin O-deethylase in assay buffer (0.05 M Tris, 0.1 M NaCl, pH 7.8), was then added to each well. Immediately, an initial fluorescence measurement ($t = 0$) at excitation/emission (545/575 nm) followed by additional set of fluorescence measurements of the samples were recorded every 5 min for 40 min interval using the Bio-Tek Synergy H1Hybrid Multi-Mode Microplate Readers (Bio-Tek Instruments, Winooski, VT, USA).

3.3.15. Statistical analysis

Compiled data were presented as mean and standard error of the mean (mean ± SEM). Where possible, data were statistically analyzed by SigmaPlot® for Windows (Systat Software, Inc, CA) or GraphPrism with a p-value<0.05 being considered statistically significant. One-way analysis of variance (ANOVA) followed by Tukey-Kramer multiple comparison test were employed to assess which treatment group(s) showed a significant difference from the control group.

3.4. RESULTS

3.4.1. In vitro Drug Release

To assess the post-administration fate of DoxQ, the *in vitro* release of the conjugate was examined. The *in vitro* drug release scheme is shown in Figure.3.2. The release of doxorubicin was due to the enzyme digestion of the amide bond. The release of doxorubicin from the

conjugate showed a first-order kinetic profile and the release half-life ($t_{1/2}$) was approximately 60 h (Figure 3.3). Quercetin was released from the conjugate by hydrolyzing the carbamate bond. The release of quercetin exhibited second-order kinetics in aqueous medium with $t_{1/2}$ of approximately 100 h.

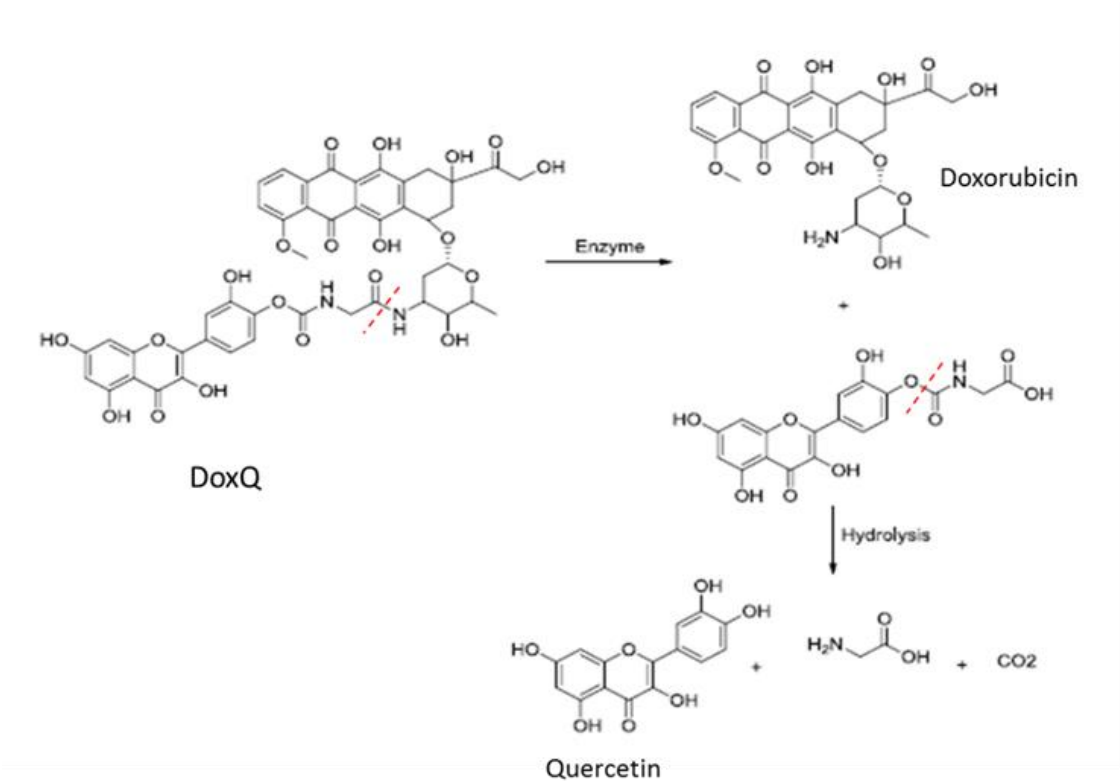

Figure. 3.2. A schematic representation of the release of doxorubicin and quercetin from DoxQ.

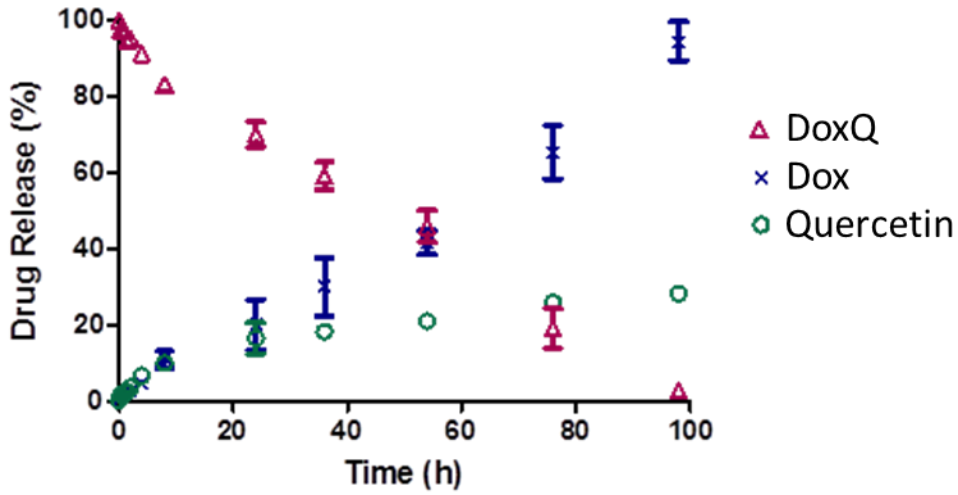

Figure 3.3. *In-vitro* release of doxorubicin and quercetin from DoxQ quantified by HPLC (n=3, mean±SEM).

3.4.2. Cellular Uptake by MDCK-MDR Cells

To assess the efficacy of DoxQ, the uptake of the novel conjugate was examined in MDCK-MDR cells, a P-gp positive cell line. Confocal microscopy was used to examine if the novel derivative can improve doxorubicin's uptake by P-gp positive cells. The fluorescence signal detected in cells treated with a mixture of doxorubicin and quercetin or DoxQ was higher than the group treated with free doxorubicin (Figure. 3.4). Images were analyzed by ImageJ (Figure. 3.5a). After 5 min treatment, there was no significant improvement of drug uptake by the cells treated with doxorubicin plus quercetin mixture compared to that of free doxorubicin. However, the fluorescence signal was significantly enhanced in the cells treated with DoxQ ($p < 0.05$).

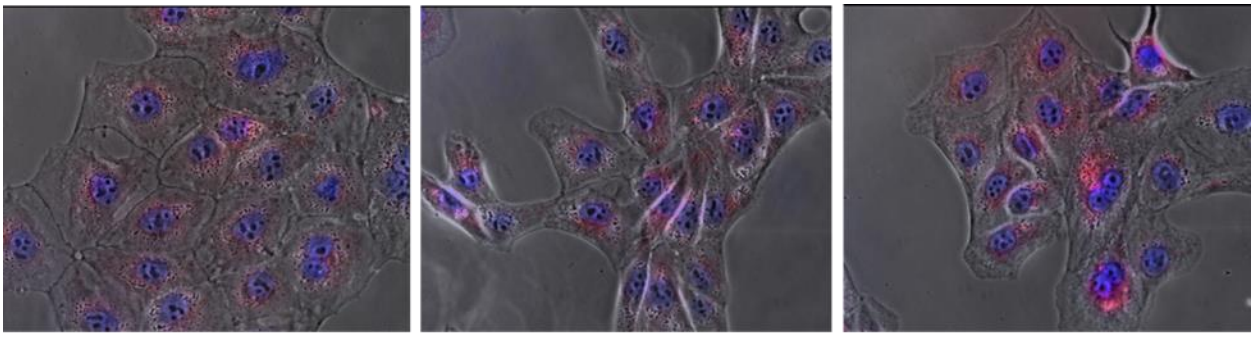

Figure. 3.4. Fluorescence imaging study of cell uptake of doxorubicin by MDCK-MDR cells (P-gp positive). Cells were treated with **(A)** 50 nM free doxorubicin **(B)** 50 nM doxorubicin and 50 nM quercetin **(C)** 50 nM DoxQ for 15 min prior to cell imaging.

Drug uptake by the cells was quantified by HPLC as shown in Fig. 2.5B. The novel formulation significantly improved drug uptake compared to both free doxorubicin and a mixture of doxorubicin and quercetin. This is consistent with the fluorescence imaging study (Figure 3.4 and Figure 3.5A).

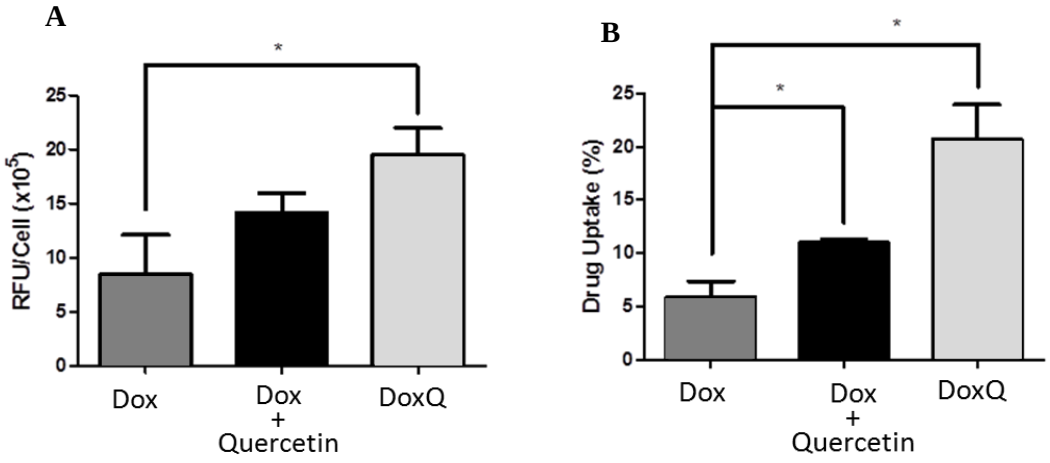

Figure. 3.5. (A) The fluorescence signals analyzed by ImageJ of the images of MDCK-MDR cells after 6 h treatment (n=3, mean±SD) **(B)** HPLC quantification of % drug uptake by MDCK-MDR cells (P-gp positive) after 6 h treatment (n=3, mean±SD). *P<0.05

3.4.3. Effect of DoxQ on Murine Breast Cancer Cells

The cytotoxicity of doxorubicin was evaluated in a triple negative murine breast cancer line by resazurin blue assay in comparison to DoxQ or a mixture of doxorubicin and quercetin to assess its anti-cancer activity. DoxQ was substantially less toxic than doxorubicin or a mixture of doxorubicin and quercetin mixture (Figure 3.6). The IC_{50} of DoxQ was more than two fold higher than doxorubicin alone or a mixture of doxorubicin and quercetin mixture. The decreased cytotoxicity of DoxQ could be partially due to the very poor water solubility and the relatively slow release of doxorubicin from the conjugate.

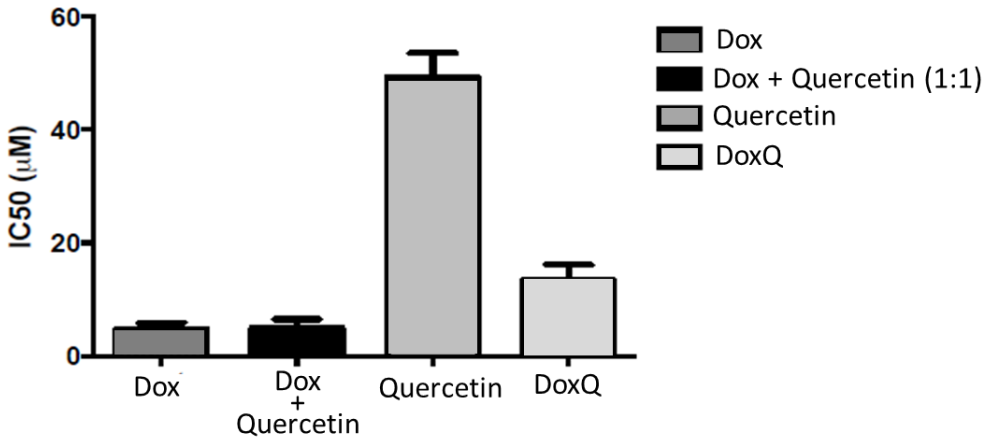

Figure. 3.6. The cytotoxic effects of doxorubicin, a mixture of doxorubicin and quercetin, or DoxQ in murine breast cancers were determined by resazurin blue assay. Cells were treated with various concentrations of test compounds for 72 hours. The result is expressed as IC_{50} (n=4, mean±SD).

3.4.4. Antioxidant Activity

To understand the possible mechanism involved in attenuating doxorubicin induced cardiotoxicity by DoxQ, the antioxidant capacity of DoxQ was investigated. The antioxidant effect was studied utilizing an assay that compares the antioxidant capacity of the investigational compound to that of a positive control (Trolox). The antioxidant capacity of doxorubicin, DoxQ, quercetin and a mixture of doxorubicin and quercetin was evaluated at 1, 10, 50 and 100 mM and showed a dose response effect in all study groups (Figure 3.7). DoxQ showed significantly higher antioxidant effect compared to doxorubicin at all concentrations studied. Similarly, the antioxidant capacity of DoxQ at 10 and 50 mM DoxQ was significantly higher than a mixture of doxorubicin and quercetin, while at 1 and 10 mM DoxQ it was significantly higher than quercetin alone.

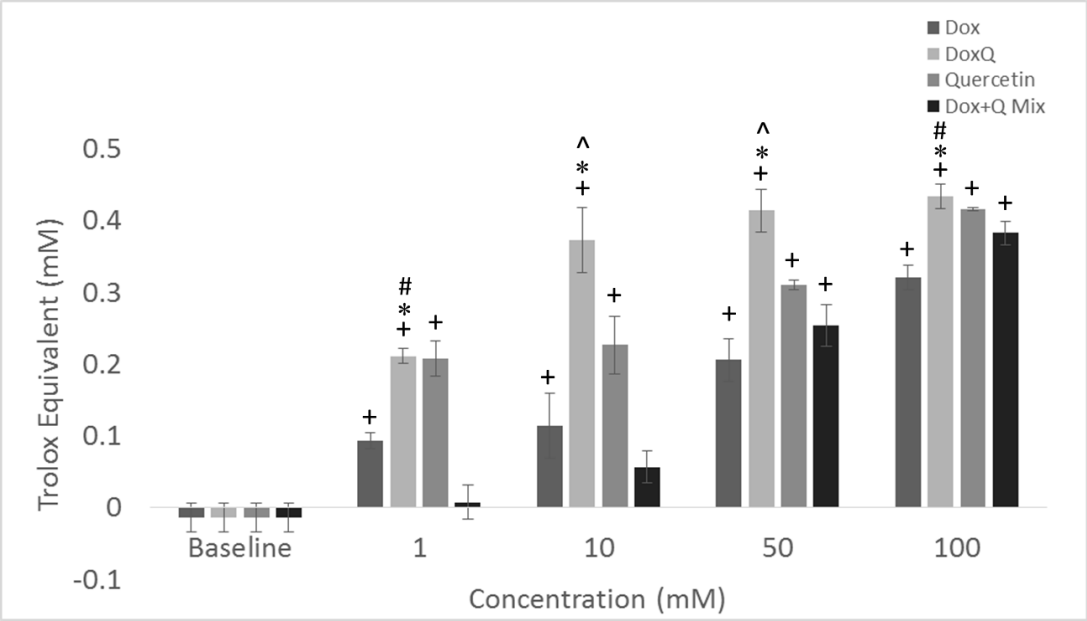

Figure 3.7. Antioxidant activity of DoxQ in comparison to doxorubicin, a mixture of doxorubicin and quercetin, or quercetin alone expressed as Trolox equivalents (n=4; mean±SEM). +P<0.05 compared to control, *P<0.05 compared to doxorubicin, ^P<0.05 compared to quercetin, #P<0.05 compared to Dox+quercetin mixture.

3.4.5. Effect on CYP3A4 Inhibition

To elucidate the possible mechanisms involved in improving the bioavailability of doxorubicin, the effect of DoxQ on CYP3A4 inhibition effect was investigated. CYP3A4 is the major metabolic enzyme involved in first pass effect. Inhibitory effects of CYP3A4 by test compounds were compared to that of ketoconazole at 0.01, 0.1, 1, 10, 50, and 100 μM and the result was expressed as % inhibition relative to ketoconazole. The results show that DoxQ inhibited CYP3A4 at all the concentrations tested, with the highest inhibition at 0.01 μM (Figure 3.8). A mixture of doxorubicin and quercetin did not inhibit CYP3A4 except at 100 μM, which could be due to instability of quercetin, dimerization or its precipitation (35).

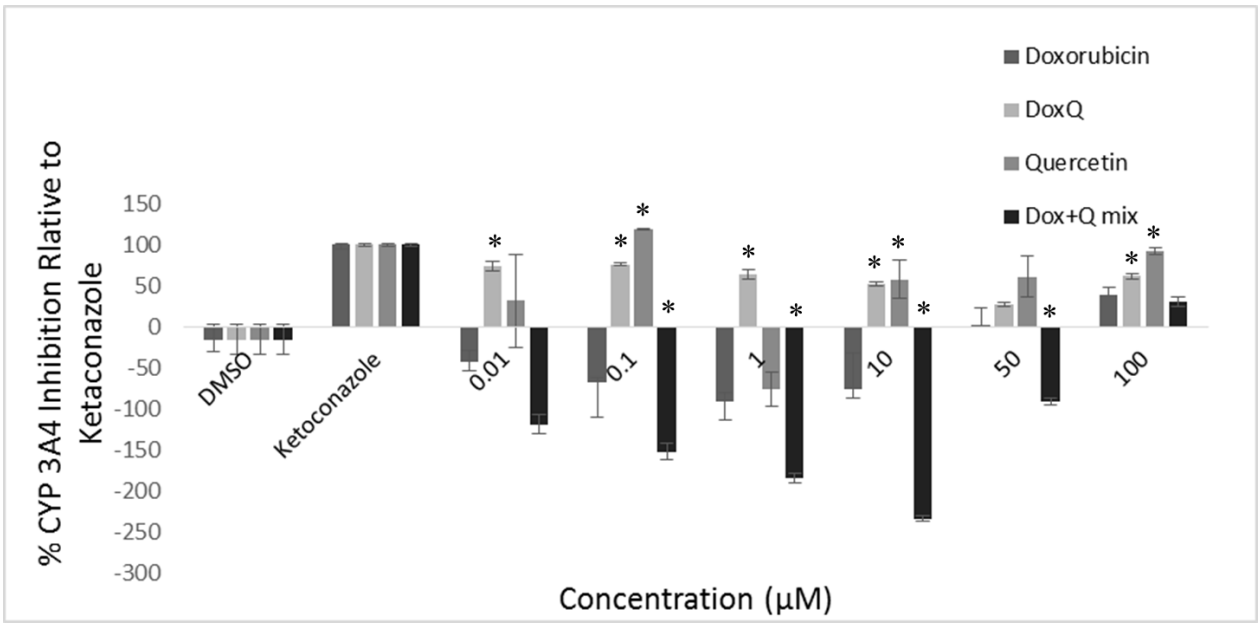

Figure 3.8. CYP3A4 enzyme inhibition expressed as % of the positive inhibitor (ketoconazole) (n=4; mean±SEM). *P<0.05 compared to doxorubicin.

3.4.6. Effect on P-gp ATPase Activity

The effects of DoxQ on P-gp were examined in comparison to doxorubicin, quercetin or a mixture of doxorubicin and quercetin to elucidate the possible role of P-gp inhibition in improving the bioavailability of doxorubicin. At the concentration range of 1-100 μM there was no statistically different ATPase activity between DoxQ and doxorubicin. At 200 μM, P-gp ATPase activity of DoxQ was lower than doxorubicin by 0.6 folds suggesting slight P-gp inhibition effects. However; a mixture of doxorubicin and quercetin mixture significantly reduced P-gp ATPase activity by 0.8-1.2 folds at 50 - 200 μM concentration compared to free doxorubicin (Figure 3.9). Quercetin alone reduced P-gp ATPase activity at all concentrations supporting its P-gp inhibitory effects documented in the literature.

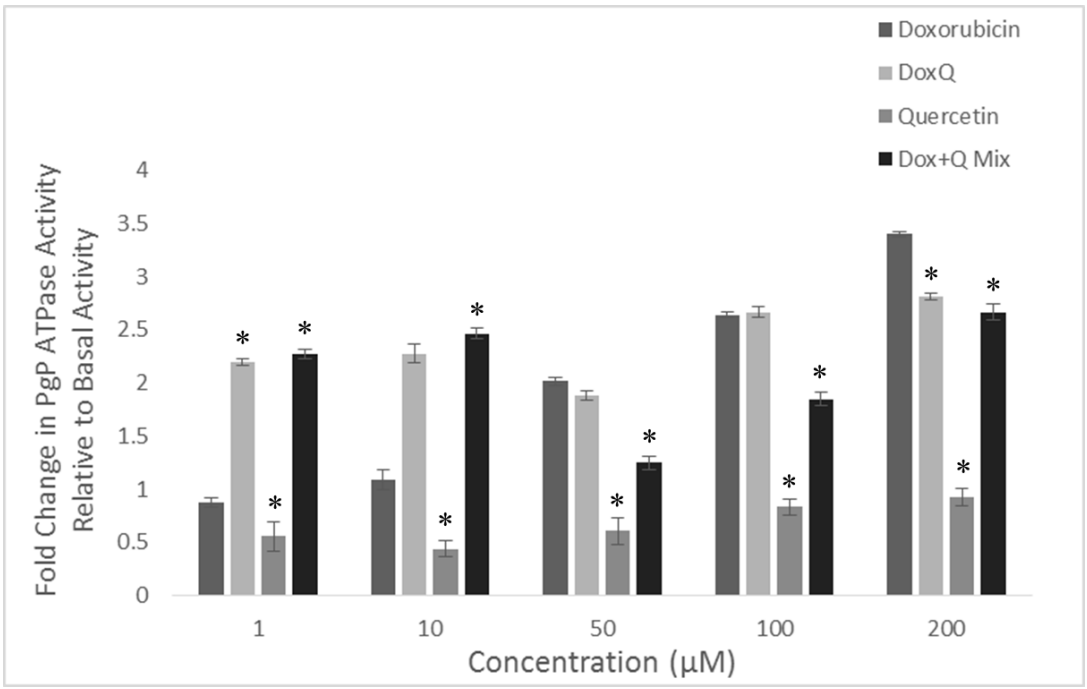

Figure 3.9. Fold change in P-gp ATPase activity of doxorubicin, DoxQ, a mixture of doxorubicin and quercetin, or quercetin on P-gp ATPase activity at 1, 10, 50, 100, and 200 μM relative to basal activity (n=4, mean±SEM). *P<0.05 compared to doxorubicin.

3.4.6. Effect of DoxQ on Rat Cardiomyocytes Cell Viability

To assess the safety of DoxQ, the effects of DoxQ on rat cardiomyocytes were examined at 1, 5, and 10 μM in comparison to doxorubicin by trypan blue assay**.** A dose response effect was observed with both doxorubicin and DoxQ (Figure 3.10A). At 10 μM doxorubicin treatment resulted in ~22% cell death, while DoxQ treatment resulted in ~17% death both were statistically significant from the baseline. Additionally, the lower % of cell death in cells with DoxQ at 10 μM was statistically significant from the cells treated with doxorubicin alone at the same concentration (Figure 3.10b).

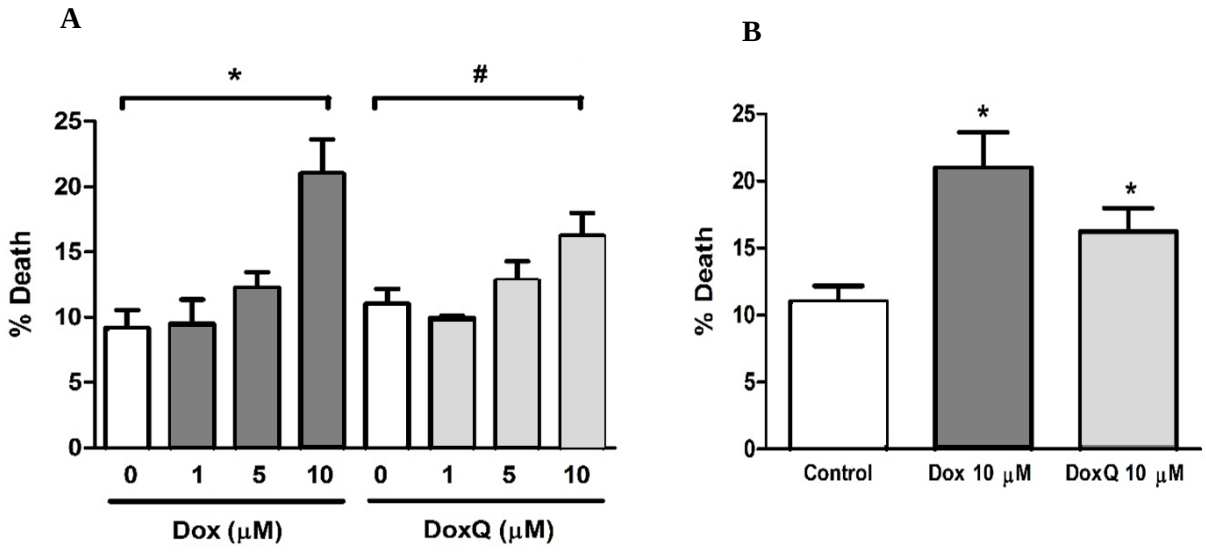

Figure 3.10. Effect of doxorubicin and DoxQ on adult rat cardiomyocyte viability after treatment for 18 h **(A)** Dox versus DoxQ dose response (n=3, mean±SEM * P<0.05 Dox compared to control; # P<0.05 DoxQ compared to control **(B)** Dox versus DoxQ (10μM) (n=3; mean±SEM) .* P<0.05 DoxQ compared to doxorubicin.

3.4.7. Effect of DoxQ on RL-14 Cell Viability

To further confirm the safety of DoxQ, the effects of DoxQ or doxorubicin on human cardiomyocytes was investigated after treatment at 10 μM for 24 h by MTT assay. The results show that cell viability was higher in the group treated with DoxQ (77%) than the group of cells treated with free doxorubicin (52%) indicating that DoxQ prevented the cytotoxicity mediated by doxorubicin by ~25% (Figure 3.11).

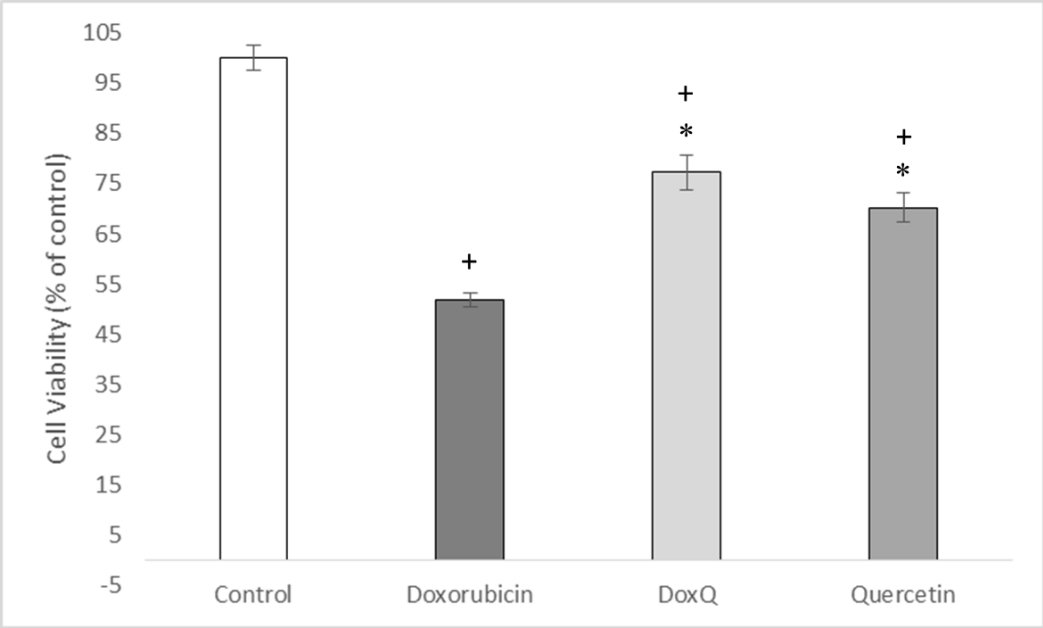

Figure 3.11. Cell viability of human cardiac myocytes (RL-14) measured by MTT assay after drug treatment at 10 μM for 24 hours (n=4, mean±SEM) *P<0.05 compared to doxorubicin, +P<0.05 compared to control.

3.4.8. Effect of DoxQ on Reactive Oxygen Species

To elucidate whether DoxQ may protect cardiomyocytes from the damage caused by doxorubicin via generating ROS, the levels of ROS generated after treatment of RL-14 cells with doxorubicin, DoxQ, or quercetin were measured by DCF assay. The levels of ROS in cells

treated with DoxQ (556%) was lower than cells treated with free doxorubicin (322%) by ~234% (Figure 3.12).

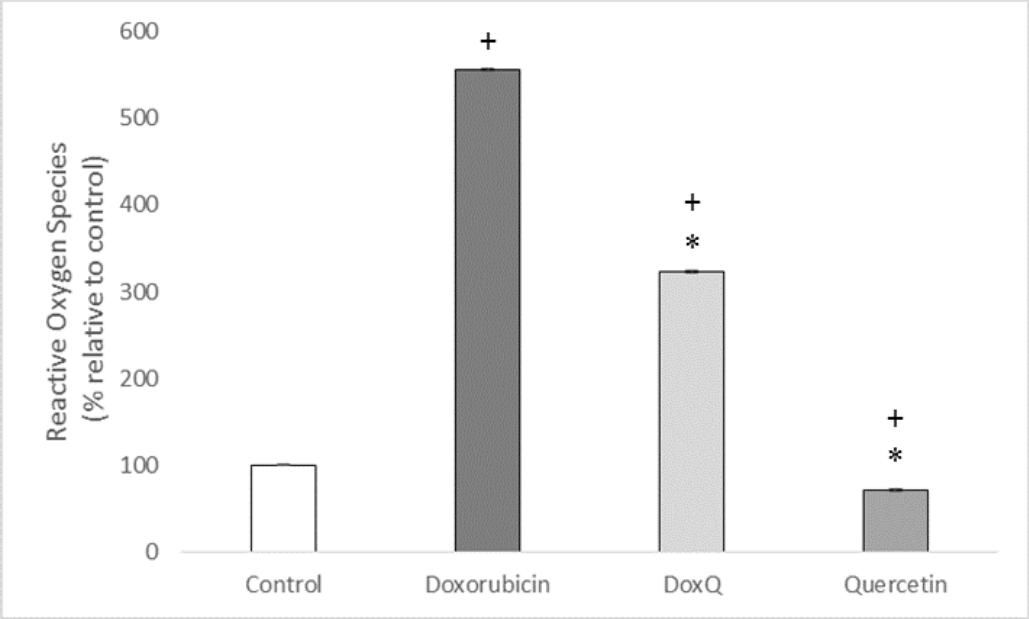

Figure 3.12. Reactive Oxygen Species levels quantified fluorometrically by dichlorofluorescein (DCF) assay after drug treatment of RL-14 cells at 10 μM for 24 hours (n=4, mean±SEM). *P<0.05 compared to doxorubicin, +P<0.05 compared to control.

3.4.9. Effect of DoxQ on Induction of Cellular Cardiotoxicity Markers

To further confirm the protective effects of DoxQ against doxorubicin induced cardiotoxicity, the expression of three cardiac hypertrophy markers α-MHC, β-MHC, and BNP was examined in RL-14 cells after treatment at 10μM for 24 h of test compounds.

DoxQ significantly inhibited the induction of mRNA expression of α-MHC by 1.5-folds, and β-MHC by 2.5-folds, and BNP by 6-folds compared to doxorubicin (Figure 3.13). The expression of all three hypertrophic markers in the group of cells treated with quercetin was similar to control untreated cells, supporting the protective role of quercetin on cardiomyocytes.

A

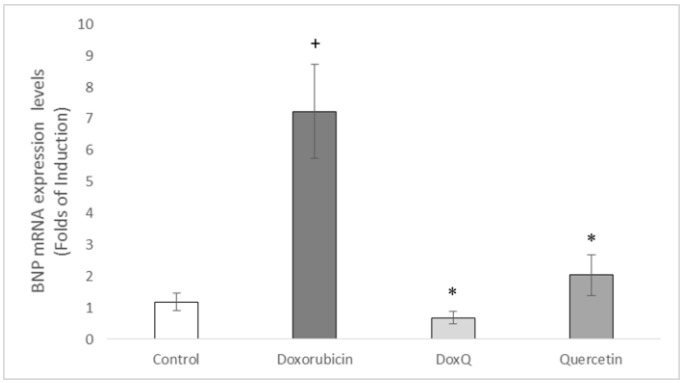

B

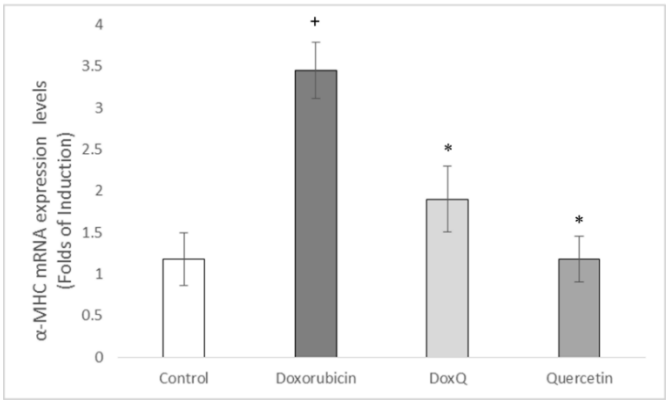

C

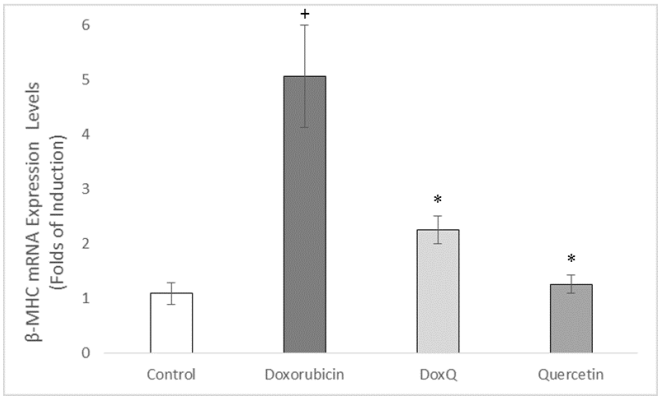

Figure 3.13. Fold expression of cardiac hypertrophy markers in RL-14 cells after treatment at 10μM for 24 h of doxorubicin, DoxQ, or quercetin. The mRNA expression of **(A)** BNP **(B)** α-MHC and **(C)** β-MHC in RL-14 cells. The mRNA expression was quantified by RT-PCR and normalized to β-actin as housekeeping gene (n=6, mean±SEM). *P<0.05 compared to doxorubicin.

3.4.10. Effect of DoxQ on the Induction of Cellular Oxidative Stress Markers

To further confirm the cardioprotective effects of DoxQ and the role of oxidative stress in promoting cardiotoxicity by doxorubicin, the expression of oxidative stress markers GST-A1 and HO-1 was investigated in RL-14 cells. DoxQ significantly lowered the mRNA expression of GST-A1 by 1.5 in comparison to doxorubicin (Figure 3.14A). The expression of HO-1 was lower by one fold in cells treated with doxorubicin compared to cells treated with DoxQ (Figure 3.14B)

A

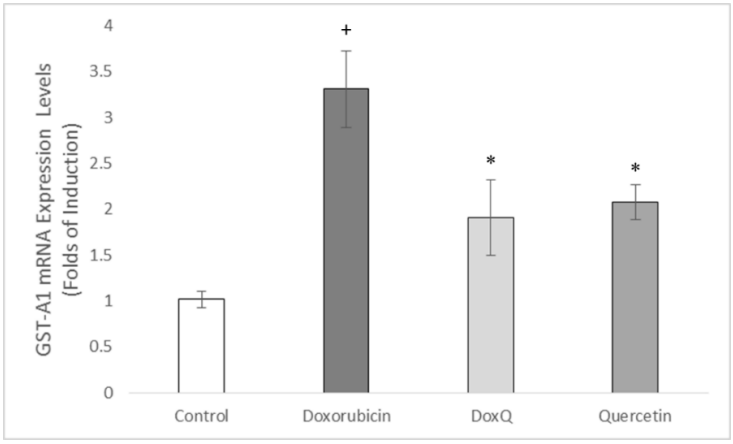

B

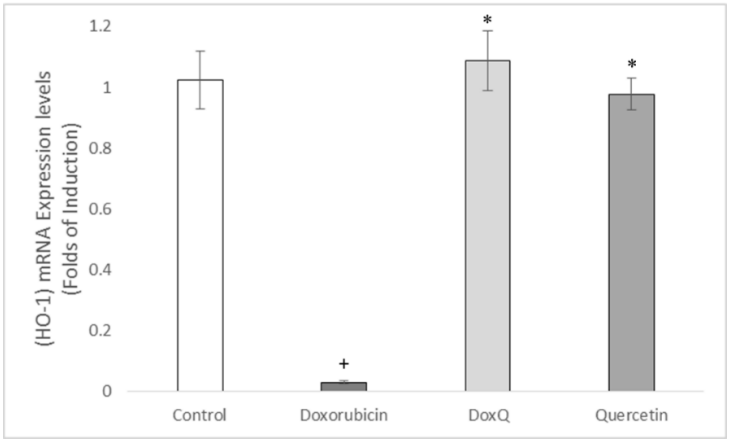

Figure 3.14. Fold expression of oxidative stress markers in RL-14 cells after treatment at 10μM for 24 h of doxorubicin, DoxQ, or quercetin. The mRNA expression of **(A)** GST-A1 and **(B)** HO-1 in RL-14 cells. The mRNA expression was quantified by RT-PCR and normalized to β-actin as housekeeping gene (n=6, mean±SEM). * $P<0.05$ compared to doxorubicin.

3.4.11. Effect of DoxQ on Gene Expression and Catalytic Activity of CYP1B1

To further elucidate the cardioprotective effects of DoxQ, the capacity of DoxQ to alter the induction of CYP1B1 gene by doxorubicin as well as its catalytic activity was investigated in RL-14 cells. Fig 14a demonstrate that DoxQ inhibited the mRNA expression of CYP1B1 by more than 4 folds compared to doxorubicin (Figure 2.15A). The catalytic activity of CYP1B1 was also significantly inhibited by DoxQ compared to doxorubicin alone (Figure 3.15 B & C).

A

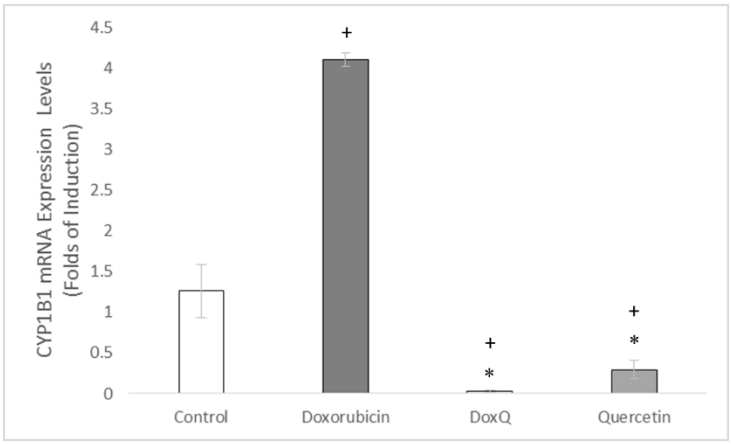

B

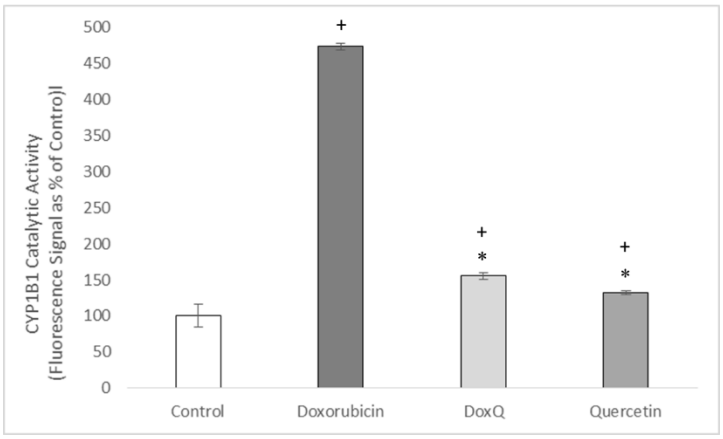

C

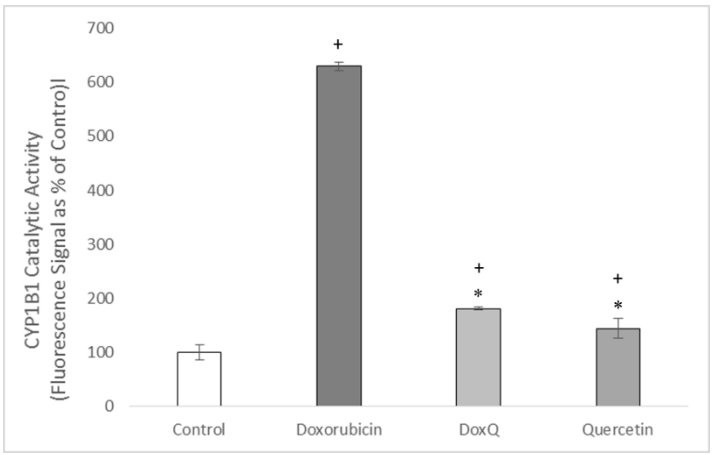

Figure 3.15. (A) The mRNA expression of CYP1B1 quantified by RT-PCR and normalized to β-actin as housekeeping gene (n=6, mean±SEM) **(B)** CYP1B1 catalytic activity determined by MROD assay (n=3, mean±SEM) **(C)** CYP1B1 catalytic activity determined by EROD assay (n=3, mean±SEM) * $P<0.05$ compared to doxorubicin.

3.5. DISCUSSION

Doxorubicin is an effective chemotherapeutic anticancer agent used in in a variety of cancers. However, its use is often limited by dose related cardiotoxicity as the cumulative dose of doxorubicin concentrates in the heart and may progress to severe cardiomyopathy and even death. The cardiotoxicity of doxorubicin is related to the generation of reactive oxygen species such as superoxides and subsequently hydrogen peroxide. In addition, the expression of certain cardiotoxicity markers and metabolic enzymes is altered with doxorubicin therapy and are involved in doxorubicin induced cardiotoxicity.

The currently available pegylated liposomal formulation of doxorubicin Doxil^{TM} preferentially concentrates in the skin resulting in palmar plantar erythrodysesthesia (PPE) syndrome (10, 36). There is another liposomal non-pegylated formulation of doxorubicin called Myocet^{TM} that significantly reduces hand palm syndrome. Both liposomal formulations provide sustained release of doxorubicin, thus minimizing the acute cardiotoxicity caused by high maximum plasma concentration (Cmax) to some extent compared to the doxorubicin hydrochloric salt when administered intravenously.

A doxorubicin-hyaluronic acid conjugate (Dox-HA) has previously shown promise in the treatment of breast cancer and metastatic lymph nodes (37). The Dox-HA was encapsulated in a nanocarrier and administered subcutaneously into the mammary tumors of nude mice. The Dox-HA provided localization in the breast tissue and also provided a sustained release of doxorubicin both contributing to lower systemic toxicities caused by doxorubicin while retaining efficacy.

Consistent with the promising results of a Doxorubicin-HA conjugate (37) we designed a novel derivative of doxorubicin utilizing a flavonoid that is naturally consumed in fruits and

vegetables and reported to have health benefits, P-gp and CYP3A4 inhibitory activities (25) as well as a preferential tendency to intestinal lymphatics absorption (26,38,39). The novel compound (DoxQ) was chemically synthesized by conjugating doxorubicin to a naturally occurring flavonoid quercetin via a peptide linker "glycine" (Figure 3.1) and can be administered orally or intravenously. The release of doxorubicin is accomplished by a simple cleavage of the peptide bond of glycine by proteases followed by the cleavage of the carbamate bond to release quercetin (Figure 3.2).

The purpose of this study is to elucidate the *in vitro* efficacy and safety of DoxQ with a potential to mitigate the poor oral bioavailability and dose related cardiotoxicity of doxorubicin. The possible mechanisms by which DoxQ mitigates these therapeutic limitations are also described. In terms of efficacy, we have shown that both doxorubicin and quercetin are released from the conjugate *in vitro*. The slow *in vitro* release of doxorubicin from the conjugate over more than 4 days (Figure 2.3) may translate to lower peak plasma concentration thus limiting acute cardiotoxicity. Additionally, DoxQ retained its anti-cancer activity in triple negative murine breast cancers with IC_{50} in the micromolar range.

The low oral bioavailability of doxorubicin is due to its limited uptake by intestinal cells expressing P-gp as it is a substrate of P-gp efflux pump and also its extensive first pass metabolism by CYP3A4 (40-42). The cellular uptake of DoxQ as well as a mixture of doxorubicin and quercetin by P-gp positive cells (Figure 3.4 & Figure 3.5) and the inhibitory effects on P-gp ATPase by a mixture of doxorubicin and quercetin (Figure 3.9) suggest that the release of quercetin from DoxQ plays a role in minimizing the P-gp efflux effect of doxorubicin and enhances its uptake by P-gp positive cells. We then investigated the effect of DoxQ on CYP3A4 inhibition, as it is the major metabolic enzyme contributing to first pass effect and also

many compound that inhibit P-gp are inhibitors of CYP3A4. Fig 3.8 shows that DoxQ acts as inhibitor of CYP3A4, which could limit the loss of doxorubicin by first pass metabolism and potentially improve its bioavailability. The overall improvement in the bioavailability of doxorubicin by DoxQ sheds the light on the therapeutic utility of DoxQ as a novel delivery approach for oral administration of doxorubicin and may also lower the required dose of doxorubicin to achieve effective concentrations when administered intravenously.

To assess the safety of DoxQ, the effects of the novel conjugate were initially investigated in isolated adult rat cardiomyocytes. DoxQ showed lower cytotoxicity profile in rat cardiomyocytes at the concentration range tested in comparison to doxorubicin alone (Figure 3.10). The effects of DoxQ were then examined in RL-14 cells, a commercially available cell line isolated from human ventricular tissues, which is commonly used to investigate molecular mechanisms and toxic effects induced by chemotherapeutic agents like doxorubicin (43,44). Before conducting experiments in RL-14 cells, 10 μM concentration was selected based on reported therapeutic plasma concentration of doxorubicin in humans (45,46) as well as other in vitro studies that examined cardiotoxic effects of doxorubicin (47,48). Our study shows that DoxQ was less toxic to RL-14 (Figure 2.11) as evident by MTT assay and consistent with the observation from the trypan blue assay in rat cardiomyocytes. The expression of cardiac hypertrophy markers α-MHC, β-MHC, and BNP were examined in RL-14 cells to further confirm the protective effects of DoxQ on cardiomyocytes. Chronic treatment with doxorubicin causes cardiotoxicity that may progress to cardiac myopathy and heart failure via multiple cellular pathways (49). Mayyah Z et al reported that treatment of RL-14 cells with doxorubicin caused cardiotoxicity manifested by induction in the expression of β-MHC/ α-MHC genes (50). Furthermore, Chen Y-L et al showed that doxorubicin enhanced protein expression of BNP and

β-MHC while reducing the expression of α-MHC in a rat model (49). These observations are supported by our findings in this study as doxorubicin induced the expression of β-MHC more than α-MHC (Figure 3.13) and also induced the expression of BNP. Interestingly, the expression of α-MHC, β-MHC, and BNP was inhibited by DoxQ, confirming the protective effects of DoxQ on cardiomyocytes.

To elucidate cardioprotective mechanisms of DoxQ against doxorubicin induced cardiotoxicity, several *in vitro* assays were utilized. Given the role of reactive oxygen species in doxorubicin induced cardiotoxicity and the antioxidant effects of quercetin, the antioxidant capacity of DoxQ was initially examined using a commercial kit in comparison to doxorubicin alone and a mixture of doxorubicin plus quercetin. Our results show that the antioxidant capacity of DoxQ was higher than doxorubicin in non-cell environment (Figure 3.7). Based on this observation, DCF assay was undertaken to measure the levels of reactive oxygen species in RL-14 cells. The levels of reactive oxygen species generated by DoxQ were lower than doxorubicin alone (Figure 3.13), suggesting that the presence of quercetin likely scavengers reactive oxygen species generated by doxorubicin and limits its toxic effects on cardiomyocytes. This observation is also supported by the effects of DoxQ on the expression of oxidative stress markers GST-A1 and HO-1. The inhibitory effects of DoxQ on the expression of GST-A1 (Figure 3.14A), which is overexpressed when cells are under oxidative stress implies that there lower ROS generated by DoxQ than doxorubicin alone. Additionally, the inhibitory effects on mRNA expression of HO-1 by doxorubicin and not DoxQ further supports the cardioprotective effects of DoxQ as elevated HO-1 levels have protective effects on cardiomyocytes (50). To further investigate mechanisms involved in cardioprotection by DoxQ, the effects of DoxQ on the gene expression and catalytic activity of CYP1B1 were explored in RL-14 cells. CYP1B1 is a member of CYP450 metabolic

enzymes and catalyzes the formation of mid-chain HETEs metabolites of arachidonic acid, which are cardiotoxic (51). CYP1B1 also has a role in modulating cellular oxidative stress (52). A recent study showed that doxorubicin induced cytotoxicity is mediated by CYP1B1 pathway (53). Our results demonstrate that doxorubicin induced the expression of CYP1B1 and its catalytic activity in RL-14 cell, while DoxQ reversed these effects (Figure 3.15) suggesting that DoxQ attenuates doxorubicin induced cardiotoxicity at least partially by CYP1B1 inhibitory activities.

3.6. CONCLUSIONS

In conclusion we developed a novel derivative of doxorubicin with improved in vitro safety while retaining activity. DoxQ was less toxic than doxorubicin in both rat and human cardiomyocytes and retained anti-cancer activity in triple negative murine cancer cells. The lower level of reactive oxygen species generated by DoxQ compared to doxorubicin as well as the results of the oxidative stress markers examined also suggests cardioprotection *in vitro*. DoxQ inhibited both the expression of CYP1B1 and also its catalytic activity proposing an additional mechanism by which DoxQ attenuates cardiotoxicity induced by doxorubicin and improves its tolerability.

In terms of mitigating the drug delivery barriers of poor oral bioavailability, the initial *in vitro* results of DoxQ are promising. The cellular uptake of DoxQ by MDCK-MDR cells was higher than doxorubicin alone or doxorubicin plus quercetin mixture. The CYP450 inhibitory activities of DoxQ were higher than doxorubicin. DoxQ inhibited CYP3A4 while a mixture of doxorubicin plus quercetin demonstrated higher inhibition of P-gp ATPase activity compared to DoxQ and free doxorubicin. If DoxQ is less susceptible to first pass effect (F=1-E) and the

release of quercetin from DoxQ lowers the P-gp efflux effect, then oral absorption of doxorubicin and the possibility that DoxQ is shunted to intestinal lymphatics could potentially increase when E is lowered. To the best of our knowledge, this is the first study that utilizes quercetin as a lymphatically targeted carrier for doxorubicin to improve its bioavailability and safety and mechanistically elucidate efficacy and safety of the novel conjugate DoxQ. Future *in vivo* experiments in light of the *in vitro* observations using this novel drug delivery approach are warranted and are in progress by our laboratory.

3.7. REFERENCES

1. Thorn CF, Oshiro C, Marsh S, Hernandez-Boussard T, McLeod H, Klein TE, Altman RB. Doxorubicin pathways: pharmacodynamics and adverse effects. Pharmacogenet Genomics. 2011;21(7):440-6.
2. Swift LP, Rephaeli A, Nudelman A, Phillips DR, Cutts SM. Doxorubicin-DNA adducts induce a non-topoisomerase II-mediated form of cell death. Cancer Res. 2006;66(9):4863-71.
3. Agudelo D, Bourassa P, Bérubé G, Tajmir-Riahi HA. Intercalation of antitumor drug doxorubicin and its analogue by DNA duplex: structural features and biological implications. Int J Biol Macromol. 2014;66:144-50.
4. Carvalho FS, Burgeiro A, Garcia R, Moreno AJ, Carvalho RA, Oliveira PJ. Doxorubicin-induced cardiotoxicity: from bioenergetic failure and cell death to cardiomyopathy. Med Res Rev. 2014;34(1):106-35.
5. Gustafson DL, Merz AL, and Long ME. Pharmacokinetics of combined doxorubicin and paclitaxel in mice. Cancer Lett. 2005;220:161-9.

6. Lee HJ, Lee MG. Effects of dexamethasone on the pharmacokinetics of adriamycin after intravenous administration to rats. Res. Commun. Mol. Pathol. Pharmacol. 1999;105: 87-96.
7. Matsumura Y, Hamaguchi T, Ura T, Muro K, Yamada Y, Shimada Y, Shirao K, Okusaka T, Ueno H, Ikeda M, Watanabe N. Phase I clinical trial and pharmacokinetic evaluation of NK911, a micelle-encapsulated doxorubicin. Br J Cancer. 2004; 91(10):1775-81.
8. Ríhová B, Strohalm J, Prausová J, Kubácková K, Jelínková M, Rozprimová L, Sírová M, Plocová D, Etrych T, Subr V, Mrkvan T, Kovár M, Ulbrich K. Cytostatic and immunomobilizing activities of polymer-bound drugs: experimental and first clinical data. J Control Release. 2003;91(1-2):1-16.
9. Tolcher AW, Sugarman S, Gelmon KA, Cohen R, Saleh M, Isaacs C, Young L, Healey D, Onetto N, Slichenmyer W. Randomized phase II study of BR96-doxorubicin conjugate in patients with metastatic breast cancer. J Clin Oncol. 1999;17(2):478-84.
10. Soloman R, Gabizon AA. Clinical pharmacology of liposomal anthracyclines: focus on pegylated liposomal Doxorubicin. Clin Lymphoma Myeloma. 2008;8(1):21–32.
11. Davies NM, Yanez JA. Flavonoid Pharmacokinetics: Methods of Analysis, Preclinical and Clinical Pharmacokinetics, Safety, and Toxicology. 1st Ed. John Wiley and Sons; 2013.
12. Liu L, Gao C, Yao P, and Gong Z. Quercetin Alleviates High-Fat Diet-Induced Oxidized Low-Density Lipoprotein Accumulation in the Liver: Implication for Autophagy Regulation. BioMed Research International. 2015; 2015:607531.
13. He Y, Cao X, Liu X , Li X, Xu Y, Liu J, Shi J. Quercetin reverses experimental pulmonary arterial hypertension by modulating the TrkA pathway. Experimental Cell Research. 2015; 339(1) :122–34.

14. Gormaz JG, Quintremil S, Rodrigo R. Cardiovascular Disease: A Target for the Pharmacological Effects of Quercetin. Curr Top Med Chem. 2015;15(17):1735-42.
15. Chirumbolo S. The role of quercetin, flavonols and flavones in modulating inflammatory cell function. Inflamm Allergy Drug Targets. 2010;9(4):263-85.
16. Wang G, Wang J, Luo J, Wang L, Chen X, Zhang L, Jiang S. PEG2000-DPSE-coated quercetin nanoparticles remarkably enhanced anticancer effects through induced programed cell death on C6 glioma cells. J Biomed Mater Res A. 2013;101(11):3076-85.
17. Jiang P, Burczynski F, Campbell C, Pierce G, Austria J.A., Briggs CJ, Rutin and flavonoid contents in three buckwheat species Fagopyrum esculentum, F. tartaricum, and F. homotropicum and their protective effects against lipid peroxidation. Food Res. Int., 2007; 40:356–64.
18. Kang JT, Moon JH, Choi JY, Park SJ, Kim SJ, Saadeldin IM, Lee BC. Effect of Antioxidant Flavonoids (Quercetin and Taxifolin) on In vitro Maturation of Porcine Oocytes.Asian-Australas J Anim Sci. 2016;29(3):352-8.
19. Atashpour S, Fouladdel S, Movahhed TK, Barzegar E, Ghahremani MH, Ostad SN, Azizi E. Quercetin induces cell cycle arrest and apoptosis in CD133(+) cancer stem cells of human colorectal HT29 cancer cell line and enhances anticancer effects of doxorubicin. Iran J Basic Med Sci. 2015;18(7):635-43.
20. Minaei A, Sabzichi M, Ramezani F, Hamishehkar H, Samadi N. Co-delivery with nano-quercetin enhances doxorubicin-mediated cytotoxicity against MCF-7 cells. Mol Biol Rep. 2016;43(2):99-105.
21. Wang G, Zhang J, Liu L, Sharma S, Dong Q. Quercetin potentiates doxorubicin mediated antitumor effects against liver cancer through p53/Bcl-xl. PLoS One. 2012;7(12):e51764.

22. Chen FY, Cao LF, Wan HX, Zhang MY, Cai JY, Shen LJ, Zhong JH, Zhong H. Quercetin enhances adriamycin cytotoxicity through induction of apoptosis and regulation of mitogen-activated protein kinase/extracellular signal-regulated kinase/c-Jun N-terminal kinase signaling in multidrug-resistant leukemia K562 cells. Mol Med Rep. 2015;11(1):341-8.
23. Chen JY, Hu RY, Chou HC. Quercetin-induced cardioprotection against doxorubicin cytotoxicity. J Biomed Sci. 2013;20;20:95.
24. Kaiserová H, Simůnek T, Van der Vijgh WJ, Bast A, Kvasnicková E. Flavonoids as protectors against doxorubicin cardiotoxicity: role of iron chelation, antioxidant activity and inhibition of carbonyl reductase. Biochim Biophys Acta. 2007;1772(9):1065-74.
25. Choi JS, Piao YJ, Kang KW. Effects of quercetin on the bioavailability of doxorubicin in rats: role of CYP3A4 and P-gp inhibition by quercetin. Arch Pharm Res. 2011;34(4):607-13.
26. Chen IL, Tsai YJ, Huang CM, Tsai TH. Lymphatic absorption of quercetin and rutin in rat and their pharmacokinetics in systemic plasma.J Agric Food Chem. 2010;13:58(1):546-51.
27. Kim MK, Park KS,Yeo WS, Choo H, Chong Y. In vitro solubility, stability and permeability of novel quercetin-amino acid conjugates. Bioorganic & medicinal chemistry.2009; 17:1164-71.
28. Liu Y, Schubert D. Cytotoxic amyloid peptides inhibit cellular 3-(4,5-dimethylthiazol-2-yl)-2,5-diphenyltetrazolium bromide (MTT) reduction by enhancing MTT formazan exocytosis. J Neurochem. 1997;69(6):2285-93.
29. Maayah ZH, El Gendy MA, El-Kadi AO, Korashy HM. Sunitinib, a tyrosine kinase inhibitor, induces cytochrome P450 1A1 gene in human breast cancer MCF7 cells through ligand-independent aryl hydrocarbon receptor activation. Arch Toxicol. 2013;87(5):847-56.

30. Zordoky BN, Aboutabl ME, El-Kadi AO. Modulation of cytochrome P450 gene expression and arachidonic acid metabolism during isoproterenol-induced cardiac hypertrophy in rats. Drug Metab Dispos. 2008;36(11):2277-86.
31. Maayah ZH, Ansari MA, El Gendy MA, Al-Arifi MN, Korashy HM. Development of cardiac hypertrophy by sunitinib in vivo and in vitro rat cardiomyocytes is influenced by the aryl hydrocarbon receptor signaling pathway. Arch Toxicol. 2014;88(3):725-38.
32. Livak KJ, Schmittgen TD. Analysis of relative gene expression data using real-time quantitative PCR and the 2(-Delta Delta C(T)) Method. Methods. 2001;25(4):402-8.
33. Kennedy SW, Lorenzen A, James CA, Collins BT. Ethoxyresorufin-O-deethylase and porphyrin analysis in chicken embryo hepatocyte cultures with a fluorescence multiwell plate reader. Anal Biochem. 1993;211(1):102-12.
34. Lo SN, Chang YP, Tsai KC, Chang CY, Wu TS, Ueng YF.Inhibition of CYP1 by berberine, palmatine, and jatrorrhizine: selectivity, kinetic characterization, and molecular modeling. Toxicol Appl Pharmacol. 2013;272(3):671-80.
35. Pham A, Bortolazzo A, White JB. Rapid dimerization of quercetin through an oxidative mechanism in the presence of serum albumin decreases its ability to induce cytotoxicity in MDA-MB-231 cells. Biochem Biophys Res Commun. 2012;427(2):415-20.
36. Lorusso D, Stefano AD, Carone V, Fagotti A, Pisconti S, Scambia G. Pegylated liposomal doxorubicin-related palmar-plantar erythrodysesthesia (‘hand-foot’ syndrome). Ann Oncol 2007;18(7):1159–1164.
37. Cai S, Thati S, Bagby TR, Diab HM, Davies NM, Cohen MS, Forrest ML. J Control Release.

38. Localized doxorubicin chemotherapy with a biopolymeric nanocarrier improves survival and reduces toxicity in xenografts of human breast cancer. 2010;146(2):212-8.
39. Murota K, Terao J. Quercetin appears in the lymph of unanesthetized rats as its phase II metabolites after administered into the stomach. FEBS Lett. 2005;579(24):5343-6.
40. Murota K, Cermak R, Terao J, Wolffram S.Influence of fatty acid patterns on the intestinal absorption pathway of quercetin in thoracic lymph duct-cannulated rats. Br J Nutr. 2013;109(12):2147-53.
41. Chan LM, Lowes S, Hirst BH. The ABCs of drug transport in intestine and liver: efflux proteins limiting drug absorption and bioavailability. Eur J Pharm Sci. 2004;21(1):25-51.
42. Qian F, Wei D, Liu J, Yang S. Molecular model and ATPase activity of carboxyl-terminal nucleotide binding domain from human P-glycoprotein. Biochemistry (Mosc). 2006;71 Suppl 1:S18-24, 1-2.
43. Kim JE, Cho HJ, Kim JS, Shim CK, S.J. Chung, Oak MH, Yoon IS, Kim DD. The limited intestinal absorption via paracellular pathway is responsible for the low oral bioavailability of doxorubicin. Xenobiotica; the fate of foreign compounds in biological systems. 2013; 43:579-591.
44. Maayah ZH, Elshenawy OH, Althurwi HN, Abdelhamid G, El-Kadi AO. Human fetal ventricular cardiomyocyte, RL-14 cell line, is a promising model to study drug metabolizing enzymes and their associated arachidonic acid metabolites. J Pharmacol Toxicol Methods. 2015;71:33-41.
45. Kobashigawa LC, Xu YC, Padbury JF, Tseng YT, Yano N.Metformin protects cardiomyocyte from doxorubicin induced cytotoxicity through an AMP-activated protein kinase dependent signaling pathway: an in vitro study. PLoS One. 2014;9(8):e104888.

46. Mross K, Maessen P, van der Vijgh WJ, Gall H, Boven E, Pinedo HM. Pharmacokinetics and metabolism of epidoxorubicin and doxorubicin in humans. J Clin Oncol. 1988 ;6(3):517-26.
47. Robert J, Vrignaud P, Nguyen-Ngoc T, Iliadis A, Mauriac L, Hurteloup P.Comparative pharmacokinetics and metabolism of doxorubicin and epirubicin in patients with metastatic breast cancer. Cancer Treat Rep. 1985;69(6):633-40.
48. McHowat J, Swift LM, Arutunyan A, Sarvazyan N. Clinical concentrations of doxorubicin inhibit activity of myocardial membrane-associated, calcium-independent phospholipase A(2). Cancer Res. 2001;61(10):4024-9.
49. Doroshow JH, Akman S, Chu FF, Esworthy S. Role of the glutathione-glutathione peroxidase cycle in the cytotoxicity of the anticancer quinones. Pharmacol Ther. 1990;47(3):359-70.
50. Chen YL, Chung SY, Chai HT, Chen CH, Liu CF, Chen YL, Huang TH, Zhen YY, Sung PH, Sun CK, Chua S, Lu HI, Lee FY, Sheu JJ, Yip HK. Early Administration of Carvedilol Protected against Doxorubicin-Induced Cardiomyopathy. J Pharmacol Exp Ther. 2015;355(3):516-27.
51. Yossi Issan, Ran Kornowski, Dan Aravot, Asher Shainberg, Michal Laniado-Schwartzman, Komal Sodhi, Nader G. Abraham, Edith Hochhauser. Heme Oxygenase-1 Induction Improves Cardiac Function following Myocardial Ischemia by Reducing Oxidative Stress. PLoS One. 2014; 9(3): e92246.
52. Maayah ZH, El-Kadi AO. The role of mid-chain hydroxyeicosatetraenoic acids in the pathogenesis of hypertension and cardiac hypertrophy. Arch Toxicol. 2016;90(1):119-36.
53. Yixin Tang, Elizabeth A. Scheef, Shoujian Wang, Christine M. Sorenson, Craig B. Marcus, Colin R. Jefcoate, and Nader Sheibani. CYP1B1 expression promotes the

proangiogenic phenotype of endothelium through decreased intracellular oxidative stress and thrombospondin-2 expression. Blood. 2009. 15; 113(3): 744–54.

54. Maayah ZH, Althurwi HN, Abdelhamid G, Lesyk G, Jurasz P, El-Kadi AO. CYP1B1 inhibition attenuates doxorubicin-induced cardiotoxicity through a mid-chain HETEs-dependent mechanism. Pharmacol Res. 2016;105:28-43.

CHAPTER 4

PHARMACOKINETIC AND TOXICOKINETIC CHARACTERIZATION OF A NOVEL DOXORUBICIN DERIVATIVE

A Version of this chapter has been published:

Alrushaid S, Sayre CL, Yáñez JA, Forrest ML, Senadheera SN, Burczynski FJ, Löbenberg R, Davies NM. Pharmacokinetic and Toxicodynamic Characterization of a Novel Doxorubicin Derivative. Pharmaceutics. 2017;9(3):35.

4.1. ABSTRACT

Doxorubicin (Dox) is an effective anti-cancer medication with poor oral bioavailability and systemic toxicities. DoxQ was developed by conjugating Dox to the lymphatically absorbed antioxidant quercetin to improve Dox's bioavailability and tolerability. The purpose of this study was to characterize the pharmacokinetics and safety of Dox after intravenous (IV) and oral (PO) administration of DoxQ or Dox (10 mg/kg) and investigate the intestinal lymphatic delivery of Dox after PO DoxQ administration in male Sprague–Dawley rats. Drug concentrations in serum, urine, and lymph were quantified by HPLC with fluorescence detection. DoxQ intact IV showed a 5-fold increase in the area under the curve (AUC)—18.6 ± 1.98 compared to 3.97 ± 0.71 μg * h/mL after Dox—and a significant reduction in the volume of distribution (V_{ss}): 0.138 ± 0.015 versus 6.35 ± 1.06 L/kg. The fraction excreted unchanged in urine (f_e) of IV DoxQ and Dox was ~5% and ~11%, respectively. Cumulative amounts of Dox in the mesenteric lymph fluid after oral DoxQ were twice as high as Dox in a mesenteric lymph duct cannulation rat model. Oral DoxQ increased AUC of Dox by ~1.5-fold compared to after oral Dox. Concentrations of β-N-Acetylglucosaminidase (NAG) but not cardiac troponin (cTnI) were lower after IV DoxQ than Dox. DoxQ altered the pharmacokinetic disposition of Dox, improved its renal safety and oral bioavailability, and is in part transported through intestinal lymphatics.

4.2. INTRODUCTION

Doxorubicin (Dox) is an effective anti-cancer medication that has been clinically used to treat a variety of cancers including breast, ovarian, and lymphoma (1–5). Despite the clinical effectiveness of Dox, its use is limited by off-target adverse effects, particularly dose-related cardiotoxicity and renal toxicity, which involve free radical formation and tissue damage. Dox formulations that are pegylated and in liposomes are utilized in medications, including Doxil™ and Caelyx™ (6). Pegylated (polyethylene glycol coated) liposome-encapsulated forms of Dox result in an increased concentration of Dox in the skin and a side effect called palmar plantar erythrodysesthesia or hand–foot syndrome (7). Non-pegylated liposomal Dox called Myocet™ does not have a polyethylene glycol coating, and therefore does not result in the same rate of hand–foot syndrome. This liposomal encapsulation of Dox limits but does not eliminate the cardiotoxic effects of the drug. This damage is caused by the generation of reactive oxidative species (ROS) such as superoxide and hydrogen peroxide upon the reduction of Dox to form electron-deficient semiquinone (8). Various additional drug delivery approaches have been undertaken to overcome the toxicity limitations of Dox, such as utilization of micelles (9), synthetic polymer conjugates (10), and antibody targeted carriers (11), with varied degrees of success. We have previously demonstrated that hyaluronan, a biopolymeric nanocarrier, improves survival and reduces the toxicity of Dox in xenografts of human breast cancer through the localization of Dox into the lymphatics (8).

Dox is a substrate of both the P–glycoprotein (P–gp) efflux pump (12) and cytochrome P450 metabolic enzymes (13), both of which contribute to its overall disposition, poor oral absorption, and low oral bioavailability. For this reason, Dox is only currently available as a parenteral treatment administered intravenously. We have previously reported the synthesis of a Dox-

quercetin derivative designed to overcome P–gp efflux and CYP inhibition (14) as quercetin is a natural flavonoid that exhibits inhibitory effects on CYP3A4 and P–gp (15) and an antioxidant that scavenges free radicals. Our in vitro investigation of DoxQ (14) revealed that both Dox and quercetin are released from the conjugate over time. Furthermore, DoxQ inhibited CYP3A4, a major metabolic enzyme involved in the first pass effect, and demonstrated higher cellular uptake by P–gp-positive (MDCK–MDR) cells compared to free Dox. The inhibitory effects of DoxQ on CYP3A4 and P–gp may improve the oral absorption and bioavailability of Dox in vivo. Additionally, DoxQ retained anti-cancer activity in a triple negative murine breast cancer cell line and was less toxic to both rat and human cardiomyocytes. The cardioprotective mechanism of DoxQ involved scavenging ROS, suppression of oxidative stress, and cardiac hypertrophy markers, and also inhibitory effects on CYP1B1, all of which contribute to Dox's induced cardiotoxicity. Taken together, the *in vitro* results of DoxQ showed promise at mitigating the cardiotoxicity of Dox and may also mitigate its poor oral bioavailability in vivo by inhibiting CYP3A4 and P–gp (14). The antioxidant effects of DoxQ may also mitigate the renal toxicity induced by Dox and improve its overall tolerability *in vivo*.

In addition to quercetin's antioxidant activity and inhibitory effects on CYP3A4 and P–gp, it is naturally absorbed into intestinal lymphatics after gastric or intraduodenal administration (16–18); this property may be utilized as a novel strategy to deliver Dox into lymphatics. Following oral administration, molecules and drugs are either absorbed from the intestinal mucosa into the blood stream via the hepatic portal vein or into lymphatics via the intestinal lymphatic pathway. Most small molecules and drugs administered orally enter systemic circulation via blood capillaries and become subject to hepatic metabolism before entering the vasculature. In contrast, highly lipophilic molecules and macromolecules such as proteins associate with chylomicrons in

the intestinal mucosa and enter systemic circulation via the intestinal lymphatics pathway (19). These lipophilic molecules and macromolecules are absorbed via lymphatic capillaries, which collect into the mesenteric lymph duct, followed by the thoracic lymph duct, and then drain into systemic circulation at the junction of the left subclavian and left jugular veins (19,20). Therefore, molecules that are absorbed via the intestinal lymphatic pathway enter systemic circulation without passing through the liver. This alternative absorptive pathway may be of particular importance in drug delivery and may serve as a novel drug delivery approach to minimize the first-pass effect while increasing lymphatic exposure and ultimately improving overall systemic drug exposure (21). Lipophilic drugs with LogP > 5 and solubility of >50 mg per g in long-chain triglyceride will likely have preferential absorption towards lymphatics owing to their ability to incorporate with intestinal lipoproteins (19). If the drug of interest does not meet these criteria, it is also possible to alter the physicochemical properties of a small drug molecule by chemically modifying its lipophilicity, utilizing a lipid-based drug delivery system or designing a lipophilic prodrug where the parent drug is chemically conjugated to a lipophilic moiety via a linker that can be easily cleaved *in vivo* (19–22). In this study, we utilized a novel Dox–quercetin conjugate where quercetin is designed to act as a lymphatically targeted carrier and may facilitate the intestinal transport of Dox into systemic circulation after oral administration and may also affect its disposition as well as overall systemic exposure after intravenous administration.

In the light of the studies discussed above and our promising DoxQ observations in vitro, this study was conducted to investigate the feasibility of utilizing the antioxidant quercetin as a lymphatically targeted carrier for Dox with the potential to improve its disposition, oral bioavailability, and tolerability *in vivo*. We hypothesize that the presence of quercetin in DoxQ,

intact or when released from the conjugate, will act as a carrier to transport Dox into lymphatics, at least partially, thus bypassing systemic circulation and increasing the overall bioavailability of Dox. The release of quercetin from DoxQ will likely have a beneficial effect and limit the cardiotoxic and renal side effects of doxorubicin. In addition, the synthesis and change in physicochemical properties of DoxQ may alter its pharmacokinetics and metabolism; the release of quercetin from DoxQ or DoxQ intact may also have effects on CYP3A4 and P–gp, which could further augment the disposition and bioavailability of Dox *in vivo*. Here, the acute *in vivo* disposition, safety, and lymphatic uptake of DoxQ are characterized for the first time. The pharmacokinetics, toxicodynamics, and intestinal lymphatic absorption of DoxQ in comparison to free Dox are examined in a rat model. Our results demonstrate that DoxQ improves the disposition of Dox and its oral bioavailability and safety, and is partially transported via lymphatics.

4.3. METHODS AND MATERIALS

4.3.1. Chemicals and Reagents

Doxorubicin, daunorubicin, cycloheximide, PEG-400, and DMSO were purchased from Sigma (St. Louis, MO, USA). Analytical grade formic acid and HPLC grade acetonitrile were purchased from Fisher Scientific (Ottawa, ON, Canada). Ultrapure water from a Milli-Q® system (Millipore, Billerica, MA, USA) was used for the mobile phase. HPLC columns, vials, inserts, and 0.2 μm nylon filter membranes were purchased from Phenomenex® (Torrance, CA, USA). Silastic® laboratory tubing was purchased from the Dow Corning Corporation (Midland, MI, USA). Intramedic® polyethylene tubing was purchased from Becton Dickinson Primary Care Diagnostics, Becton Dickinson and Company (Sparks, MD, USA). Monoject® 23 gauge (0.6 mm

× 25 mm) polypropylene hub hypodermic needles were purchased from Sherwood Medical (St. Louis, MO, USA). Synthetic absorbable surgical sutures were purchased from Wilburn Medical US (Kernesville, NC, USA). Sterile heparin/50% dextrose catheter lock solution and blunt needles were obtained from SAI Infusion Technologies, Strategic Applications (Lake Villa, IL, USA).

4.3.2. Synthesis of the DoxQ Conjugate

DoxQ was synthesized by conjugating Dox to quercetin via a glycine linker, as previously described (14).

4.3.3. Physicochemical Properties

LogP and LogS values of DoxQ were predicted using an online computer software (VCCLAB, Virtual Computational Chemistry Laboratory) (23,24). pKa, logP, logD at pH 7.4, intrinsic solubility, and solubility at pH 7.4 were calculated using MarvinSketch v. 17.2.20.0 (ChemAxon Ltd., Cambridge, MA, USA), pKa and logP were calculated using GastroPlus v. 9.0.0007 (Simulations Plus, Inc., Lancaster, CA, USA). Portions of these results were generated by GastroPlus™ software (Version 8.0) provided by Simulations Plus, Inc. (Lancaster, CA, USA). The melting point of DoxQ was experimentally determined by MEL-TEMPII melting point apparatus from Laboratory Devices (Holliston, MA, USA).

4.3.4. Analytical System and Conditions

The analytical method described in (25) was adapted with some modifications. The HPLC system used was a Shimadzu LC-2010A (Kyoto, Japan) with Fluorescence RF-535 detector at

470/560 nm (excitation/emission) wavelengths. Separation was achieved using C18 Phenomenex Kintex® column (250 μm, 250 × 4.6 mm) for serum and lymph samples or (2.6 μm, 100 × 4.60 mm) joined to (250 μm, 250 × 4.6 mm) for urine samples. The mobile phase was prepared by mixing acetonitrile with 0.1% formic acid in water (35:65, *v*/*v*), which was filtered through 0.2 μm nylon filter and degassed under reduced pressure prior to use. The separation was carried out isocratically at ambient temperature (22 ± 1 °C) with a flow rate of 0.6 mL/min. Shimadzu EZStart (Version 7.4) software was used for data collection and integration. On the day of the analysis, samples were prepared and injected into the HPLC system.

4.3.5. Preparation of Standard Solutions

Stock solutions of Dox (1 mg/mL) and the internal standard (IS) daunorubicin (1 mg/mL) were prepared in methanol, protected from light and stored at −20 °C between uses for no longer than one week. Using the stock solutions of Dox, calibration standards in serum, urine, and lymph were freshly prepared by sequential dilution with blank rat serum, urine, and lymph. A series of concentrations were obtained, particularly 0.1, 0.5, 1.0, 10.0 and 100 μg/mL.

Stock solutions of intact DoxQ (10 mg/mL) were freshly prepared in DMSO and protected from light. Calibration standards of DoxQ in serum and urine were prepared by serial dilution with blank rat serum or urine to yield concentrations of 1, 10, 20, and 100 μg/mL. The final concentration of DMSO in serum and urine spiked standards did not exceed 1%.

4.3.6. Calibration Curves

Calibration curves of Dox and DoxQ were obtained by plotting the peak area ratio of Dox or DoxQ to the internal standard (daunorubicin) versus calibration standards concentration of Dox or DoxQ through the unweighted least squares linear regression.

4.3.7. Animals and Surgical Procedures

Male Sprague–Dawley rats (250–300 g) were obtained from Charles River Labs (Montreal, QC, Canada) and given food (Purina Rat Chow 5001) and water ad libitum in the animal facility for at least three days before use. Rats were housed in temperature-controlled rooms with a 12 h light/dark cycle. The animal ethics protocol was revised and approved by the Bannatyne Campus Animal Care Committee at the University of Manitoba, (protocol #16-004, approved 29 March 2016).

4.3.8. Pharmacokinetic Study

Eight surgically modified, with exposed jugular vein catheterization (polyurethane–silastic blended catheter), adult male Sprague–Dawley rats (average weight: 250 g) were purchased from Charles River Laboratories (Saint-Constant, QC, Canada). The cannula was flushed daily with a sterile heparin/50% dextrose catheter lock solution to maintain the patency of the cannula, as advised in the technical sheet supplied with the animals from Charles River. Each animal was placed in a separate metabolic cage overnight and fasted for 12 h before dosing. On the day of experiment, the animals were dosed either intravenously or orally with Dox (10 mg/kg) or equimolar DoxQ (n = 4 for each treatment group). Both Dox and DoxQ were freshly reconstituted in 3% DMSO and 97% PEG-400 prior to dosing. Animals received water ad

libitum pre- and post-dosing, and food (Purina Rat Chow 5001) was provided 2 h post-dosing. Doses were selected based on previous use in similar pharmacokinetic studies (13,15) and sensitivity of analytical instrumentation. Serial blood samples (0.30 mL) were collected at 0, 1 min, 15 min, and 30 min, then 1, 2, 4, 6, 12, 24, 48 and 72 h after IV administration. The same blood collection time points were applied following oral administration except for 1 min. At 72 h after administration, the animals were euthanized and exsanguinated. Immediately after all the blood collection time points (except the terminal point); the cannula was flushed with the same volume of 0.9% saline to replenish the collected blood volume. The dead volume of the cannula was filled with a small volume (~0.15 mL) of heparinized lock solution after each blood draw to maintain the patency of the cannula. The samples were collected into regular polypropylene microcentrifuge tubes, centrifuged at 15,000 rpm for 5 min (Beckman Microfuge centrifuge, Beckman Coulter Inc., Fullerton, CA, USA), and the serum collected and stored at −20 °C until further sample preparation for HPLC analysis. Urine samples were also collected at 0, 2, 6, 12, 24, 48 and 72 h following Dox or DoxQ administration. The exact urine volume of each sample was recorded then stored at −20 °C until further sample preparation for HPLC analysis.

4.3.9. Intestinal Lymphatic Drug Delivery

The intestinal transport of DoxQ via lymphatics was examined in vivo by two methods. In the first method, mesenteric lymph cannulated rat model was used to directly measure the concentrations of Dox in the lymph after administration of DoxQ or Dox. In the second method cycloheximide, a chylomicron blocking drug, was administered intraperitoneally prior to oral administration of DoxQ or Dox then concentrations of Dox were measured in serum to indirectly assess lymphatic transport.

For the mesenteric lymph cannulation surgery, six male Sprague–Dawley rats (~300 g) were obtained from Charles River Labs (Montreal, QC, Canada) and given food (Purina Rat Chow 5001) and water ad libitum in the animal facility for at least three days before use. On the day of surgical operation, rats were anesthetized by isoflurane and the abdominal hair was shaved. Rats were maintained under inhaled anesthesia on a warm surgical table. A ~2.5 cm abdominal midline skin incision was made and extended through the musculature using blunt dissection beginning the incision at a point just above the xyphoid cartilage and proceeding distally. The intestine and liver were retracted using surgical retractors to locate the superior mesenteric lymph duct, which is filled with opaque white chyle. The lymph duct was isolated from the surrounding connective tissue and a small incision was made with a bent 23 G needle in the ventral wall of the lymph. A catheter was inserted through the incision and secured by placing a small cellulose patch with a drop of Vetbond^{TM} over the point of insertion into the lymph duct. When a gradual and continuous flow of lymph was observed, an initial lymph sample was collected into a normal microtube. A single dose (10 mg/kg) of DoxQ (n = 3) or Dox (n = 3) was administered by oral gavage while the rat was under anesthesia. Thereafter, lymph samples were collected over one hour after dosing. The animals were euthanized after the last lymph sample collection.

For the determination of intestinal lymphatic transport by lymph blockage method, cycloheximide (3 mg/kg) was administered intraperitoneally (IP) to jugular vein cannulated male Sprague-Dawley rats (~250 g) (n = 4) 1.5 h prior to oral administration of DoxQ to block the formation of chylomicrons in lymph (26–35). DoxQ was then administered orally (10 mg/kg). Blood samples were collected at 0 h, 15 min, 30 min, 1 h, 2 h, 6 h, 12 h, 24 h and 48 h. The animals were euthanized after the last blood sample collection.

4.3.10. Treatment of Serum and Lymph Samples For Analysis

To a 100 μL serum or lymph sample (except 0 h), 10 μM of the internal standard (daunorubicin) was added then vortexed for 30 s (Vortex Genie–2, VWR Scientific, West Chester, PA, USA). One milliliter of cold HPLC grade acetonitrile (pre-stored at −20 °C) was added to the precipitate proteins, vortexed for 2 min (Vortex Genie–2, VWR Scientific, West Chester, PA, USA), and centrifuged at 15,000 rpm for 5 min; the supernatant was transferred to new, labeled 2 mL centrifuge tubes. The samples were evaporated to dryness using a Savant SPD1010 SpeedVac Concentrator (Thermo Fisher Scientific, Inc., Asheville, NC, USA). The residue was reconstituted with 100 μL of mobile phase, vortexed for 1 min, and centrifuged at 15,000 rpm for 5 min; the supernatant was transferred to HPLC vials and 100 μL were injected into the HPLC system.

4.3.11. Treatment of Urine Samples For Analysis

Two hundred microliters of urine and 10 μM of the internal standard were combined and vortexed for 30 s. The proteins present in the urine samples were precipitated using 1.6 mL cold HPLC-grade acetonitrile (pre-stored at −20 °C), vortexed for 2 min, and centrifuged at 15,000 rpm for 15 min. The supernatant was transferred to new, labeled 2-mL centrifuge tubes. The samples were evaporated to dryness using SpeedVac. The residue was reconstituted with 200 μL of mobile phase, vortexed for 1 min, and centrifuged at 15,000 rpm for 15 min. The supernatant was transferred to HPLC vials and vortexed, and 100 μL was injected into the HPLC system.

4.3.12. Pharmacokinetic Analysis

Pharmacokinetic analysis was performed using data from individual rats, and the mean and standard error of the mean (SEM) were calculated for each group. The elimination rate constant (k_{el}) was estimated by linear regression of the serum concentrations in the log-linear terminal phase. Non-compartmental modeling of the serum concentration versus time data points was performed using Phoenix® WinNonlin® software (Version 6.3) (Pharsight Corporation, Mountain View, CA, USA) to calculate the pharmacokinetic parameters in the terminal phase, namely total clearance (CL_{tot}), and volume of distribution (V_{ss}). The initial maximum serum concentration (C_0) was calculated by back extrapolation using WinNonlin software. Based on the cumulative urinary excretion data, the fraction excreted in urine (f_e by dividing the total cumulative amount excreted in urine (ΣXu) by the dose), renal clearance (CL_{renal} by multiplying f_e by CL_{tot}), and hepatic clearance ($CL_{hepatic}$ by subtracting CL_{renal} from CL_{tot}, assuming that hepatic clearance is equivalent to non-renal clearance) were calculated. The fraction of a dose converted to a specific metabolite (F_m) was calculated using the following equation: $F_m = AUC_{(m,D)}/AUC_{(m)}$, where $AUC_{(m,D)}$ is the AUC of the metabolite after IV or PO administration of its precursor (Dox after DoxQ) and $AUC_{(m)}$ is the AUC of the metabolite after IV administration of an equimolar dose of the preformed metabolite (Dox after Dox) (36,37).

4.3.13. Assessment of Cardiac Toxicity of DoxQ and Dox

The cardiac toxicity was assessed after a single IV dose of Dox or DoxQ utilizing a rat cardiac Troponin-I (cTnI) ultra-sensitive ELISA kit from Life Diagnostics, Inc. (West Chester, PA, USA). Blood samples from pharmacokinetic studies were collected at 0, 12, 24, and 48 h from the jugular vein after a single 10 mg/kg IV dose of Dox (n = 4) or an equimolar dose of

DoxQ (n = 4). Samples were centrifuged to obtain the serum and stored at −20 °C in a freezer until analysis. On the day of the analysis, cTnI concentrations were measured in serum samples following the manufacturer's instructions. The area under the effect curve (AUEC) was calculated for cTnI concentrations at 12–48 h post-dosing using the trapezoidal rule (38,39) by WinNonlin® software.

4.3.14. Assessment of Renal Toxicity of Dox and DoxQ

The urinary output of rats over 24 h was monitored before and after administration of a single IV dose of Dox (10 mg/kg) or equimolar DoxQ to assess potential renal toxicity. Acute renal toxicity induced by Dox and other drugs may result in a reduction in the total urinary output (40–42). The total urine volume excreted over 24 h post-dosing was compared to the total urine volume excreted over 24 h pre-dosing.

The potential renal toxicity of Dox and DoxQ was also determined by measuring β-*N*-acetylglucosaminidase (NAG), a marker of ongoing renal damage, in rat urine (8,43). Urine samples from pharmacokinetics experiments were collected from metabolic cages at 0 h, 12 h, 24 h, and 48 h and stored at −20 °C until analysis. Concentrations of NAG urine samples were measured using an assay kit from ALPCO Diagnostics (Salem, NH, USA, cat. No. 73-1290050) on a Medica EasyRA automated clinical chemistry analyzer (Medica Corporation, Bedford, MA, USA) (44,45).

3.3.15. Statistical Analysis

Compiled data were presented as mean and standard error of the mean (mean ± SEM). Where possible, the data were analyzed for statistical significance using SigmaPlot software (v.

13.0, Systat Software, Inc., San Jose, CA, USA). Student's *t*-test was employed for unpaired samples to compare means between two groups, while one-way ANOVA was employed to compare the means of three or more groups, with subsequent *t*-tests between groups if necessary; a value of $p < 0.05$ was considered statistically significant.

4.4. RESULTS

4.4.1. Physicochemical Properties

As DoxQ is a chemical derivative of Dox, the change in the chemical structure of Dox will likely alter the physiochemical properties of the parent drug, which may affect its disposition into biological fluids and pharmacokinetic profile. Therefore, exploring the physicochemical properties of DoxQ in comparison to Dox provides insight into the differences in their dispositions and pharmacokinetics. Computer software, namely VCCLAB (23,24), MarvinSketch, and GastroPlus, were used to predict the physicochemical properties of DoxQ and Dox (Table 1). The estimated partition coefficient (LogP) value of DoxQ (2.6–3.8) was 3–5-fold higher than Dox (logP 0.49–1.3), suggesting higher lipophilicity of DoxQ. The distribution coefficient at pH 7.4 ($LogD_{7.4}$), which takes into account the ionizable groups at specific pH, of DoxQ was 25-fold higher than Dox (0.097) and may be a better predictor of lipophilicity. The predicted LogP and $LogD_{7.4}$ values of DoxQ are in agreement with the low predicted solubility (0.006 mg/mL) of DoxQ compared to Dox (0.243 mg/mL) at physiological pH and higher logS values of DoxQ. The predicted pKa values of DoxQ were also different than those of Dox. Furthermore, the experimentally determined melting point of DoxQ was 175 °C compared to 242 °C. The difference in the predicted pKa values of DoxQ versus Dox as well as other

physicochemical properties described above indicate that DoxQ is distinct from Dox and exhibits unique physicochemical properties.

Table 4.1. Physicochemical properties of Dox, quercetin, and DoxQ.

Compound	**Doxorubicin (Free Base)**	**Quercetin**	**DoxQ**
Structure	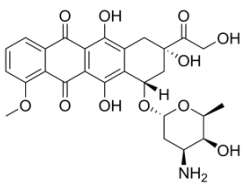	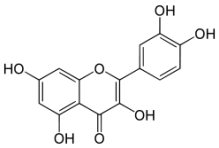	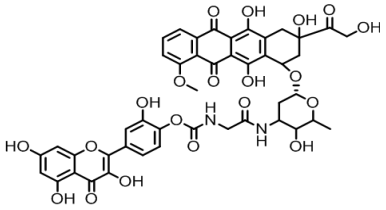
Molecular Weight (g/mol)	543.53	302.238	928.82
Formula	$C_{27}H_{29}NO_{11}$	$C_{15}H_{10}O_7$	$C_{45}H_{40}N_2O_{20}$
pKa (MarvinSketch)	8.00, 9.17, 9.93, 12.67, 13.49, 14.10	6.38, 7.85, 8.63, 10.29, 12.82	6.37, 7.72, 7.94, 8.97, 9.51, 10.21, 12.53, 13.10, 13.57, 14.06, 14.77
pKa (GastroPlus)	6.77, 8.43, 9.5	7.24, 8.15, 9.12, 10.25, 11.35	7.21, 8.08, 8.78, 9.38, 9.91, 10.64, 11.26
pKa (GastroPlus, after fitting solubility)	6.974, 10.08	6.582, 8.15, 10.25, 11.35	7.978, 8.08, 8.78, 9.38, 10.64, 11.26
logP (MarvinSketch)	1.30	1.75	2.60
logP (neutral, GastroPlus)	0.49	1.96	2.61
logP (VCCLAB)	1.3	1.44 ± 0.55	3.8 ± 1.5
$logD_{7.4}$ (MarvinSketch)	0.097	1.00	2.407
Intrinsic solubility (MarvinSketch)	−4.05 logS	−2.49 logS	−6.47 logS
Solubility at pH 7.4 (MarvinSketch)	−3.27 logS	−1.42 logS	−5.34 logS
Solubility at pH 7.4 (MarvinSketch)	0.243 mg/mL	15.15 mg/mL	0.006 mg/mL
logS (VCCLAB)	2.7	2.78	3.43
Melting point (experimental)	242 °C	316.5 °C *	175 °C

*PubChem (46)

4.4.2. HPLC Analysis of Dox

Optimal separation of Dox, DoxQ, and daunorubicin (IS) in serum, urine, and lymph was achieved with a mobile phase composed of acetonitrile with 0.1% formic acid in water 35:65, *v*/*v* and a flow rate of 0.6 mL/min on a C18 Phenomenex Kintex® column. Chromatograms were free of any interfering peaks co-eluted with peaks of interest (Figure 4.1). Calibration curves of Dox in serum and lymph were linear over the range of 0.05–100 μg/mL in serum and lymph and 0.1–100 μg/mL for urine, with excellent linearity ($r^2 > 0.99$) in all three matrices. Calibration curves of DoxQ in serum and urine were linear over the range of 1–100 μg/mL ($r^2 > 0.99$). The observed maximum serum concentration (C_{max}) of both Dox and DoxQ at 1 min post-dosing was within the linear range. The limit of quantification (LOQ) was 0.05 μg/mL and 1 μg/mL for Dox and DoxQ intact, respectively.

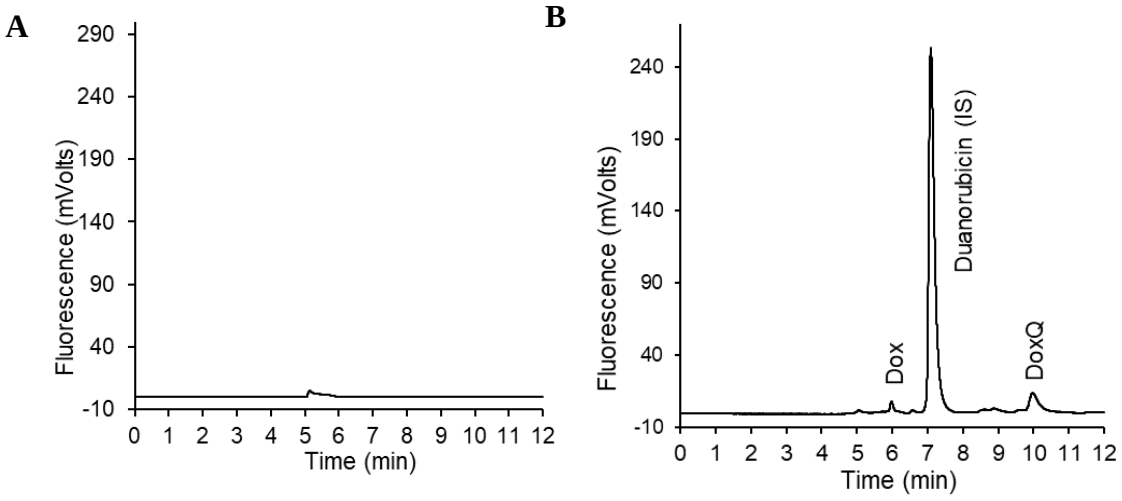

Figure 4.1. (**A**) Representative chromatogram of blank serum; (**B**) representative chromatogram of Dox, DoxQ, and the internal standard daunorubicin after 30 min of DoxQ IV dosing.

4.4.3. Pharmacokinetics of Dox and DoxQ After IV Administration

The disposition profiles of Dox and DoxQ intact in serum and urine following a single IV dose of Dox and an equimolar dose of DoxQ were examined (Figures 4.2 and 4.3). The serum concentration–time profile of IV DoxQ showed a rapid decline over the first 30 min and was quantifiable up to 1 h post-dosing. The concentrations of Dox after Dox were quantifiable up to 6 h post-dosing (Figure 4.2), with a maximum serum concentration (C_0) of Dox after Dox of ~25 μg/mL. The disposition profile of Dox after Dox, as well as its pharmacokinetic parameters, are consistent with the literature (13,15,25). Following IV administration of DoxQ, both DoxQ intact and Dox were detected with maximum serum concentration (C_0) of intact DoxQ of ~108 μg/mL and ~1 μg/mL for free Dox (Table 3.2). Concentrations of intact DoxQ demonstrated a rapid decline over one hour, while concentrations of Dox after DoxQ dosing showed a slower decline and were quantifiable up to 2 h post-dosing. Notably, the maximum serum concentration (C_0) of intact DoxQ after equimolar IV DoxQ was 4–5-fold higher than C_{max} of Dox after IV Dox. The area under the concentration–time curve (AUC) of intact DoxQ (18.6 ± 1.98 μg * h/mL) was also 5-fold higher than that of Dox (3.97 ± 0.71 μg * h/mL), demonstrating higher systemic exposure to DoxQ. The volume of distribution V_{ss} of Dox was ~80-fold higher than that of DoxQ, suggesting significantly greater tissue distribution of Dox. The fraction of DoxQ metabolized into Dox was ~12%.

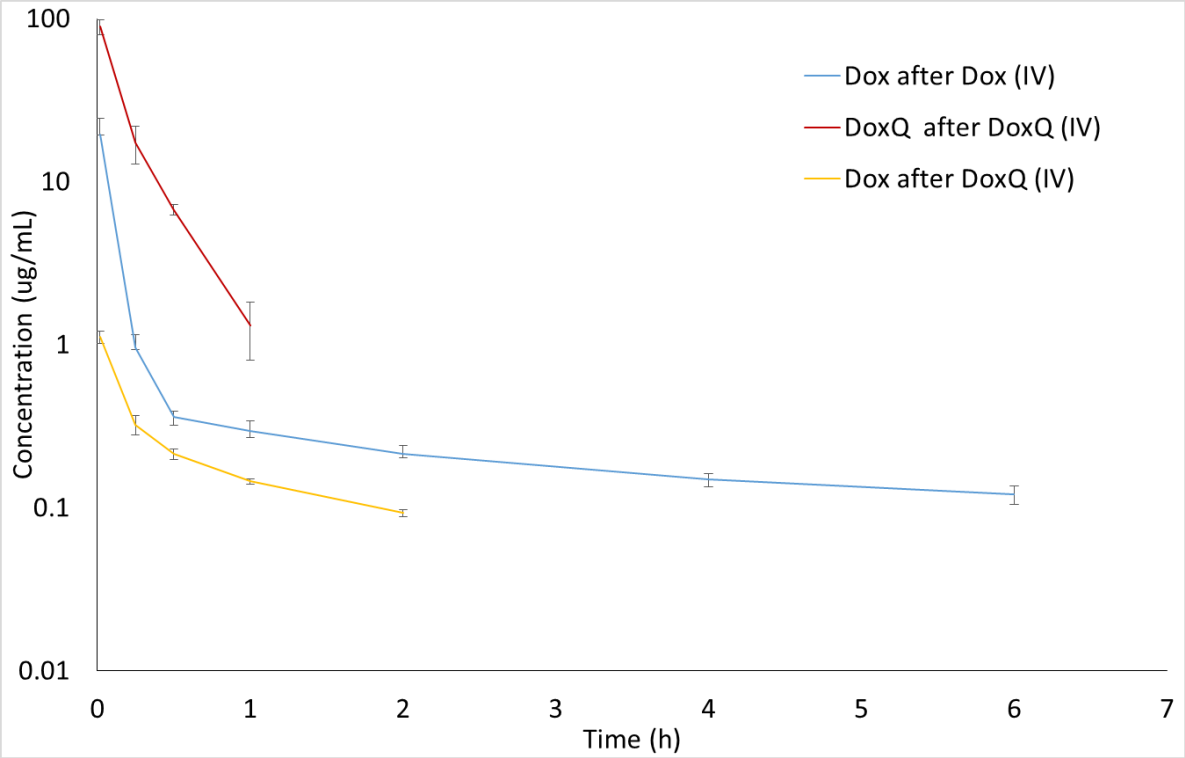

Figure 4.2. Concentrations of Dox and DoxQ intact after IV administration of Dox (10 mg/kg, n = 4 mean ± SEM) or DoxQ (equimolar dose, n = 3, mean ± SEM) in rat serum.

Table 4.2. Pharmacokinetics of Dox and DoxQ intact in rat serum after IV administration of Dox (10 mg/kg) and an equimolar dose of DoxQ (mean ± SEM, n = 4 unless otherwise stated).

Pharmacokinetic Parameter	Dox Administered	DoxQ Administered	
	Dox	DoxQ [1]	Dox
C_0 (μg/mL)	24.7 ± 14.2	108 ± 26.4 *	1.23 ± 0.11 [+]
k_{el} (h^{-1})	0.16 ± 0.02	4.59 ± 0.78 *	0.75 ± 0.076 [+]
$t_{1/2}$ (h)	4.69 ± 0.8 [@]	0.16 ± 0.3 *	0.87 ± 0.07
C_{last} (μg/mL)	0.12 ± 0.03	1.11 ± 0.17 *	0.09 ± 0.01 [+]
T_{last} (h) [2]	6	1	2
AUC_{last} (μg * h/mL)	3.97 ± 0.7 [@]	18.6 ± 1.98 *	0.46 ± 0.04 [+]
AUC_{inf} (μg * h/mL)	4.79 ± 1.83	NC	0.62 ± 0.03
V_{ss} (L/kg)	6.35 ± 2.11	0.08 ± 0.015	NA
CL_{renal} (L/h/kg) [1]	0.28 ± 0.84	0.02 ± 0.005	NA
$CL_{hepatic}$ (L/h/kg) [1]	2.35 ± 0.36	0.51 ± 0.06*	NA
CL_{total} (L/h/kg) [1]	2.63 ± 0.39	0.53 ± 0.01 *	NA
f_e (%)	10.73 ± 3.14	4.32 ± 1.005	NA
f_m (%)	NA	NA	11.66 ±0.86

[1] $n = 3$; [2] Median; NC = not calculable because $r^2 < 0.8$ or AUC% extrapolated > 27%; NA = not applicable; * $p < 0.05$ Dox after Dox versus DoxQ after DoxQ, [+] $p < 0.05$ DoxQ after DoxQ versus Dox after DoxQ, [@] $p < 0.05$ Dox after Dox versus Dox after DoxQ.

In the urine, both DoxQ intact and Dox were detected after DoxQ IV dosing. Likewise, Dox was excreted unchanged after Dox IV dosing (Figure 4.3). The total cumulative urinary excretion plots demonstrate that DoxQ is predominantly excreted as intact DoxQ and, to a much lower extent, as free Dox after DoxQ dosing. The total cumulative amount of free Dox excreted unchanged was much higher after Dox dosing than after DoxQ. The fraction of the dose excreted unchanged in the urine (f_e) of DoxQ and Dox were 4.32 ± 1.005 and 10.73 ± 3.14, respectively, indicating that both drugs are mainly eliminated by non-renal routes.

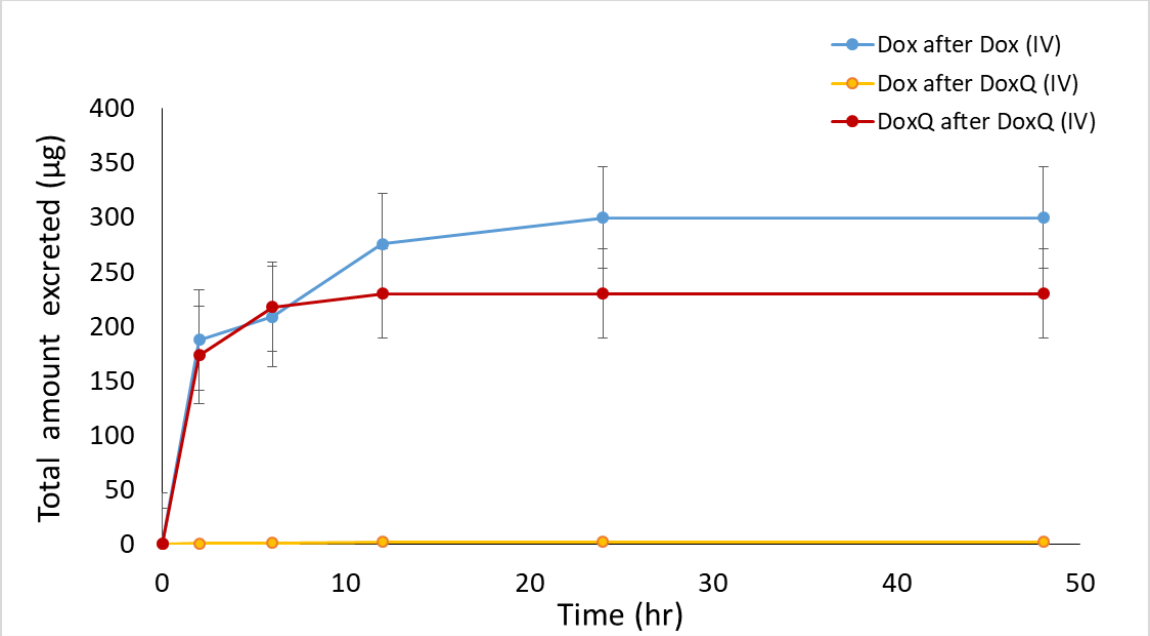

Figure 4.3. Cumulative amounts of Dox and DoxQ intact excreted unchanged in the urine after IV administration of Dox (10 mg/kg; n = 3, mean ± SEM) and equimolar DoxQ (n = 4, mean ± SEM) during the 48 h post-dosing.

4.4.4. Pharmacokinetics of Dox and DoxQ After Oral Administration

Following oral administration of DoxQ only the metabolite Dox was detected in serum as opposed to both DoxQ intact and Dox after IV administration (Figure 4.4). Following oral administration of Dox, Dox was also detected in serum. The serum concentration time plots demonstrate that concentrations of Dox after DoxQ were higher than after Dox at all time points, with resultant higher calculated AUC_{last} values of Dox after DoxQ than Dox after Dox when each was orally administered (Table 4.3). Bioavailability of Dox after Dox was ~8.5%, while the fraction of DoxQ metabolized into Dox was ~10.3%.

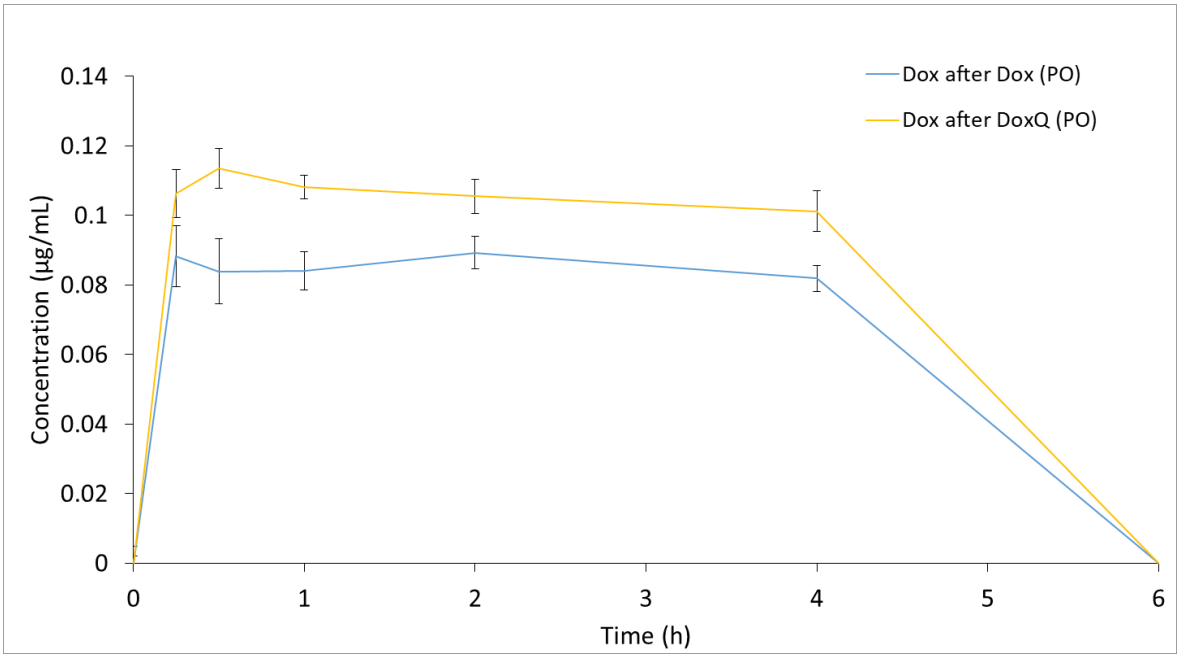

Figure 4.4. Concentrations of Dox after PO administration of Dox (10 mg/kg) and equimolar DoxQ in rat serum over 6 h. (n = 3 mean ± SEM for Dox, n = 4 mean ± SEM for DoxQ).

Table 4.3. Pharmacokinetics of Dox after oral administration of 10 mg/kg Dox and equimolar DoxQ in rat serum (mean ± SEM, n = 4 unless otherwise stated).

Pharmacokinetic Parameter	**Dox Administered**	**DoxQ Administered**	**Cycloheximide + DoxQ Administered**
	Dox [1]	**Dox**	**Dox**
C_{max} (µg/mL)	0.09 ± 0.01	0.11 ± 0.01 [+]	0.07 ± 0.001
C_{last} (µg/mL)	0.08 ± 0.01	0.10 ± 0.01	0.07 ± 0.02
T_{last} (h) [2]	4	4	4
AUC_{last} (µg * h/mL)	0.33 ± 0.04	0.41 ± 0.03 [+]	0.27 ± 0.005
F_m (%)	NA	10.32 ± 0.42 [+]	6.81 ± 0.14
F (%)	8.57 ± 0.71	NA	NA

[1] n = 3; [2] Median; NA = Not applicable; [+] $p < 0.05$ Dox after DoxQ versus Dox after Cycloheximide + DoxQ.

4.4.5 Intestinal Lymphatic Drug Delivery

The mesenteric lymph duct cannulation rat model is commonly used as to directly examine the transport of drugs after oral administration because it enables the collection of lymphatic fluids as it flows from the intestine (20,35). The intestinal lymphatic transport of Dox after oral administration DoxQ and Dox was investigated in a mesenteric lymph duct cannulated model to assess whether the presence of quercetin facilitates lymphatic transport of Dox. Following oral DoxQ or Dox dosing, lymph samples were collected up to one hour post-dosing and concentrations of Dox were measured by HPLC. The cumulative amount of Dox in mesenteric lymph fluid after oral DoxQ were two-fold higher than after Dox (Figure 4.5), suggesting that quercetin in DoxQ, intact or when released, increased the intestinal delivery of Dox into lymphatics.

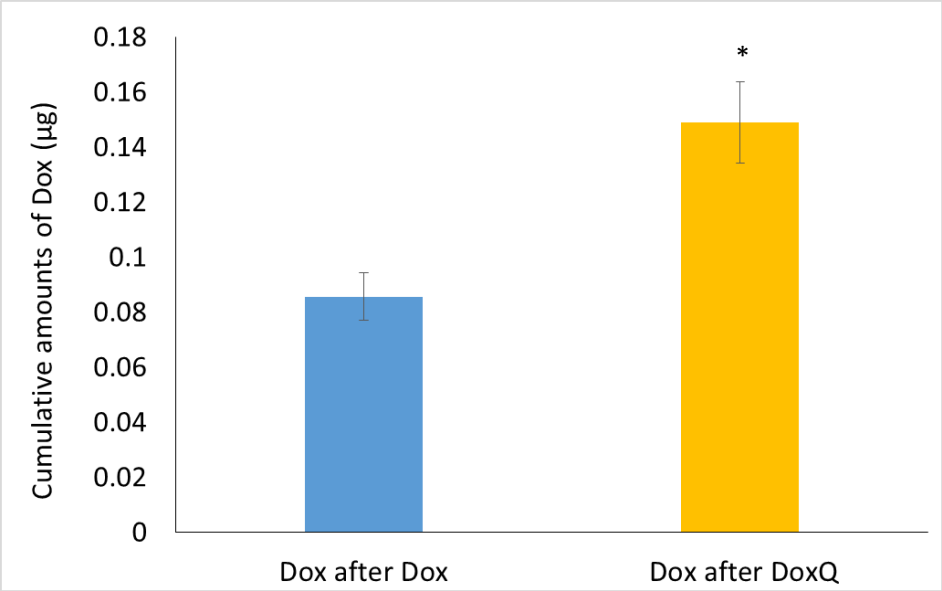

Figure 4.5. Cumulative amounts of Dox in mesenteric lymph fluid over one hour after oral administration of Dox (10 mg/kg) and equimolar DoxQ (n = 3, mean ± SEM). * $p < 0.05$ Dox after DoxQ versus Dox after Dox.

Intestinal lymphatic delivery of Dox was also examined indirectly in the cycloheximide treated rat model. Lymph blockage was achieved by pre-administration of cycloheximide 1.5 h prior to oral administration of DoxQ. A 3 mg/kg intraperitoneal dose of cycloheximide was chosen based on previous studies published in the literature (26–35). Likewise, a 1.5-h time delay prior to oral DoxQ dosing was chosen to achieve maximum lymph blockage (29).

Figure 4.6 demonstrates that pre-administration of cycloheximide prior to oral DoxQ reduced the systemic exposure of Dox compared to DoxQ administered alone. Given that quercetin is naturally transported via intestinal lymphatics and could act as a carrier for Dox's (Dox in DoxQ) lymphatic transport, blockage of the intestinal lymphatic pathway may reduce systemic exposure. The results suggest that quercetin in DoxQ, intact or when released from the conjugate, facilitates intestinal lymphatic transport of Dox, and that blocking the lymphatic pathway resulted in lower levels of circulating Dox.

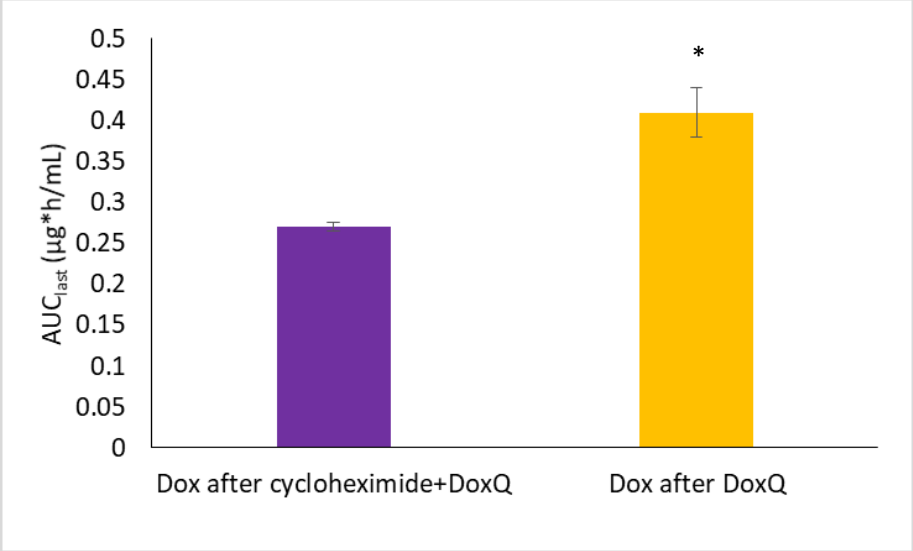

Figure 4.6. Systemic exposure (AUC_{last}) of Dox after PO administration of DoxQ alone or after cycloheximide IP followed by DoxQ PO in rat serum (n = 4, mean ± SEM). * $p < 0.05$ Dox after DoxQ versus Dox after cycloheximide + DoxQ.

4.4.6. Cardiotoxicity of Dox and DoxQ

The clinical use of Dox is limited by its dose-related cardiotoxicity, which can result in cardiac muscle injury. The extent of myocardial injury can be assessed by measuring the levels of cardiac troponins in blood. Cardiac troponins are highly sensitive and specific biomarkers of cardiac muscle damage, induced by chemotherapeutics as well as other pathological conditions (47). cTnI is commonly used as an early marker of cardiotoxicity induced by Dox (8,48) as it is released within 2–3 h of myocardial injury and peaks at 24 h (49,50). Based on the reported peak troponin concentrations following myocardium injury, levels of cTnI were measured in serum samples from pharmacokinetic study at 12, 24, and 48 h after a single acute IV dose (10 mg/kg) of Dox or equimolar DoxQ utilizing an ELISA kit. Figure 4.7 illustrates that the concentrations of cTnI at 12, 24, and 48 h post-IV-dosing of DoxQ were lower than after Dox dosing, though this did not reach statistical significance and thus the cardiac toxicity induced by DoxQ and Dox was not different using this biomarker. Although the calculated area under the effect curve (AUEC) of cTnI concentrations at 12–48 h post-DoxQ-dosing (Figure 4.8) was lower than the AUEC after Dox, it did not result in cardioprotective effects of DoxQ as there were no statistical differences between the treatment groups.

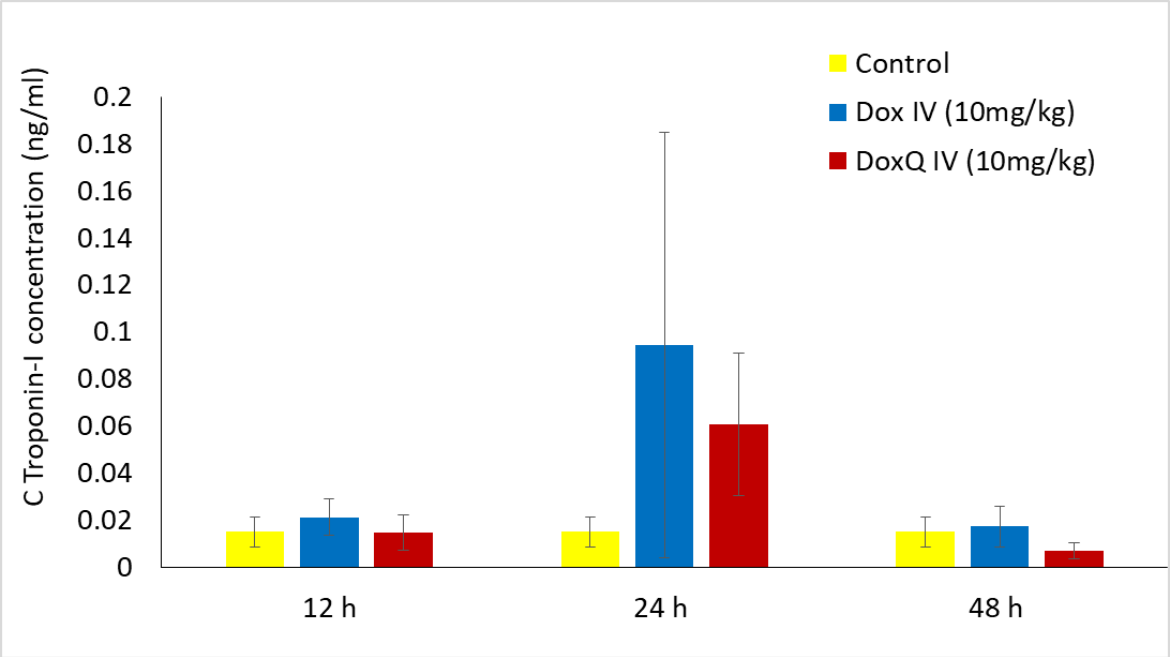

Figure 4.7. cTnI concentrations after IV (10 mg/kg) administration of Dox and equimolar DoxQ (n = 4, mean ± SEM). Data were not statistically significant.

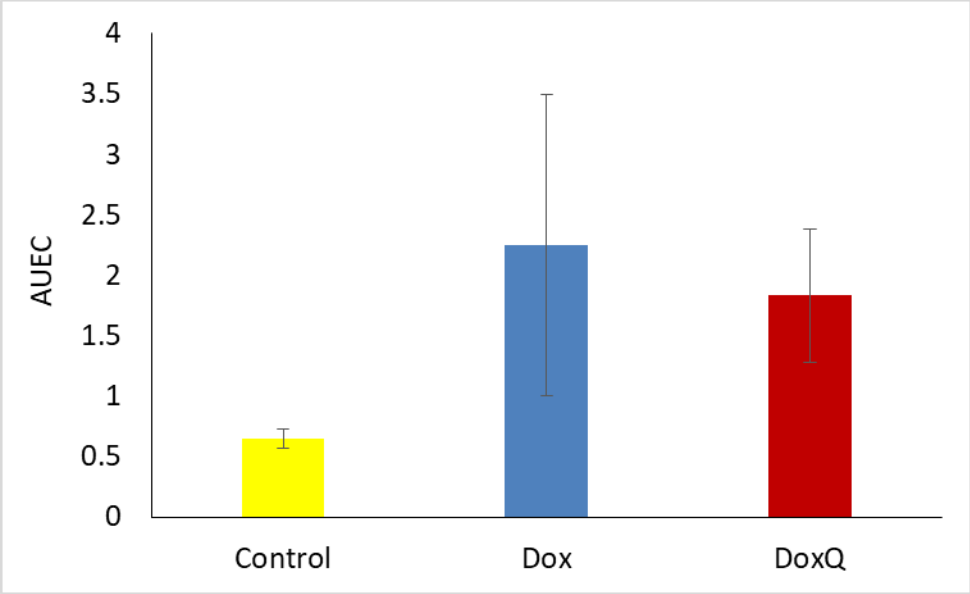

Figure 4.8. AUEC of cTnI concentrations 12-48 h after IV (10 mg/kg) administration of Dox and equimolar DoxQ (n = 4, mean ± SEM). Data were not statistically significant.

4.4.7. Renal Toxicity of Dox and DoxQ

Dox can also induce renal toxicity, which could be manifested as reduced urinary output. Thus, the effect of DoxQ on the total urinary output of rats over 24 h was examined in comparison to rats treated with Dox after a single acute IV dose. Figure 4.9 shows that there was no significant difference in the total urine volume over 24 h in rats treated with Dox or an equimolar dose of DoxQ.

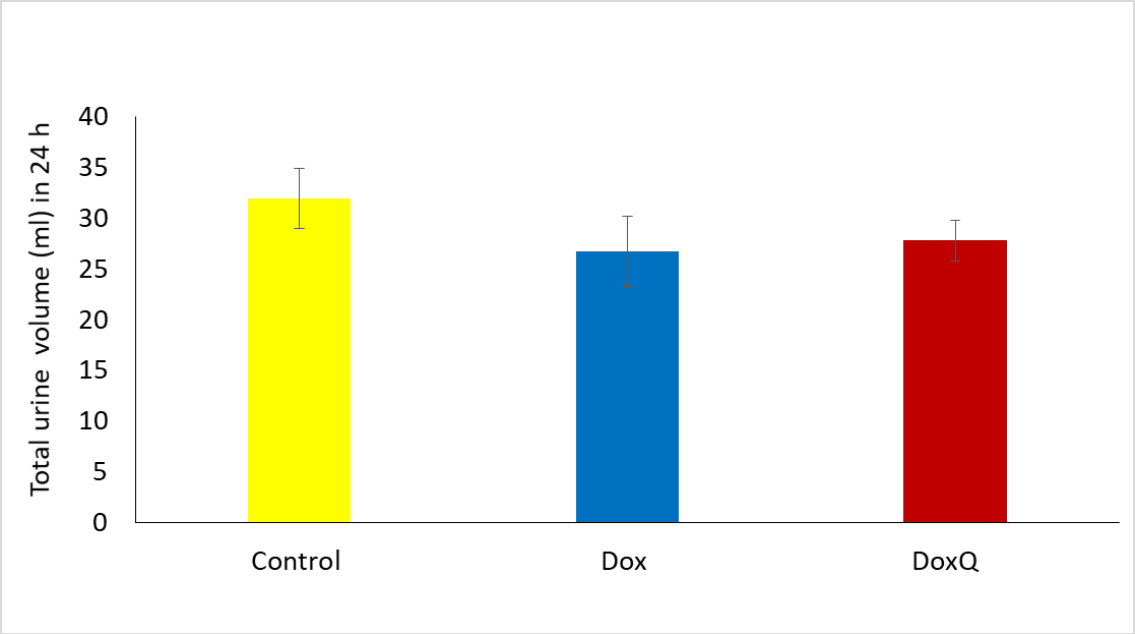

Figure 4.9. Average total urine volume 24 h post IV Dox (10 mg/kg) and equimolar DoxQ compared to control untreated. Dox (n = 3, mean ± SEM), DoxQ (n = 4, mean ± SEM), control (n = 7, mean ± SEM). Data were not statistically significant

The potential renal toxicity of Dox and DoxQ was determined by measuring β-*N*-acetylglucosaminidase (NAG), a lysosomal enzyme found in large concentrations in kidney tubules and a sensitive and early marker of renal damage (8,51,52). Urine samples from

pharmacokinetic studies after a single IV dose of DoxQ or Dox collected at 0, 2, 6, 12, 24 and 48 h were analyzed on a Medica easy RA analyzer for NAG concentrations. Cumulative amounts of NAG in 24 h after DoxQ dosing were lower than after Dox (Figure 4.10), suggesting lower renal toxicity induced after DoxQ administration compared to Dox.

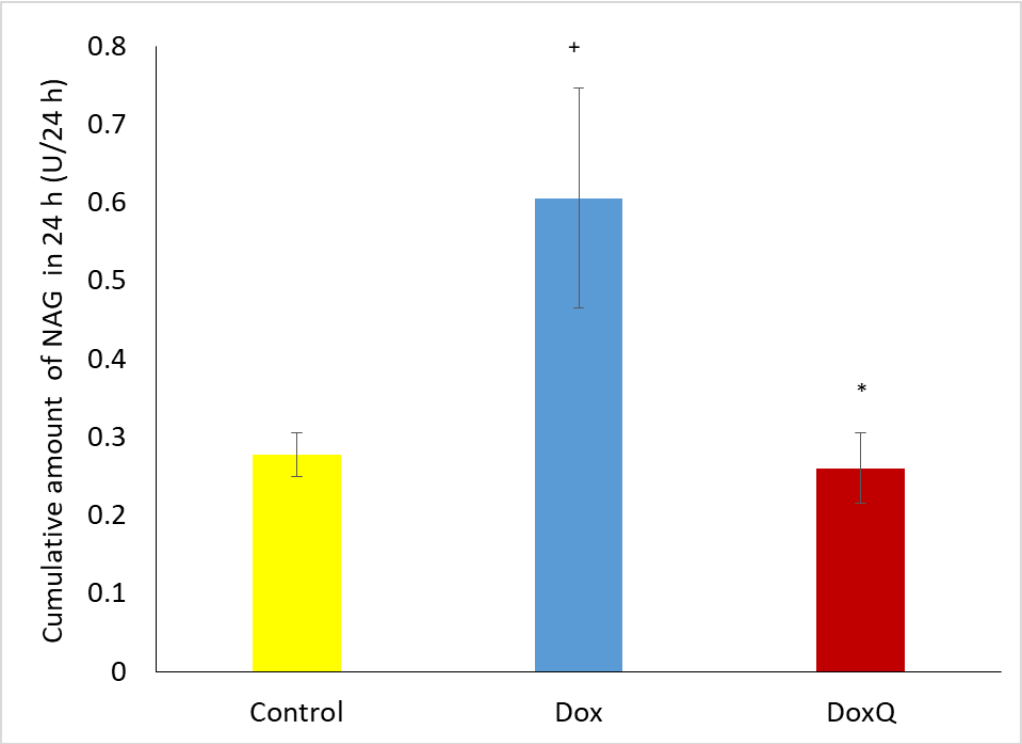

Figure 4.10. Total amount of NAG excreted in urine after IV administration of Dox (10 mg/kg) mean ± SEM) and equimolar DoxQ compared to control untreated (n = 4, mean ± SEM). + $p < 0.05$ Dox versus control ,* $p < 0.05$ DoxQ versus Dox.

4.5. DISCUSSION

Dox is an anthracycline antibiotic widely used in cancer chemotherapy; however, its dose-dependent toxicity limits its clinical use. The purpose of this study was to investigate the feasibility of utilizing a Dox-bound derivative with the lymphatically absorbed antioxidant quercetin as a proof of concept linker, delivering Dox and Dox–quercetin to the systemic

circulation via intestinal lymphatics after oral dosing. In addition, the flavonoid–Dox conjugate may lead to sustained release of the anti-cancer agent after IV dosing, resulting in lower peak serum concentration, which may be associated with the dose-limiting cardiotoxicity of the drug. Furthermore, the protective antioxidant effects of quercetin in DoxQ, when intact or when released, may further limit the cardiac and renal toxicity induced by Dox.

Various liposome-encapsulated formulations of Dox are currently available in human studies with the advantage of reduced acute cardiotoxicity compared to IV Dox and improved pharmacokinetics (53). However, pegylated liposomal Dox is associated with an additional side effect of palmar plantar erythrodysesthesia (7). In this study, we sought to examine the performance of a controlled-release Dox–quercetin conjugate with reduced side effects in vitro, which may have better tolerability compared to conventional Dox–HCl and liposomal Dox treatments.

The Dox–quercertin conjugate was synthesized using a glycine linker, resulting in a new derivative with increased lipophilicity and improved *in vitro* pharmacological activities. Our previous in vitro study demonstrated a controlled release of both Dox and quercetin released from DoxQ over four days (14). Furthermore, DoxQ was less cardiotoxic than Dox to both rat and human cardiomyocytes and the mechanism of cardioprotection involved a reduction in the levels of ROS and oxidative stress markers as well as inhibitory effects on the expression and catalytic activity of CYP1B1. Additionally, DoxQ mitigated the therapeutic barriers contributing to the low oral bioavailability of Dox as it inhibited CYP3A4 and demonstrated higher cellular uptake by P–gp-positive cells (MDCK–MDR) *in vitro*.

In this study, our intestinal lymphatic delivery strategy was applied to the DoxQ delivery system, increasing the serum concentrations of Dox at all time points, with an overall increase in

AUC_{last} of Dox after oral DoxQ administration compared to after Dox, reflecting an overall increase in the systemic exposure of Dox. In addition, only free Dox was released from oral DoxQ and detected analytically, thus it was analyzed for systemic exposure. Given that DoxQ was not detected as the intact conjugate after oral dosing of DoxQ, calculating the F of DoxQ intact was not possible; however, it was appropriate to calculate the fraction of DoxQ metabolized to Dox, as described in Section 4.2.9. Therefore, the extent of systemic exposure of Dox after oral Dox and DoxQ was assessed by comparing the AUCs of Dox (Table 4.3).

After IV administration DoxQ was detected intact, which we have shown to be a pharmacologically active form as it retained anti-cancer activity in a triple-negative murine breast cancer cell line (14). The actual total concentration of DoxQ intact in the serum after an equimolar dose of Dox was 5-fold higher than the concentration of Dox after Dox, allowing a greater AUC compared to the standard Dox treatment. This could result in a lower dose of DoxQ being required to achieve the same effective serum concentrations. DoxQ injections could conceivably be as effective as Dox with reduced toxicity. With regard to its pharmacokinetics, the difference in the volume of distribution between the IV Dox after Dox group and the IV DoxQ intact group was possibly due to the change in physicochemical properties and inhibition of P–gp by quercetin. Dox with a log P value of 1.3, pKa of 8.4, and a molecular weight of 543.53 g/mol rapidly crosses the lipid membrane and binds to tissues, resulting in a larger V_{ss}. On the other hand, DoxQ with a smaller V_{ss} (0.08 L/kg) indicates that it is should mainly reside in the vascular compartment with much lower affinity to distribute across biological membranes compared to Dox, regardless of its higher lipophilicity (logP 2.60–3.8). This could be due to the large molecular weight of 982 g/mol and the presence of multiple potential ionization sites, which may impede its distribution across biological membranes while intact. Similar effects

were observed for clozapine nano-formulation, where tissue distribution of clozapine incorporated in solid lipid nanoparticles was lower than clozapine solution because free clozapine could only be distributed after its release from nanoparticles (54). Therefore, it is possible that DoxQ intact will distribute to a lower extent than when it is released from the conjugate or when Dox alone is administered. Examination of the total cumulative amounts of Dox and DoxQ excreted unchanged after IV dosing revealed lower cumulative amounts of DoxQ intact after DoxQ than of Dox after Dox. This could be due to the large molecular weight of DoxQ (928.8 g/mole) to be filtered at the glomerulus and also its high lipophilicity (LogP 2.6–3.8, Table 4.2), as opposed to Dox with a smaller size and lower lipophilicity.

With regard to intestinal lymphatic absorption of DoxQ, our results show that cumulative amounts of Dox following DoxQ oral dosing were twice as high after Dox in a mesenteric lymph cannulated rat model. This observation is likely due to the presence of quercetin in DoxQ, intact or when released, acting as a lymphatically targeted carrier to facilitate the transport of Dox into lymphatics, as quercetin has been reported to be transported via intestinal lymphatics following intragastric or intraduodenal administration (16–18). Additionally, compounds with high lipophilicity, high logP, and large molecular size favor association with chylomicrons in the intestine, facilitating their uptake by lymphatic capillaries into the mesenteric lymph duct (19,21). The new derivative is more lipophilic (LogP 2.6–3.8) and larger in size (molecular weight 928.8 g/mole) compared to Dox (LogP 1.3, 543.53 g/mol), both of which may in part facilitate DoxQ's lymphatic intestinal absorption. Furthermore, formulation effects of PEG-400 on the intestinal absorption and pharmacokinetics of DoxQ and even Dox are possible. PEG-400 is often utilized in dosing of rodent species (45,55) and was used as a vehicle in this study for both oral and IV administration of DoxQ and Dox because DoxQ has poor water solubility and

reconstitution in 0.9% NaCl is not feasible. The diverse effects of PEG-400 on solubility, permeability, drug metabolizing enzymes, transporters, and gastrointestinal transit time may have influences on the intestinal absorption and systemic exposure of oral drugs (56–58).

In spite of the efficacy of Dox chemotherapy, its clinical use is limited due to its dose-limiting cardiac toxicity along with its renal toxicity, caused in part by the generation of oxygen species in the conversion from Dox to semiquinone, yielding very reactive hydroxyl radicals. The free radical may also cause damage to various membrane lipids and other cellular components (59). Following a large single-dose injection of Dox (10 mg/kg IV), there was an increase in cTnI released from cardiac tissues at the 12, 24, and 48 h time points, consistent with the literature. In parallel, rats that received DoxQ (equimolar dose of Dox) also had an increase in cTnI at each time point. The significant 4-5-fold increase of circulating intact DoxQ as compared to Dox and its overall increase in systemic exposure, as well as the metabolism of DoxQ to Dox, did not result in higher cTnI compared to rats that received Dox as no statistically significant difference in cardiac toxicity was observed between the two treatment groups (Figures 4.7 and 4.8). The *in vivo* cardiac effects of DoxQ in this study are different from our in vitro observations, where DoxQ formulation greatly reduced the cardiac toxicity induced by Dox in both rat and human cardiomyocytes (14). This observation is also different from a reported study in which the combination of Dox with resveratrol and quercetin polymeric micelles was shown to mitigate Dox-induced cardiotoxicity both *in vitro* and *in vivo* (60). The *in vivo* cardioprotective effects of this combination strategy were assessed by measuring levels of aspartate amino transferase (AST), amino alanine transferase (ALT), and Creatine kinase (CK) in mice and showed a significant reduction in all three biochemical markers as opposed to Dox administered alone. The observations from the later reported study (60) and our *in vitro* study

(14) demonstrate the protective effects of quercetin on Dox-induced cardiotoxicity. The cardioprotective effects reported in (60) were attributed to the synergistic action of resveratrol and quercetin micelles when co-administered with Dox at a ratio of 10:10:1 resveratrol:quercetin:Dox, whereas our DoxQ conjugate is designed to release Dox and quercetin at a ratio of 1:1, which may have not been enough to show cardioprotection *in vivo* after one dose. Additionally, the use of two antioxidants, namely resveratrol and quercetin, together could have provided a greater ability to scavenge reactive oxygen species and attenuate the cardiotoxicity induced by Dox as opposed to only quercetin in the DoxQ formulation.

Urine analysis following a single acute dose of Dox showed higher cumulative amounts of β-N-acetylglucosaminidase (NAG), a lysosomal enzyme in the epithelial cells of the proximal tubules and a sensitive marker of renal damage, compared to DoxQ. This is likely due to the antioxidant protective effects of quercetin in DoxQ on Dox-induced renal toxicity and is consistent with similar studies reported in the literature (61,62).

DoxQ by injection could have greater benefits over standard dosing regimens in terms of tolerance and potential improved toxicity. Further translational efforts will focus on optimizing dose frequency, completing preclinical proof of concept in chronic studies, and examining other natural lymphatic carriers for oral delivery.

4.6. CONCLUSION

DoxQ alters the pharmacokinetic disposition of Dox both orally and intravenously and is in part transported through intestinal lymphatics. DoxQ may increase therapeutic safety compared to Dox in a rodent model and further long-term studies are warranted.

4.7. REFERENCES

1. Minotti G, Menna P, Salvatorelli E, Cairo G, Gianni L. Anthracyclines: Molecular advances and pharmacologic developments in antitumor activity and cardiotoxicity. harmacol Rev. 2004;56(2):185-229.
2. Cortés-Funes H, Coronado C. Role of anthracyclines in the era of targeted therapy. Cardiovasc Toxicol. 2007;7(2):56-60.
3. Gibbs DD, Pyle L,Allen M, Vaughan M, Webb A, Johnston SR, Gore ME. A phase I dose-finding study of a combination of pegylated liposomal doxorubicin (Doxil), carboplatin and paclitaxel in ovarian cancer. Br J Cancer. 2002;86(9):1379-84.
4. Gianni L, Dombernowsky P, Sledge G, Martin M, Amadori D, Arbuck SG, Ravdin P, Brown M, Messina M, Tuck D, Weil C, Winograd B. Cardiac function following combination therapy with paclitaxel and doxorubicin: An analysis of 657 women with advanced breast cancer. Ann Oncol. 2001;12(8):1067-73.
5. McBride NC, Cavenagh JD, Ward MC, Grant I, Schey S, Gray A, Hughes A, Mills MJ, Cervi P, Newland AC, Kelsey SM. Liposomal daunorubicin (DaunoXome) in combination with cyclophosphamide, vincristine and prednisolone (COP-X) as salvage therapy in poor-prognosis non-Hodgkins lymphoma. Leuk Lymphoma. 2001 Jun;42(1-2):89-98.
6. Soloman R, Gabizon AA. Clinical pharmacology of liposomal anthracyclines: Focus on pegylated liposomal Doxorubicin Clin Lymphoma Myeloma. 2008;8(1):21-32.
7. Lorusso D, Di Stefano A, Carone V, Fagotti A, Pisconti S, Scambia G. Pegylated liposomal doxorubicin-related palmar-plantar erythrodysesthesia (‘hand-foot’ syndrome). Ann Oncol. 2007;18(7):1159-64

8. Cai S, Thati S, Bagby TR, Diab HM, Davies NM, Cohen MS, Forrest ML. Localized doxorubicin chemotherapy with a biopolymeric nanocarrier improves survival and reduces toxicity in xenografts of human breast cancer. J Control Release. 2010;146(2):212-8.
9. Matsumura Y, Hamaguchi T, Ura T, Muro K, Yamada Y, Shimada Y, Shirao K, Okusaka T, Ueno H, Ikeda M, Watanabe N.Phase I clinical trial and pharmacokinetic evaluation of NK911, a micelle-encapsulated doxorubicin. Br. J. Cancer. 2004; 91(10): 1775–81.
10. Ríhová B1, Strohalm J, Prausová J, Kubácková K, Jelínková M, Rozprimová L, Sírová M, Plocová D, Etrych T, Subr V, Mrkvan T, Kovár M, Ulbrich K. Cytostatic and immunomobilizing activities of polymer-bound drugs: Experimental and first clinical data J Control Release. 2003;91(1-2):1-16.
11. Tolcher AW, Sugarman S, Gelmon KA, Cohen R, Saleh M, Isaacs C, Young L, Healey D, Onetto N, Slichenmyer W. Randomized phase II study of BR96-doxorubicin conjugate in patients with metastatic breast cancer. J Clin Oncol. 1999;17(2):478-84.
12. Gustafson DL, Merz AL, Long ME.Pharmacokinetics of combined doxorubicin and paclitaxel in mice. Cancer Lett. 2005;220(2):161-9.
13. Lee HJ, Lee MG. Effects of dexamethasone on the pharmacokinetics of adriamycin after intravenous administration to rats. Res Commun Mol Pathol Pharmacol. 1999;105(1-2):87-96.
14. Alrushaid S, Zhao Y, Sayre CL, Maayah ZH, Laird Forrest M, Senadheera SN, Chaboyer K, Anderson HD, El-Kadi AOS, Davies NM. Mechanistically Elucidating the In-Vitro Safety and Efficacy of a Novel Doxorubicin Derivative. Drug Deliv Transl Res. 2017;7(4):582-597.
15. Choi JS1, Piao YJ, Kang KW. Effects of quercetin on the bioavailability of doxorubicin in rats: Role of CYP3A4 and P-gp inhibition by quercetin. Arch Pharm Res. 2011;34(4):607-13.

16. Chen IL, Tsai YJ, Huang CM, Tsai TH. Lymphatic absorption of quercetin and rutin in rat and their pharmacokinetics in systemic plasma. J Agric Food Chem. 2010;58(1):546-51.
17. Murota K, Cermak R, Terao J, Wolffram S. Influence of fatty acid patterns on the intestinal absorption pathway of quercetin in thoracic lymph duct-cannulated rats. Br J Nutr. 2013;109(12):2147-53.
18. Murota K, Terao J. Quercetin appears in the lymph of unanesthetized rats as its phase II metabolites after administered into the stomach. FEBS Lett. 2005;579(24):5343-6.
19. Trevaskis NL, Kaminskas LM, Porter CJ. From sewer to saviour—Targeting the lymphatic system to promote drug exposure and activity. Nat Rev Drug Discov. 2015;14(11):781-803.
20. Trevaskis NL, Hu L, Caliph SM, Han S, Porter CJ. The mesenteric lymph duct cannulated rat model: Application to the assessment of intestinal lymphatic drug transport J Vis Exp. 2015;(97).
21. Yáñez JA, Wang SW, Knemeyer IW, Wirth MA, Alton KB. Intestinal lymphatic transport for drug delivery. Adv Drug Deliv Rev. 2011;63(10-11):923-42
22. Porter CJ, Trevaskis NL, Charman WN. Lipids and lipid-based formulations: Optimizing the oral delivery of lipophilic drugs. Nat Rev Drug Discov. 2007;6(3):231-48.
23. Tetko IV, Gasteiger J, Todeschini R, Mauri A, Livingstone D, Ertl P, Palyulin VA, Radchenko EV, Zefirov NS, Makarenko AS, Tanchuk VY, Prokopenko VV. Virtual computational chemistry laboratory—Design and description, J Comput Aided Mol Des. 2005;19(6):453-63.
24. Virtual Computational Chemistry Laboratory. Available online: http://www.vcclab.org (accessed on 24 August 2017).

25. Daeihamed M, Haeri A, Dadashzadeh S. A Simple and Sensitive HPLC Method for Fluorescence Quantitation of Doxorubicin in Micro-volume Plasma: Applications to Pharmacokinetic Studies in Rats. Iran J Pharm Res. 2015 Winter;14(Suppl):33-42.
26. Dahan A, Hoffman A. Evaluation of a chylomicron flow blocking to investigate the intestinal lymphatic transport of lipophilic drugs. Eur J Pharm Sci. 2005;24(4):381-8.
27. Bhalekar MR, Upadhaya PG, Madgulkar AR, Kshirsagar SJ, Dube A, Bartakke US. In-Vivo bioavailability and lymphatic uptake evaluation of lipid nanoparticulates of darunavir. Drug Deliv. 2016;23(7):2581-86.
28. Fu Q, Sun J, Ai X, Zhang P, Li M, Wang Y, Liu X, Sun Y, Sui X, Sun L, Han X, Zhu M, Zhang Y, Wang S, He Z. Nimodipine nanocrystals for oral bioavailability improvement: Role of mesenteric lymph transport in the oral absorption. Int J Pharm. 2013;448(1):290-7
29. Attili-Qadri S, Karra N, Nemirovski A, Schwob O, Talmon Y, Nassar T, Benita S. Oral delivery system prolongs blood circulation of docetaxel nanocapsules via lymphatic absorption. Proc Natl Acad Sci U S A. 2013;110(43):17498-503.
30. Sun M, Zhai X, Xue K, Hu L, Yang X, Li G, Si L.Intestinal absorption and intestinal lymphatic transport of sirolimus from self-microemulsifying drug delivery systems assessed using the single-passintestinal perfusion (SPIP) technique and a chylomicron flow blocking approach: Linear correlation with oral bioavailabilities in rats. Eur J Pharm Sci. 2011;43(3):132-40.
31. Lind ML, Jacobsen J, Holm R, Müllertz A. Intestinal lymphatic transport of halofantrine in rats assessed using a chylomicron flow blocking approach: The influence of polysorbate 60 and 80. Eur J Pharm Sci. 2008;35(3):211-8

32. Gao F, Zhang Z, Bu H, Huang Y, Gao Z, Shen J, Zhao C, Li Y. Nanoemulsion improves the oral absorption of candesartan cilexetil in rats:Performance and mechanism. J Control Release. 2011;149(2):168-74.
33. Mishra A, Vuddanda, PR, Singh S. Intestinal Lymphatic Delivery of Praziquantel by Solid Lipid Nanoparticles: Formulation Design, In Vitro and In Vivo Studies. J. Nanotechnol. 2014;2014:1-12.
34. Makwana V, Jain R, Patel K, Nivsarkar M, Joshi A. Solid lipid nanoparticles (SLN) of Efavirenz as lymph targeting drug delivery system: Elucidation of mechanism of uptake using chylomicron flow blocking approach. Int J Pharm. 2015;495(1):439-446.
35. Tsai YJ, Tsai TH. Mesenteric lymphatic absorption and the pharmacokinetics of naringin and naringenin in the rat. J Agric Food Chem. 2012;60(51):12435-42.
36. Rowland M, Tozer TN. Metabolites and drug response. In. Clinical Pharmacokinetics and Pharmacodynamics: Concepts and applications, 4th ed.; Tozer RM, Thomas N Eds.; Lippincott Williams & Wilkins: Baltimore, MD, USA. 2011: 603–631.
37. Mehvar R, Jamali F, Watson MW, Skelton D. Pharmacokinetics of tetrabenazine and its major metabolite in man and rat. Bioavailability and dose dependency studies. Drug Metab Dispos. 1987;15(2):250-5.
38. Hanafy S, Dagenais NJ, Dryden WF, Jamali F. Effects of angiotensin II blockade on inflammation-induced alterations of pharmacokinetics and pharmacodynamics of calcium channel blockers. Br J Pharmacol. 2008;153(1):90-9.
39. Sattari S, Dryden WF, Eliot LA, Jamali F. Despite increased plasma concentration, inflammation reduces potency of calcium channel antagonists due to lower binding to the rat heart. Br J Pharmacol. 2003;139(5):945-54.

40. Singh NP, Ganguli A, Prakash A. Drug-induced kidney diseases. J Assoc Physicians India. 2003;51:970-9.
41. Naughton CA. Drug-induced nephrotoxicity. Am Fam Physician. 2008;78(6):743-50.
42. Okuda S, Oh Y, Tsuruda H, Onoyama K, Fujimi S, Fujishima M. Adriamycin-induced nephropathy as a model of chronic progressive glomerular disease Kidney Int. 1986;29(2):502-10.
43. Le JM, Han YH, Choi SJ, Park JS, Jang JJ, Bae RJ, Lee MJ, Kim MJ, Lee YH, Kim D, Lee HY, Park SH, Park CB, Kang JS, Kang JK. Variation of nephrotoxicity biomarkers by urinary storage condition in rats. Toxicol Res. 2014;30(4):305-9
44. Martinez SE, Davies NM. Enantiospecific pharmacokinetics of isoxanthohumol and its metabolite 8-prenylnaringenin in the rat. Mol Nutr Food Res. 2015;59(9):1674-89.
45. Oliveira AL, Martinez SE, Nagabushnam K, Majeed M, Alrushaid S, Sayre CL, Davies NM. Calebin A: Analytical Development for Pharmacokinetics Study, Elucidation of Pharmacological Activities and Content Analysis of Natural Health Products. J Pharm Pharm Sci. 2015;18(4):494-514.
46. PubChem. Available online: https://pubchem.ncbi.nlm.nih.gov/compound/5280343#section=Entrez-Crosslink (accessed on 24 August 2017).
47. Tian S, Hirshfield KM, Jabbour SK, Toppmeyer D, Haffty BG, Khan AJ, Goyal S.Serum biomarkers for the detection of cardiac toxicity after chemotherapy and radiation therapy in breast cancer patients. Front Oncol. 2014;4:277

48. Hadi N, Yousif NG, Al-amran FG, Huntei NK, Mohammad BI, Ali SJ. Vitamin E and telmisartan attenuates doxorubicin induced cardiac injury in rat through down regulation of inflammatory response. BMC Cardiovasc Disord. 2012;12:63.
49. Adamcova M, Sterba M, Simunek T, Potacova A, Popelova O, Mazurova Y, Gersl V. Troponin as a marker of myocardiac damage in drug-induced cardiotoxicity. Expert Opin Drug Saf. 2005;4(3):457-72.
50. Babuin L, Jaffe AS. Troponin: The biomarker of choice for the detection of cardiac injury. CMAJ. 2005 Nov 8;173(10):1191-202.
51. Teng XW1, Abu-Mellal AK, Davies NM. Formulation dependent pharmacokinetics, bioavailability and renal toxicity of a selective cyclooxygenase-1 inhibitor SC-560 in the rat J Pharm Pharm Sci. 2003;6(2):205-10.
52. Burke JF Jr, Laucius JF, Brodovsky HS, Soriano RZ. Doxorubicin Hydrochloride-Associated Renal Failure. Arch Intern Med. 1977;137(3):385-8.
53. Luo R, Li Y, He M, Zhang H, Yuan H, Johnson M, Palmisano M, Zhou S, Sun D. Distinct biodistribution of doxorubicin and the altered dispositions mediated by different liposomal formulations. Int J Pharm. 2017;519(1-2):1-10.
54. Manjunath K, Venkateswarlu V. Pharmacokinetics, tissue distribution and bioavailability of clozapine solid nanoparticles after intravenous and intraduodenal administration. J Control Release. 2005;107(2):215-28.
55. Martinez SE, Sayre CL, Davies NM. Pharmacometrics of 3-Methoxypterostilbene: A Component of Traditional Chinese Medicinal Plants. Evid Based Complement Alternat Med. 2013;2013:261468.

56. Schulze JD, Waddington WA, Eli PJ, Parsons GE, Coffin MD, Basit AW. Concentration-Pharm Res. 2003;20(12):1984-8.
57. Schulze JD, Waddington WA, Eli PJ, Parsons GE, Coffin MD, Basit AW.The effect of polyethylene glycol 400 on gastrointestinal transit: Implications for the formulation of poorly-water soluble drugs. Pharm Res. 2003;20(12):1984-8.
58. Ma BL, Yang Y, Dai Y, Li Q, Lin G, Ma YM. Polyethylene glycol 400 (PEG400) affects the systemic exposure of oral drugs based on multiple mechanisms: Taking berberine as an example. RSC Adv. 2017; 7: 2435–42.
59. Olson RD, Mushlin PS. Doxorubicin cardiotoxicity: Analysis of prevailing hypotheses. FASEB J. 1990;(13):3076-86.
60. Cote B, Carlson LJ, Rao DA, Alani AWG. Combinatorial resveratrol and quercetin polymeric micelles mitigate doxorubicin induced cardiotoxicity in vitro and in vivo. J Control Release. 2015;213:128-133
61. Yagmurca M, Yasar Z, Bas O. Effects of quercetin on kidney injury induced by doxorubicin. Bratisl Lek Listy. 2015;116(8):486-9.
62. Heeba GH, Mahmoud ME. Dual effects of quercetin in doxorubicin-induced nephrotoxicity Environ Toxicol. 2016;31(5):624-36.

CHAPTER 5

PHARMACEUTICAL CHARACTERIZATION OF MYONOVIN®, A NOVEL SKELETAL MUSCLE REGENERATOR: *IN SILICO, IN VITRO, IN VIVO* STUDIES

A version of this chapter has been published:

Alrushaid S, Davies NM, Anderson JE, Le T, Yáñez JA, Maayah ZH, El-Kadi AOS, Rachid O, Sayre CL, Löbenberg R, Burczynski FJ. Pharmaceutical Characterization of MyoNovin®, a Novel Skeletal Muscle Regenerator: in silico, in vitro, in vivo Studies. J Pharm Pharm Sci. 2018;21(1s):1-18.

5.1. ABSTRACT

PURPOSE: MyoNovin® is a novel skeletal muscle-regenerating compound developed through synthesis of two nitro groups onto a guaifenesin backbone to deliver nitric oxide to skeletal muscle with a potential to treat muscle atrophy. The purpose of this study was to utilize *in silico*, *in vitro*, and *in vivo* approaches to characterize MyoNovin® and examine its safety, biodistribution, and feasibility for drug delivery. **METHODS:** *In silico* software packages were used to predict the physicochemical and biopharmaceutical properties of MyoNovin®. In vitro cardiotoxicity was assessed using human cardiomyocytes (RL-14) while effects on CYP3A4 metabolic enzyme and antioxidant activity were examined using commercial kits. A novel HPLC assay was developed to measure MyoNovin® concentration in serum, and delineate initial pharmacokinetic and acute toxicity after intravenous administration (20 mg/kg) to male Sprague-Dawley rats. **RESULTS:** MyoNovin® showed relatively high lipophilicity with a LogP value of 3.49, a 20-fold higher skin permeability (19.89 cm/s*10^7) compared to guaifenesin (0.66 cm/s*10^7), and ~10-fold higher effective jejunal permeability (2.24 cm/s*10^4) compared to guaifenesin (0.26 cm/s*10^4). In vitro, MyoNovin® was not cytotoxic to cardiomyocytes at concentrations below 8 μM and did not inhibit CYP3A4 or show antioxidant activity. *In vivo*, MyoNovin® had a short half-life ($t_{1/2}$) of 0.16 h, and a volume of distribution V_{ss} of 0.62 L/kg. Biomarkers of MyoNovin® cardiac and renal toxicity did not differ significantly from baseline control levels. **CONCLUSIONS:** The predicted high lipophilicity and skin permeability of MyoNovin® render it a potential candidate for transdermal administration while its favourable intestinal permeation suggests it may be suitable for oral administration. Pharmacokinetics following IV administration of MyoNovin® were delineated for the first time in a rat model.

Preliminary single 20 mg/kg dose assessment of MyoNovin® suggest no influence on serum troponin or β-N-Acetylglucosaminidase.

5.2. INTRODUCTION

Skeletal muscle atrophies are characterized by loss of skeletal muscle mass due to aging, prolonged immobility, denervation, and/or other factors. To our knowledge, there is no clinically available pharmacological treatment specifically for muscle atrophy. Recent work revealed that nitric oxide (NO) plays an important role in skeletal muscle regeneration. The mechanism of regeneration involves the activation of satellite cells that are located in close proximity to the skeletal muscle fiber and are mitotically quiescent in adult muscle under normal physiological conditions. Under some conditions, however, such as mechanical stretching of muscle fibers and exercise, satellite cells are activated, resulting in their proliferation (1, 2). Both NO and hepatocyte growth factor are required for satellite cell activation (3, 4). NO triggers the activation of resting satellite cells to enter the cell cycle (5) and hepatocyte growth factor also promotes satellite cell cycling by binding to the c-met receptor and enhancing cell migration by activated myogenic precursor cells (6). The activation of satellite cells, thus, contributes to skeletal muscle growth from exercise and repair following injury or disease onset (7,8).

A study published by our group showed that transdermal administration of a clinically utilized nitric oxide donor, isosorbide dinitrate, to normal mice promoted satellite cell cycling as it increased DNA synthesis by 19-24% in adult muscle (9). Similarly, administration of methocarbamol produced a 28% increase in DNA synthesis. Co-administration of isosorbide dinitrate and methocarbamol had an additive effect, producing a 38% increase in DNA synthesis. Such observations led to the development of MyoNovin® (10), a novel nitric oxide donor

designed to specifically deliver NO to skeletal muscles. MyoNovin® was chemically synthesized by attaching two nitro groups to guaifenesin. Guaifenesin is a mucolytic agent with muscle relaxant activity and is an active metabolite of methocarbamol. The guaifenesin backbone of MyoNovin® is anticipated to act as a carrier for delivery of NO to skeletal muscle fibers, triggering satellite cell activation and ultimately muscle growth and repair (9). The same report showed that NO was released from homogenates of both liver and skeletal muscle after treatment with MyoNovin® using experiments with electron paramagnetic resonance (EPR) spectroscopy. Furthermore, MyoNovin® increased satellite cell activation and proliferation in normal mice as it increased DNA synthesis by 37-39% 24 h after a single transdermal treatment and 40-55% following 24 h of a single oral dose (9).

Given the essential role of NO in muscle regeneration, the promising results of MyoNovin® efficacy both *in vitro* and *in vivo* in normal (9) and dystrophic mice (11) and the fact that there are no viable pharmacological treatments to treat muscle atrophy or promote skeletal muscle regeneration, MyoNovin® could be a feasible therapeutic approach to treat conditions such as skeletal muscle injury and atrophy of various origins. MyoNovin® is a relatively new chemical derivative of guaifenesin, and synthesis of MyoNovin® from guaifenesin would be expected to alter the physicochemical and biopharmaceutical properties, and pharmacokinetic and toxicity profiles of the molecule. Thus, for further development of MyoNovin® as a potential drug to promote muscle growth and repair, it is necessary to characterize its safety and explore its pharmacokinetics following IV administration.

We, therefore, conducted the current study to determine the feasibility of MyoNovin® for drug delivery and delineate preliminary pharmacokinetic and selected acute toxicity by characterizing the compound *in silico*, *in vitro*, and *in vivo*. The physicochemical and

biopharmaceutical properties of MyoNovin® were examined for the first time utilizing in silico tools, while its effects on CYP450 enzymes and cardiac safety were examined in vitro. Furthermore, a novel reverse-phase high-performance liquid chromatography (RP-HPLC) assay was developed to measure MyoNovin® serum concentrations and to delineate its pharmacokinetics in a rat model. The cardiac toxicity of MyoNovin® was assessed by examining its effects on cardiomyocytes in vitro and as measured by plasma concentrations of cardiac troponin *in vivo*, while renal toxicity was assessed by measuring *in vivo* levels of a renal toxicity biomarker, β-N-acetylglucosaminidase (NAG) and urinary output 24 h post-dose.

5.3. METHODS

5.3.1. Chemicals and Materials

Methoxy-phenol (guaiacol), guaifenesin, allybromide, silver nitrate, acetone, brine, pinostrobin, PEG-400 and DMSO were purchased from Sigma (St. Louis, MO, USA). Beta-2-methoxyphenoxy-lactic acid was obtained from BOC Sciences (Shirley, NY, USA). HPLC grade acetonitrile and methanol, ethyl acetate, and hexane were purchased from Fisher Scientific (Ottawa, ON, CA). Ultrapure water from a Milli-Q® system (Millipore, Billerica, MA, USA) was used for the mobile phase. HPLC C18 Phenomenex Kinetex® column (5 μm, 250 x 4.6 mm), vials, inserts, and, 0.2 um nylon filter membranes were purchased from Phenomenex® (Torrance, CA, USA). Sterile heparin/50% dextrose catheter lock solution and blunt needles were obtained from SAI Infusion Technologies, Strategic Applications (Lake Villa, IL, USA). Cytochrome P450 kit catalogue # P2857 was from Life Technologies (Burlington, ON, CA). Cayman

antioxidant assay kit catalogue # 709001 was purchased from Cayman Chemical (Ann Arbor, MI), cytochrome P450 kit catalogue # P2857 was from Life Technologies (Burlington, ON).

5.3.2. Chemical Synthesis of MyoNovin®

MyoNovin® was synthesized by modifying the Wang et al procedure (9). A schematic representation of MyoNovin®'s synthesis is illustrated in Figure 5.1. To a stirred suspension of methoxy-phenol 1 (1.24 g, 0.01 mol) in 20 mL of dry acetone, allyl bromide (1.45 g, 0.012 mol) was added, and the mixture was heated overnight at 70˚C. The resulting solution was cooled to room temperature (RT) and filtered through sintered glass funnel to remove any solid residues. The filtrate was evaporated under reduced pressure to obtain 2 allyloxy-2-methoxy-benzene (1.51 g) as a colourless liquid. To an ice-cooled stirred solution of compound 2 (1.0 g; 6.09 mmol) in 12 mL of acetonitrile (CH_3CN) , silver nitrate ($AgNO_3$, 0.024 mol) was added followed by iodine (I_2, 1.56 g, 0.024 mol). After iodine has dissolved, the reaction was refluxed for 12 h, filtered, poured into water and extracted with ethyl acetate (EtOAc). The organic layer was washed with brine and evaporated under reduced pressure. The oil obtained was purified by flash chromatography (eluent from hexanes/EtOAc 10/1 to 3/1 v/v) to isolate compound 3 (1.24 g) as a yellow liquid. The chemical structure of MyoNovin® was confirmed by H_1NMR. H_1NMR ($CDCl_3$): δ = 3.85 (s, 3H), 4.28 (d, 2H, J= 5.2 Hz), 4.81 (dd, 1H, J = 6.6 Hz, J = 12.9 Hz), 4.98 (dd, 1H, J = 3.3 Hz, J = 12.9 Hz), 5.56-5.64 (m, 1H), 6.87-7.08 (m, 4H).

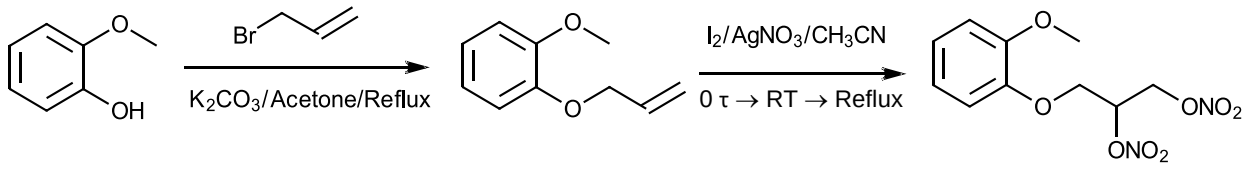

2-methoxy-phenol

allyloxy-2-methoxy-benzene

1-(3,4-bis-nitrooxy-butoxy)-2-methoxy-benzene

1 **2** **3**

Figure 5.1. A schematic diagram of MyoNovin® synthesis.

5.3.3. Physicochemical and Biopharmaceutical Properties

Gastro-Plus™, Marvin Sketch®, and Virtual Computational Chemistry Laboratory Computer modelling software were utilized to predict the physicochemical properties of MyoNovin® compared to its precursor guaifenesin. Portions of these results were generated by GastroPlus™ software (Version 9.0) provided by Simulations Plus, Inc. (Lancaster, California, USA). ADMET Predictor™ was used for modeling the biopharmaceutical and physicochemical as well pharmacokinetic parameters.

LogP and LogS values of MyoNovin® were predicted using online computer software (VCCLAB, Virtual Computational Chemistry Laboratory) (12,13). pKa, logP, logD at pH 7.4, and solubility at pH 7.4 were calculated using MarvinSketch™ (ChemAxon Ltd., Cambridge, MA, USA), pKa and logP were calculated using GastroPlus™ (Simulations Plus, Inc., Lancaster, CA, USA).

5.3.4. Effect of MyoNovin® on Metabolic Enzymes

The effect of MyoNovin® on CYP3A4 was examined using a CYP Vivid kit from Life Technologies following the manufacturer's instructions. On the day of the experiment stock solutions of MyoNovin® and the positive control were prepared in DMSO then further diluted with the assay buffer to achieve a final concentration of 0.01, 0.1, 1, 10, 50, and 100 μM/well. The assay was performed using black clear bottom 96-well plates in quadruplicates. To run the assay 40 μl of the test compounds or the positive control, 50 μl of a master pre-mix of CYP450 BACULOSOMES® (microsomes of insect origin expressing a single human CYP 450) and the regeneration system were combined in each well and incubated for 20 min at room temperature (23 ± 1℃). The reaction was initiated by adding 10 μl a mixture of the Vivid® fluorescent substrate and $NADP^+$. The fluorescence was measured immediately after the initiation of the reaction at excitation/emission wavelengths of 485 and 520 nm using a Synergy HT multi-well plate reader (Biotek Instruments Inc., Winooski, VT, USA). The inhibitory effect of MyoNovin® on CYP3A4 was compared to ketoconazole, a positive inhibitor of CYP3A4 and results expressed as % inhibition. The concentration of the positive control ketoconazole (10 μM) was chosen based on the manufacture's guidelines. More information about the assay can be found in the technical bulletin of the assay kit.

5.3.5. Antioxidant Activity of MyoNovin®

The antioxidant capacity of MyoNovin® and derivatives was examined at 1, 10, 50, and 100 μg/mL using a commercial assay kit from Cayman Chemical following manufacturer's instructions. The assay is based on the ability of the antioxidant in the sample to inhibit the

oxidation of ABTS® (2,2'-azino-di-[3-ethylbenzthiazoline sulphonate]) to ABTS®.+ by metmyoglobin. The amount of ABTS produced is measured at 750 nm. Presence of antioxidants will supress absorbance at 750 nm. Stock solutions of MyoNovin®, guaifenesin, β methoxy-phenoxy-lactic acid, allyloxy-2-methoxy-benzene and the positive control were prepared in DMSO on the day of the experiment then further diluted with DMSO to achieve a final concentration of 1, 10, 50 and 100 μg/mL. The assay was performed in clear 96-well plates with 4 replicates at each concentration. To run the assay, 10 μl of test compounds were added to each well followed by 10 μl of metmyoglobin and 150 μl of chromogen. Afterwards, 40 μl of hydrogen peroxide working solution was added to each well with 1 min to initiate the reaction. The 96-well plate was covered and incubated on a shaker for 5 min at room temperature (23 ± 1°C). The absorbance was measured at 750 nm using a Synergy HT multi-well plate reader and Gen5™ software for data analysis (Biotek Instruments Inc., Winooski, VT, USA). The antioxidant activity of MyoNovin®, guaifenesin, β methoxy-phenoxy-lactic acid, and allyloxy-2-methoxy-benzene was compared to that of Trolox® (6-hydroxy,2,5,7,8-tetramethylchroman-2-carboxylic acid), which is a water soluble vitamin E (α-tocopherol) analog and commonly used as a standard for antioxidant activity. Results were expressed as molar equivalents of Trolox®. Quercetin was used a positive control at 10 and 100 μg/mL.

5.3.6. Effects of MyoNovin® on Human Cardiomyocytes

The safety of MyoNovin® on cardiac tissue was assessed using human cardiomyocytes RL-14 cells (American Type Cell Culture Patent Deposit Designation PTA-1499 Mannanas, VA, USA). Cells were grown in 75 cm2 tissue culture flasks at 37°C in a humidified incubator with

5% CO2 containing DMEM/F-12, phenol red supplemented with 12.5% fetal bovine serum, 20 μM L-glutamate, 100 IU penicillin G and 100 μg/mL streptomycin. Following 3-4 days of incubation, cells were detached using trypsin and seeded on 12-well culture plates with DMEM/F-12 for 24 h. Cells were subsequently washed with PBS, replenished with serum free media, and treated with MyoNovin® at 2, 4, 8, 16, and 32 μM for 24 h. Effects of MyoNovin® on RL-14 viability were determined using MTT (3-(4,5-dimethylthiazol-2-yl)-2,5-diphenyltetrazolium bromide) assay. The assay measures the capacity of cells to convert MTT to coloured formazan crystals, as described previously (14,15).

5. 3.7. HPLC Analysis of MyoNovin®

The Shimadzu HPLC system (Kyoto, Japan) consisting of LC-20AB prominence liquid chromatograph, SIL-10AF auto-injector, SPD-10AV UV-VIS detector, and SCL-10A system controller was used for analysis. Separation was achieved using a C18 Phenomenex Kinetex® column (5 μm, 250 x 4.6 mm) with UV detection at 275 nm. The mobile phase was prepared by mixing acetonitrile:water:methanol (75:20:5 v/v), filtered through a 0.2 μm nylon filter and degassed using reduced pressure prior to use. Separation was carried out isocratically at ambient temperature (22±1°C) with a flow rate of 0.6 mL/min. Pinostrobin was used as the internal standard. Shimadzu EZStart (Version 7.4) software was used for data acquisition and integration. Samples were freshly prepared on day of analysis and injected into the HPLC system.

5.3.8. Preparation of Standard Solutions

Stock solutions of MyoNovin® (10 mg/mL) and the internal standard pinostrobin (1 mg/mL) were prepared in DMSO, protected from light, and stored at -20℃. Working solutions were freshly prepared in DMSO to obtain a final concentration of 0.5, 1.0, 10.0, and 100 μg/mL in rat serum or urine. Standard solutions of MyoNovin® were prepared by spiking MyoNovin® (0.5-100 μg/mL) and pinostrobin (10 μg/mL) in 100 μl of blank rat serum or urine. The final concentration of DMSO in spiked standards of serum and urine samples did not exceed 3%.

5.3.9. Calibration Curves

Calibration curves were constructed by plotting the peak area ratio of MyoNovin® to the internal standard (pinostrobin) versus calibration standard concentrations of MyoNovin®.

5.3.10. Linearity, Lower Limit of Quantification, and Lower Limit of Detection

Linearity was assessed based on the coefficient of determination (r^2) of the calibration curve using unweighted least squares linear regression. The lower limit of quantitation (LOQ) was determined based on the lowest concentration that showed a ± 15% difference between the actual added concentration and the average calculated concentration. The lower limit of detection (LOD) was estimated by comparing signals of known low concentrations of MyoNovin® spiked in serum to blank serum samples without MyoNovin®. The concentration of MyoNovin® with a 1:3 signal to noise ratio was considered the lower limit of the analytical assay.

5.3.11. Accuracy, Precision and Recovery

The analytical method was evaluated by calculating the intra-day variation of spiked MyoNovin® standards in rat serum. The intra-day variation was determined by comparing 5 replicates of different concentrations of MyoNovin® (5, 10, 25, 50, and 100 μg/mL) spiked in serum on 5 days in a 1-week period. Calibration curves were established each day. Precision was evaluated using Coefficient of Variance ($CV=SD/C_{average}$) where SD is the standard deviation and $C_{average}$ is the mean calculated concentration of five replicates. Accuracy was assessed by comparing the percentage error of calculated concentration to the actual concentration added using the equation $Bias=C_{calculated}-C_{theoretical}/C_{theoretical}$ where calculated is the concentration calculated from calibration curve and $C_{theoretical}$ is the actual concentration added (16).

Percent recovery was determined by comparing peak area ratios of MyoNovin® to the internal standard (pinostrobin) after extracting MyoNovin® from serum-spiked samples to respective samples spiked in the mobile phase without extraction.

5.3.12. Animals

This study was approved by the Bannatyne Campus Animal Care Committee at the University of Manitoba (protocol #16-004) in conformity with the Canadian Council on Animal Care guidelines. Male CD® Sprague-Dawley rats (average weight: 250±25 g) were obtained with the jugular vein surgically cannulated using polyurethane-silastic blended catheters from Charles River Labs (St. Constant, QC, Canada). Rats were housed individually in temperature-controlled rooms with a 12 h light/dark cycle. All animals had free access to Purina Rat Chow (5001) and water, except when specified below. Animals were acclimatized in standard cages with

environmental enrichment for a minimum of 3 days prior to commencing the pharmacokinetic study.

5.3.13. Pharmacokinetic study

Jugular cannulas in 5 rats were flushed daily with a sterile heparin/50% dextrose catheter lock solution to maintain the patency as advised in the technical bulletin supplied with the animals from Charles River (17). Each animal was placed in a separate metabolic cage overnight and fasted overnight (12 h) before drug administration (IV; 20 mg MyoNovin®/kg BW). The dose was selected based on our previous study whereby mice received a single oral dose of 80 mg/kg (9). MyoNovin® was freshly reconstituted in 3% DMSO and 97% PEG-400 prior to dosing. Animals received water ad libitum pre- and post-dosing. Food was provided 2 hours post-dosing. Serial blood samples (0.30 mL each) were collected at 0, 1, 5, 15, and 30 min, followed by 1, 2, 4, 6, 12, and 24 h after IV drug administration. At 24 h following drug administration, animals were euthanized and exsanguinated. Immediately after all blood-collection time points (except the terminal point), the cannula was flushed with the same volume of 0.9% saline to replenish the collected blood volume. The dead volume of the cannula was filled with a small volume (~0.15 mL) of heparinized lock solution after each blood draw to maintain the patency of the cannula. Blood samples were collected in polypropylene microcentrifuge tubes and centrifuged at 15,000 rpm for 5 min (Beckman Microfuge centrifuge, Beckman Coulter Inc., Fullerton, CA, USA) to collect serum. Serum was stored at -20℃ until sample preparation for HPLC drug analysis. Urine samples were also collected from metabolic cages at 0, 2, 6, 12, and 24 h following MyoNovin® administration. The exact urine volume of each sample was recorded and urine stored at –20℃ until preparation for HPLC drug analysis.

5.3.14. Treatment of Serum Samples for Analysis

Pinostrobin (10 μg/ml final concentration) was added to 120 μL of all serum samples with the exception of the 0 h sample. Samples were vortexed for 1 min using a Vortex Genie-2 (VWR Scientific, West Chester, PA). One (1.0) mL of cold HPLC grade acetonitrile (pre-stored at - 20℃) was added to samples to precipitate plasma proteins, vortexed for 5 min (Vortex Genie-2, VWR Scientific), and centrifuged at 15,000 rpm for 15 min before the supernatant was transferred to new, labeled 2 mL centrifuge tubes. Samples were evaporated to dryness using a Savant SPD1010 SpeedVac Concentrator without heat (Thermo Fisher Scientific, Inc., Asheville, NC). The residue was reconstituted with 100 μL of mobile phase, vortexed for 1 min and centrifuged at 15,000 rpm for 5 min; the supernatant was transferred to HPLC vials and 120 μL was injected into the HPLC system.

5.3.15. Pharmacokinetic Analysis

Pharmacokinetic analysis was performed using data from individual rats, and the mean and standard error of the mean (SEM) calculated for each group. The elimination rate constant (k_{el}) was estimated by linear regression of serum concentration in the log-linear terminal phase. A non-compartmental model was fitted to the data for serum concentration versus time using Phoenix WinNonlin® software Ver. 6.3 (Pharsight Corporation, Mountain View, CA) to calculate the pharmacokinetic parameters in the terminal phase, namely total clearance (CL_{tot}), and volume of distribution (V_{ss}). The initial maximum serum concentration (C_0) was calculated by back extrapolation using Phoenix WinNonlin® software.

5.3.16. Assessment of Renal Toxicity

The potential renal toxicity that could be induced by MyoNovin® was assessed by examining urinary output and also by measuring a biomarker of renal toxicity in rat urine. The urinary output of rats over 24 h was monitored just before (24 h pre-dose period) and after administration of a single IV dose of MyoNovin® (20 mg/kg; 24 h post-dose period). Acute renal toxicity induced by any drug may result in a reduced total urinary output (18). The total urine volume excreted over 24 h post-dosing was compared to the total urine volume excreted over the 24 h pre-dosing.

NAG is a lysosomal enzyme found at high concentration in kidney tubule cells. Appearance of NAG in the urine is used as a sensitive, early marker of renal damage (19). Urine samples (100 µl) from pharmacokinetic studies after a single IV dose of MyoNovin® collected at 0, 2, 6, 12, and 24 h were analyzed to determine NAG concentrations without dilution on a Medica EasyRa automated clinical chemistry analyzer (Medica Corporation Bedford, MA) (20). Cumulative amounts of NAG excreted in the urine over the 24 h post-dosing with MyoNovin® were compared to cumulative amounts pre-dosing to assess renal toxicity.

5.3.17. Assessment of Cardiac Toxicity

The potential cardiac toxicity of MyoNovin® was also assessed in vivo utilizing a rat cardiac Troponin-I (cTnI) ultra-sensitive ELISA kit assay from Life Diagnostics, Inc. (West Chester, PA, USA). Blood samples from pharmacokinetic studies were collected at 24 h from the jugular vein after a single 20 mg/kg IV dose (n = 4). Samples were centrifuged to obtain serum

and stored at -20° C until analysis. On the day of analysis, cTnI concentrations were measured in serum samples following manufacturer's instructions.

5.3.19. Statistical Analysis

Compiled data were presented as mean and standard error of the mean (mean ± SEM) unless otherwise stated. Where possible, data were analyzed for statistical significance using SigmaPlot software (v. 13.0, Systat Software, Inc., San Jose, CA). Student's t-tests were employed for unpaired samples to compare means between two groups, while one-way ANOVAs were employed to compare the means of three or more groups followed by Tukey-Kramer multiple comparison Test between groups if necessary. A p-value less than 0.05 was considered statistically significant.

5.4. RESULTS

5.4.1. Physicochemical and Biopharmaceutical Properties

The physiochemical and biopharmaceutical properties of MyoNovin® were compared to those of its parent compound, guaifenesin. MyoNovin® had a lower predicted water solubility and higher LogP value compared to guaifenesin (Table 5.1), indicating higher lipophilicity. The pH-solubility profile of MyoNovin® (Figure 5.2A) shows that the solubility of MyoNovin® is not affected by changes in pH, while the solubility of guaifenesin increased at pH >12 (Figure 5.2B). Examination of the solubility of MyoNovin® in simulated gastric and gastrointestinal fluids revealed that MyoNovin® has a 1000-fold lower predicted solubility in the fasted state in

simulated gastric fluid (0.004 mg/mL) compared to guaifenesin (4.574 mg/mL) (Figure 5.3). The predicted solubility of MyoNovin® in simulated intestinal fluid in the fed state (0.756 mg/mL) was more than 30-fold higher than in the fasted state (0.022 mg/mL), suggesting better oral absorption of MyoNovin® would be achieved when it is administered with food. Interestingly, prediction of guaifenesin solubility in simulated intestinal fluid showed that its solubility is higher in fasted state (2.085 mg/mL) compared to that in the fed state (0.272 mg/mL).

Predicting transmembrane permeability of MyoNovin® across skin and the intestine using ADMET predictor™ software showed that MyoNovin® is expected to have a 20-fold higher skin permeability (19.89 cm/s*10^7) compared to guaifenesin (0.66 cm/s*10^7) and approximately 10-fold higher effective jejunal permeability (2.24 cm/s*10^4) than guaifenesin (0.26 cm/s*10^4) (Figure 4.4). Moreover, prediction of MyoNovin®'s permeability across Madin-Darbey Canine Kidney (MDCK) cells, epithelial cells of kidney origin and commonly used for screening permeability of investigational compounds in drug discovery, is expected to be (554.691 cm/s*10^4) 70-fold higher than guaifenesin (7.827 cm/s*10^4). The prediction suggests that MyoNovin® likely has a useful potential to be absorbed through skin and traverse the intestine barrier. Additionally, MyoNovin® appeared to be neither a substrate nor an inhibitor of P-glycoprotein (P-gp), a membrane transporter highly expressed in intestinal and renal epithelium and responsible for efflux of many xenobiotics (e.g., chemotherapeutic drugs), as shown in table 5.2.

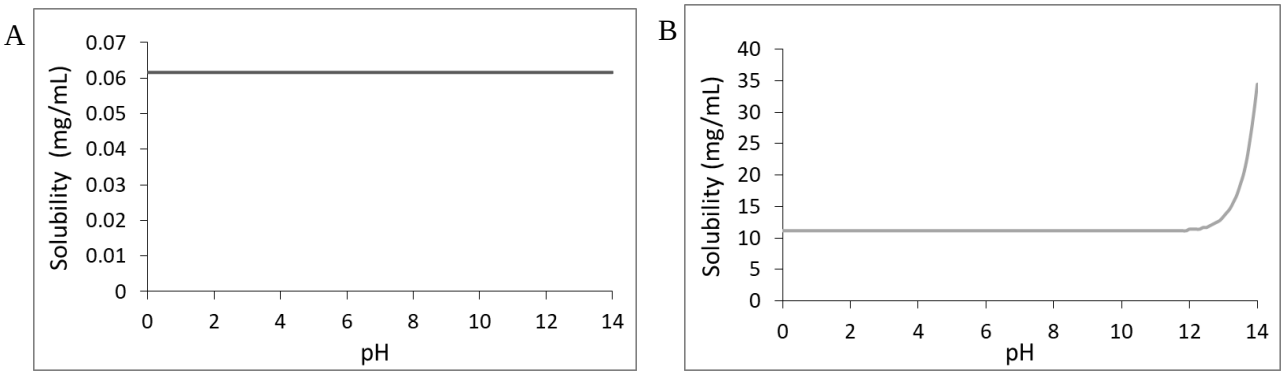

Figure 5.2. pH-solubility profile of (A) MyoNovin® and (B) guaifenesin predicted by Marvin Sketch.

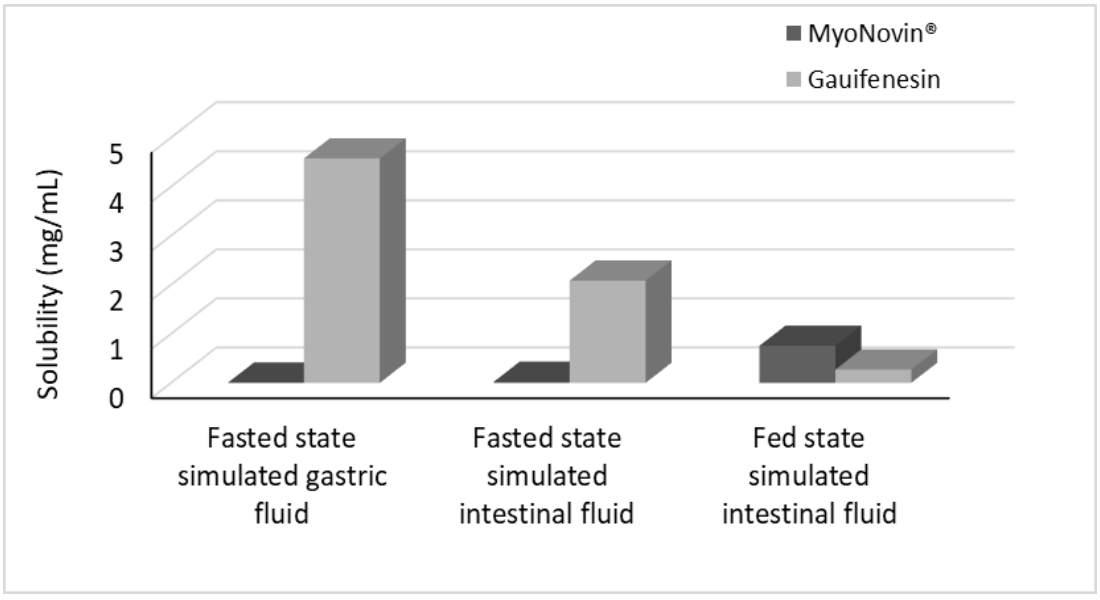

Figure 5.3. Predicted solubility of MyoNovin® and guaifenesin in human simulated gastrointestinal fluids as calculated by ADMET Predictor™ software.

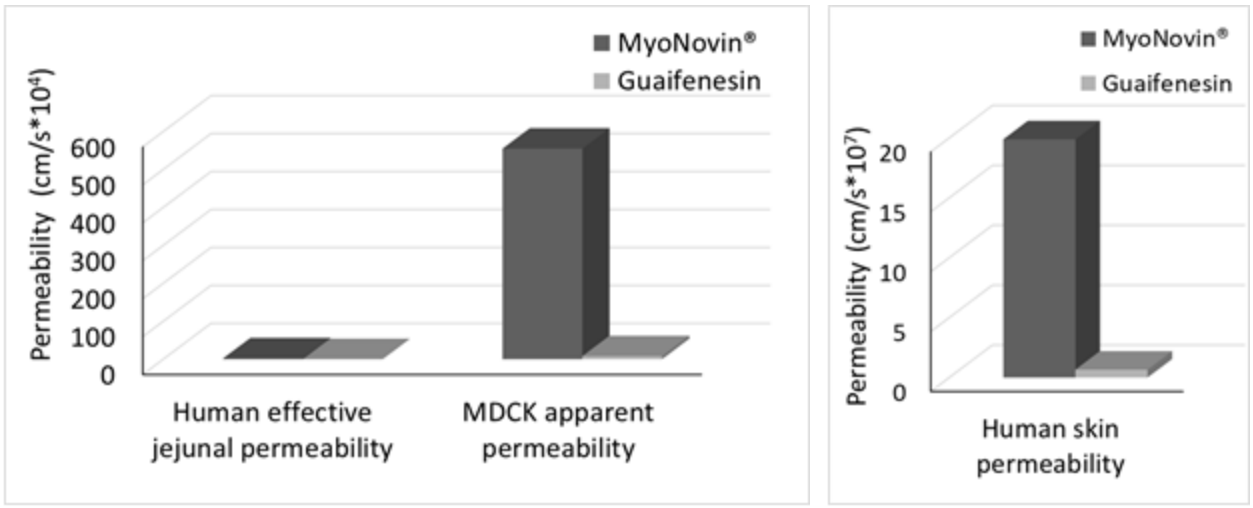

Figure 5.4. Predicted human intestinal and skin permeability of MyoNovin® and guaifenesin, and predicted permeability across MDCK (canine origin) using ADMET Predictor™ software.

Table 5.1. Physicochemical properties of MyoNovin® and guaifenesin predicted by software packages.

Compound	MyoNovin®	Guaifenesin
Structure	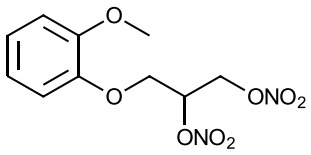	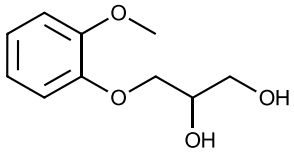
Molecular Weight (g/mol)	288.212	198.218
Formula	C10H12N2O8	C10H14O4
pKa (MarvinSketch)	No ionisable atoms	13.62, 15.56
pKa (GastroPlus™)	No ionisable atoms	No ionisable atoms
pKa (GastroPlus™, after fitting solubility)	No ionisable atoms	No ionisable atoms
logP (MarvinSketch)	2.19	0.34
logP (neutral, GastroPlus™)	3.49	0.59
logP (VCCLAB)	2.01±0.94	0.67±0.38
LogP (ADMET Predictor™, neural)	3.489	0.494
logD7.4 (MarvinSketch)	2.187	0.337
Solubility at pH 7.4 (MarvinSketch)	-3.67 logS	-1.25 logS
Solubility at pH 7.4 (MarvinSketch)	0.0616 mg/mL	11.15 mg/mL
logS (VCCLAB)	-2.44	-1.22

The predicted effects of MyoNovin® on metabolic enzymes, calculated using ADMET PredictorTM software, showed that MyoNovin® is expected to act as a substrate of CYP3A4 and as an inhibitor of CYP1A2 (Table 5.2). As well, MyoNovin® is expected to be ~90% bound to plasma proteins as opposed ~82% for guaifenesin (Table 5.3). The predicted volume of distribution for MyoNovin® was 0.389 L/kg, which is about 30-fold smaller than that of guaifenesin (11.980 L/kg).

Table 5.2. Biopharmaceutical properties of MyoNovin® and guaifenesin predicted by ADMET Predictor™ software.

Compound	**MyoNovin®**	**Guaifenesin**
Diffusion coefficient ($cm^2/s*10^5$)	0.856	0.569
P-gp Substrate (likelihood of intestinal efflux by P-gp)	No (95%)	Yes (91%)
P-gp Inhibition (intestinal)	No (94%)	No (72%)
OATP1B1 Inhibition (hepatic)	No (97%)	No (87%)
CYP3A4 Inhibition	No	No +
CYP3A4 Substrate	Yes	No +
CYP1A2 Inhibition	Yes (96%)	Yes (60%) +
CYP1A2 Substrate	No (83%)	NA
CYP2D6 Inhibition	No (95%)	No +
CYP2D6 Substrate	No (96%)	No (85%) +

+ www.Drugbank.ca (21), NA=not available

Table 5.3. Human pharmacokinetic models of MyoNovin® and guaifenesin predicted using ADMET Predictor™ software.

Compound	MyoNovin®	Guaifenesin
Human plasma protein binding (% unbound)	9.994	22.099
Human volume of distribution (Vd)	0.389	11.980
Blood-to-plasma concentration ratio (RBP)	0.890	0.869
Fraction unbound in human liver microsomes (S+fumic)	0.394	0.903

5.4.2. Effect of MyoNovin® on CYP3A4

The effect of MyoNovin® on CYP3A4 inhibition was examined utilizing a commercial assay kit. MyoNovin® did not inhibit CYP3A4 at concentrations between 0.01-50 μM (Figure 5.5). Only at 100 μM did MyoNovin® show inhibition of CYP3A4 (30%).

5.4.3. Antioxidant Activity

Nitric oxide exhibits anti-oxidant activity (22) by acting as a scavenger of reactive oxygen species. Thus, the antioxidant capacity of MyoNovin® was examined in vitro. Figure 5.6 shows that there is no difference in the antioxidant activity of MyoNovin® or its derivatives at 1, 10, 50, and 100 μg/mL compared to baseline, suggesting that MyoNovin® and derivatives do not exhibit antioxidant activity using this assay. However, a significant difference in the antioxidant activity was observed between MyoNovin® and its derivatives compared to quercetin, which is a potent antioxidant.

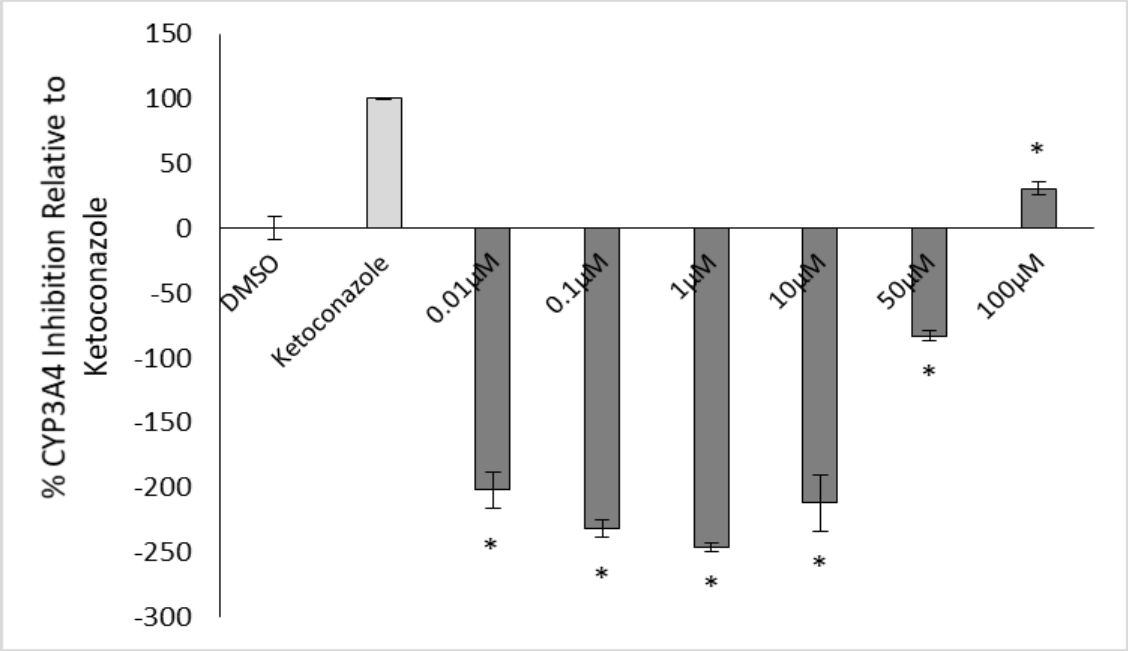

Figure 5.5. Percent (%) CYP3A4 enzyme inhibition by MyoNovin® (n=4; mean±SEM) expressed as % of the positive inhibitor (ketoconazole 10 µM). The concentration of DMSO did not exceed 0.1% in each well. *P<0.05 compared to ketoconazole.

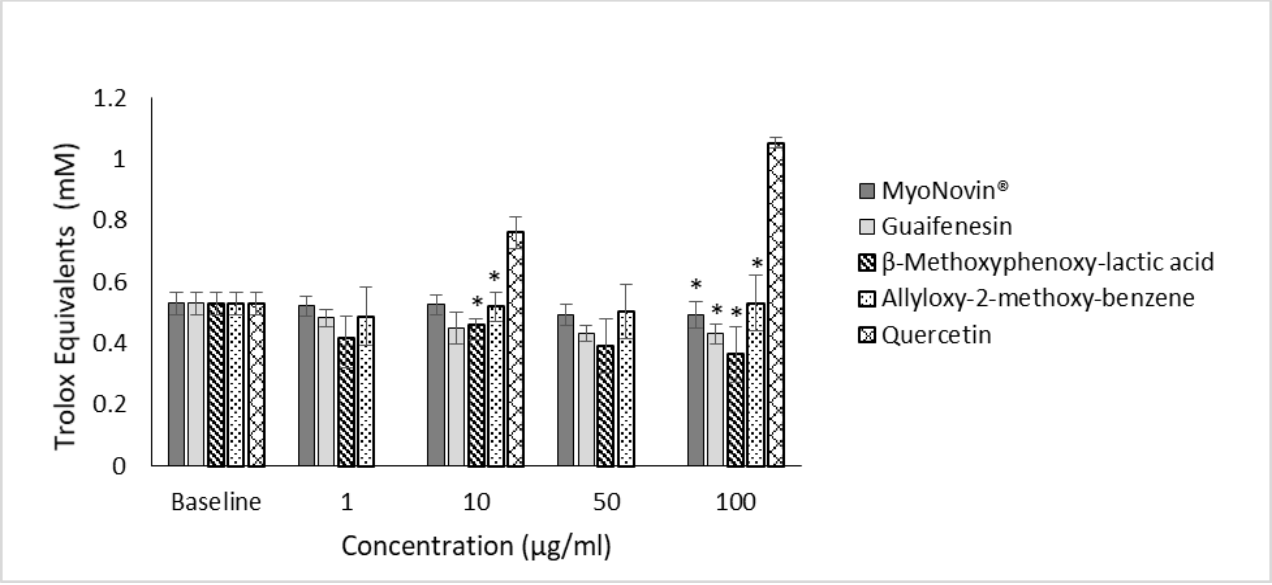

Figure 5.6. Antioxidant activity of MyoNovin® and its derivatives (n=4 mean±SEM). *P<0.05 compared to quercetin.

5.4.4. Effects on Human Cardiomyocytes (RL-14)

The effects of MyoNovin® on human cardiomyocytes was investigated after treatment (from 2-32 μM) for 24 h by the MTT assay. Figure 5.7 shows that the viability of RL-14 cells at 4 μM MyoNovin® was ~94%; since this was not statistically different from the untreated control cells, the finding indicated that MyoNovin® is likely non-toxic to cardiomyocytes at concentrations up to 4 μM. At 8 μM cell viability was only about 78%, significantly lower than controls, suggesting that MyoNovin® did induce some cardiotoxicity resulting in ~22 % cell death.

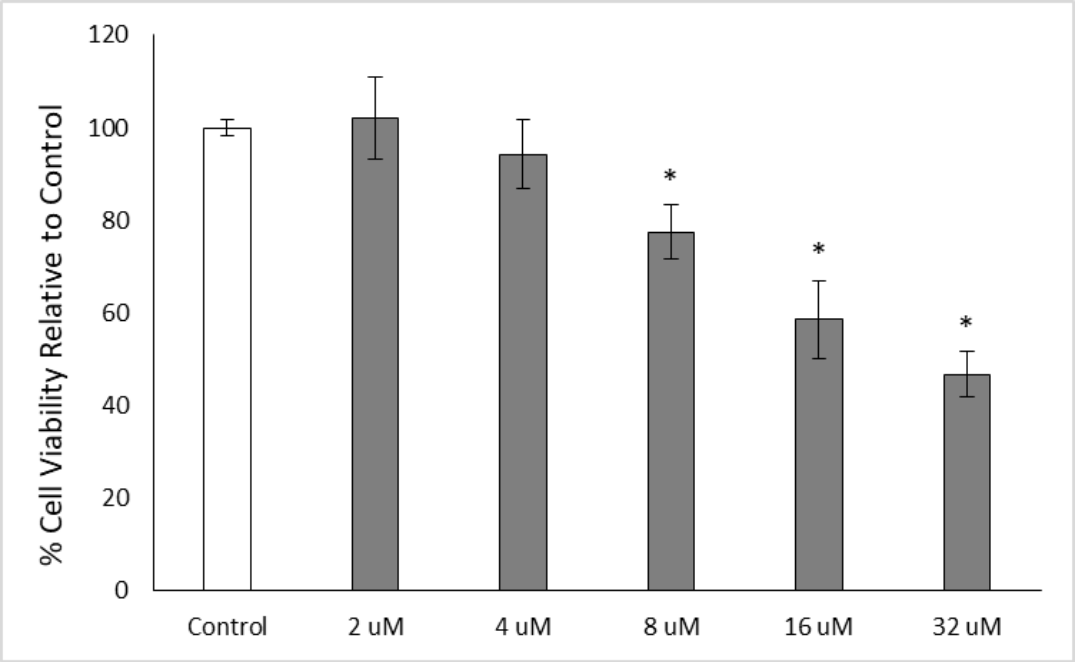

Figure 5.7. Viability of human RL-14 cardiac myocytes measured by an MTT assay after treatment with MyoNovin® at 2, 4, 8, 16 ,and 32 μM (0.6,1.2 ,2.3, 4.6, and 9.2 μg/mL) for 24 hours (n=4; mean ± SEM) relative to untreated control. *P<0.05 compared to control.

5.4.5. HPLC Analysis of MyoNovin®

A RP-HPLC assay was developed to quantitate MyoNovin® in serum and urine samples collected during pharmacokinetics experiments. Optimal separation between MyoNovin® and the internal standard, pinostrobin, was achieved using the chromatography conditions described in methods. Chromatograms were free from peaks that co-eluted with the peaks of interest. Retention times of MyoNovin® and pinostrobin were 6.2 and 7.5 min, respectively (Figure 5.8). The acceptance criteria for the analytical method were in accordance with Food and Drug Administration (FDA) guidelines (23).

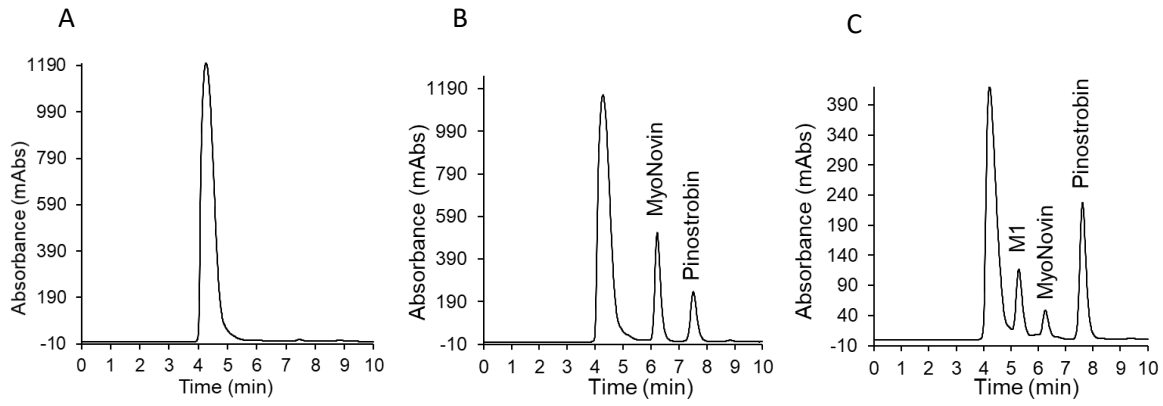

Figure 5.8. Representative chromatograms of (A) blank serum (B) MyoNovin® (100µg/mL) and pinostrobin (10 µg/mL) spiked in serum (C) MyoNovin®, pinostrobin and M1 1 min after administration of MyoNovin® (20mg/kg) to animals.

5.4.6. Linearity, LOQ, and LOD

Calibration curves of MyoNovin® showed excellent linearity and a coefficient of determination (r^2) of 0.99 over the range of 0.5-100 μg/ml. The LOQ was 5 μg/mL with corresponding CV of 13.21% and bias of -10.75% (Table 5.4). The LOD was determined to be 1 μg/mL, based on a 1:3 signal-to-noise ratio.

5.4.7. Accuracy, Precision and Recovery

The intra-day precision from five runs during one week showed that the assay CV% was <15% at the lowest concentration and <2% at the highest concentration (Table 5.4). The percent bias was -10.75% (CV=13.21%) and -2.63 (CV=1.22%) at 5 and 100 μg/mL, respectively. Percent recovery was 105% at the lower limit of quantification and 97% at 100 μg/mL MyoNovin®. The results show that intra-day coefficient of variance and bias intra-day variation were both below 15% at 5 μg/mL and within ± 5% over the range of 10-100 μg/mL when the percent recovery was >97%. These parameters indicated that the analytical method was sensitive, accurate and reproducible.

Table 5.4. Accuracy and precision of MyoNovin® in serum (n=5 days, mean ± SEM).

Concentration (Added)	Average (Calculated)	CV (%)	Bias (%)	Recovery (%)
5	4.46 ± 0.26	13.21	-10.75	105.16 ± 5.8
10	10.56 ± 0.21	4.43	5.61	105.13 ± 2.92
25	27.87 ± 0.39	3.1	11.47	99.34 ± 4.69
50	53.33 ± 0.95	3.99	6.66	98.34 ± 1.62
100	97.36 ± 0.53	1.22	-2.63	96.9 ± 4.12

5.4.8. Disposition and Pharmacokinetics of MyoNovin® after IV Administration

Following IV administration, MyoNovin® was detected in serum up to 30 min post-dosing (Figure 8) with a maximum extrapolated serum concentration (C_0) of 43.6 ± 8.8 μg/mL. The serum disposition profile of MyoNovin® showed an initial sharp decline in concentration over the first 5 min, representing a distribution phase; this was followed by a further rapid decline over the next 15-30 min (last measurable concentration), representing an elimination phase (Figure 5.9). The serum concentration versus time profile followed a bi-expotential pattern indicating that MyoNovin® resides beyond the vasculature and penetrates into tissues. Interestingly, at 1 min post-dosing, a new peak (M1) was also observed at an earlier retention time than that of MyoNovin® and was detectable for up to 1 h. The M1 peak decreased over time, similar to that of MyoNovin®, indicating that it could be a metabolite of MyoNovin® formed as result of NO release *in vivo*. Figure 5.10 shows a proposed schematic for the mechanism of NO and M1 release. Figure 5.11 illustrates possible metabolic pathways for MyoNovin® after the release of nitric oxide.

Table 5.5 demonstrates the pharmacokinetic parameters of MyoNovin® following a single IV administration (20 mg/kg). The half-life of MyoNovin® was 0.16 h (Table 5.5), suggesting that MyoNovin® remained intact for a short time before rapidly undergoing metabolism, possibly after, releasing nitric oxide. The volume of distribution (V_{ss}) of MyoNovin® was 0.62 ± 61.58 L/kg suggesting that it was distributed to tissues in a manner comparable to that predicted by ADMET Predictor™ software (Table 5.3). The total clearance was 3.10 ± 0.98 L/kg and AUC_{inf} and total body exposure was 8.13 ± 5.23 μg*h/mL.

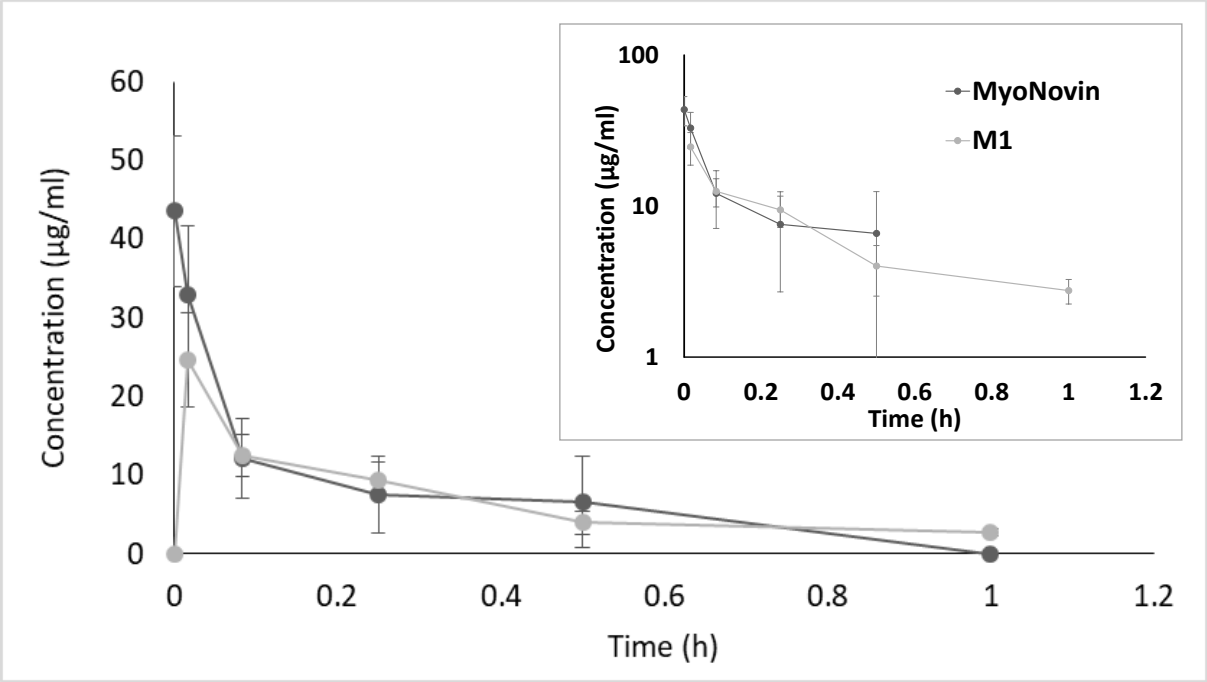

Figure 5.9. A graph of the serum concentration versus time for MyoNovin® after IV administration (20 mg/kg, n = 5, mean ± SEM). The figure insert shows the y-axis of the same serum concentration versus time curve on a Log scale.

Table 5.5. The pharmacokinetics of MyoNovin® in rat serum after IV administration (20 mg/kg) (mean ± SEM, n= 5 unless otherwise stated).

Pharmacokinetic parameter	MyoNovin®
C_0 (µg/mL)	43.6 ± 8.82
K_{el} (1/h)	12.6 ± 4.73
$t_{1/2}$ (h)	0.16 ± 0.1
AUC_{last} (µg.h/mL)	5.1 ± 2.34
AUC_{inf} (µg.h/mL)	8.13 ± 5.23
T_{last} (h)[1]	0.25
V_{ss} (L/kg)	0.62 ± 0.06
CL_{total} (L/h/kg)	3.10 ± 0.98

[1] median

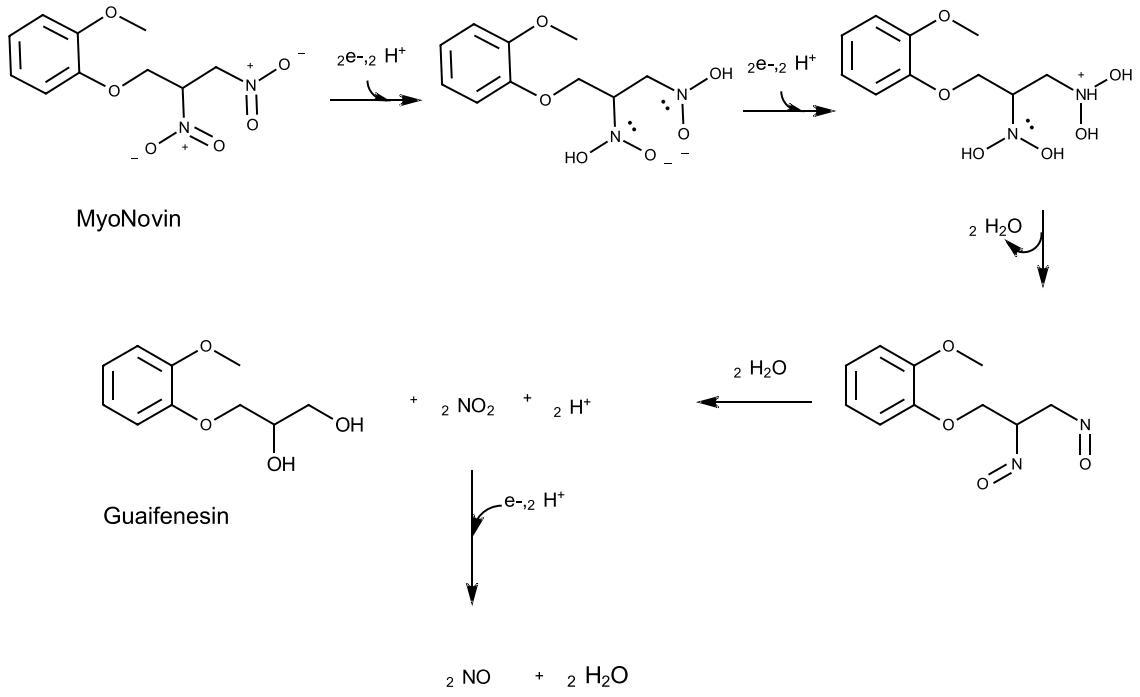

Figure 5.10. Proposed schematic representing MyoNovin® biotransformation *in vivo*, based on reference (24).

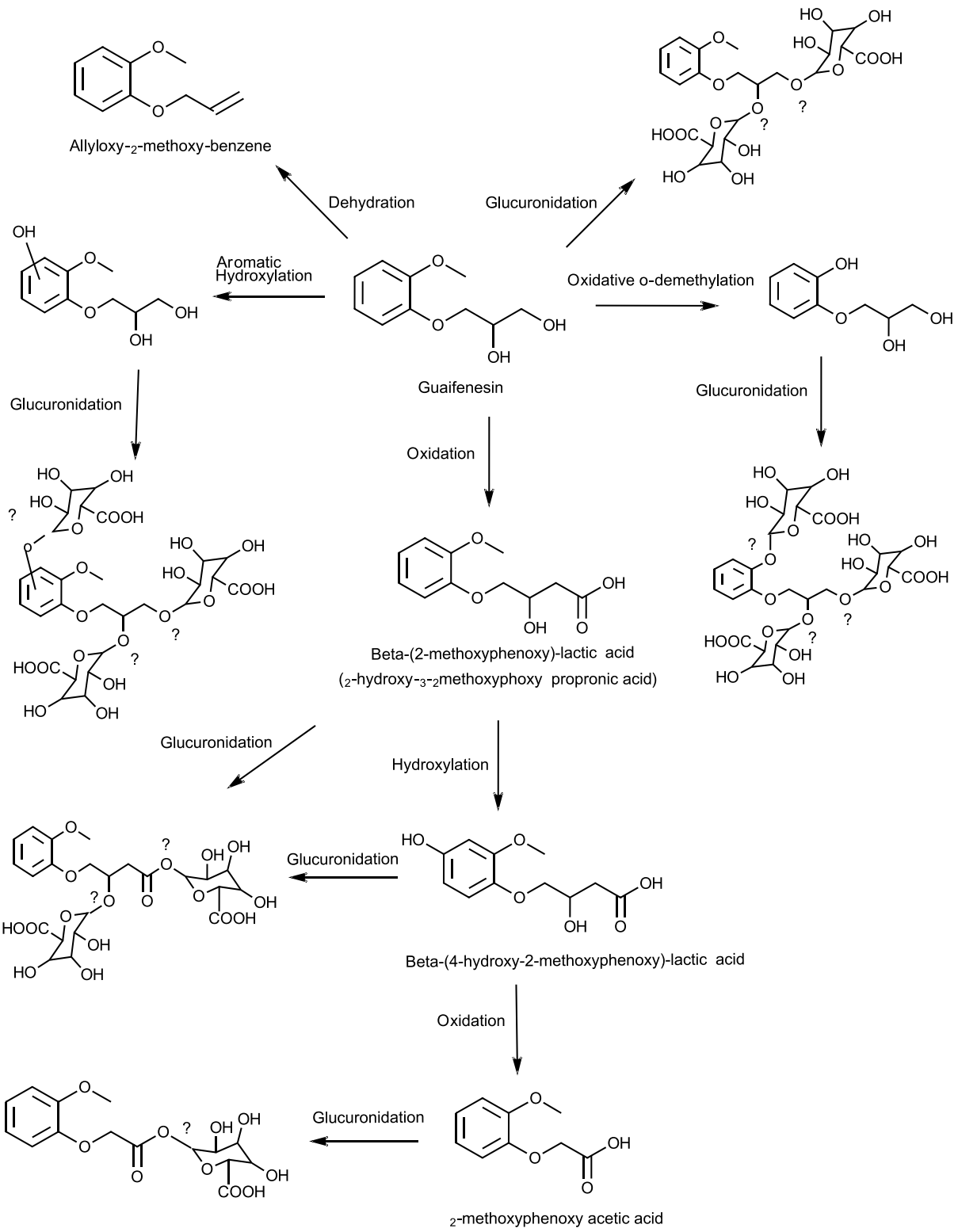

Figure 5.11. Schematic representation of proposed metabolic pathways for guaifenesin, based on references (25-29).

5.4.9. Renal Effects

Nitric oxide plays important physiological and pathophysiological roles in kidney function (30). Excessive NO production could induce renal toxicity (31). In addition, MyoNovin® could be metabolized to beta-(2-methoxyphenoxy)-lactic acid, a compound that has been localized in the presence of kidney stones (32). Therefore, the potential renal toxicity of MyoNovin® was assessed by examining the urinary output and also by measuring β-N-acetylglucosaminidase (NAG), a sensitive marker of kidney injury (33). There was no significant difference in total urine volume excreted, pre-dose suggesting that a single 20 mg/kg dose did not induce any adverse effect on the total urine excreted in 24 h post-dosing. (24.2±5.9 mL) pre-dose vs post dose (21.5 ±5.1 mL).

Cumulative NAG excreted in urine 24 h post MyoNovin® IV dosing (20 mg/kg) was not statistically different from the baseline control level of cumulative NAG excretion (Figure 5.12). A positive-control group of rats received a single IV dose of doxorubicin (10 mg/kg), a known nephrotoxic anti-cancer drug where there was a significant increase in cumulative urinary NAG excreted over the same period of time compared to baseline controls.

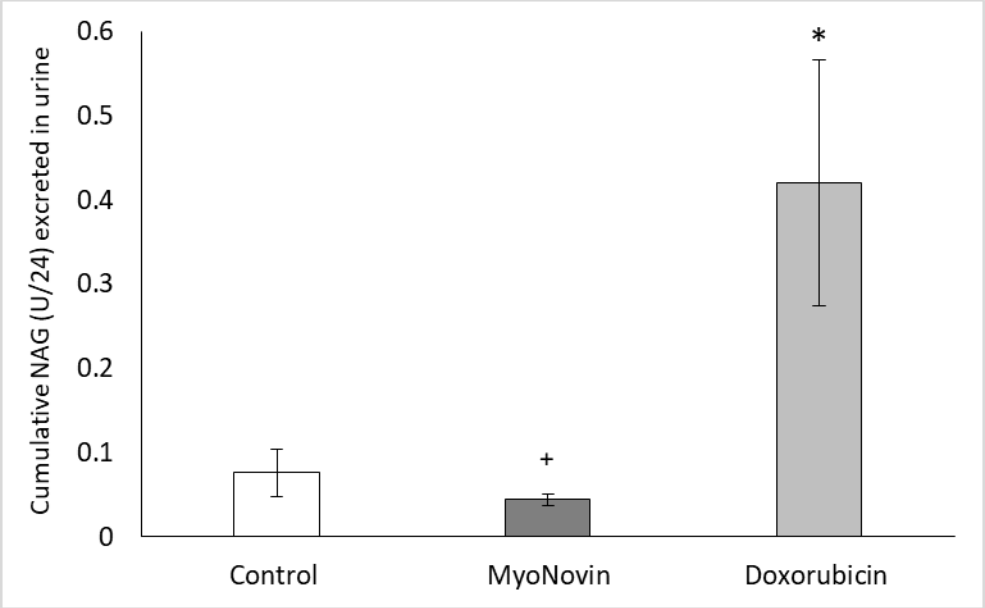

Figure 5.12. Cumulative NAG excreted in rat urine (U/24 h, mean ± SEM) post MyoNovin® IV (20mg/kg) compared to control and post doxorubicin IV (10mg/kg). Control (n=6), doxorubicin (n=3) and MyoNovin® (n=3). *P<0.05 compared to control, +p<0.05 compared to Doxorubicin.

5.4.5. Assessment of Cardiac Toxicity

Nitric oxide can play protective and/or detrimental roles in cardiac function (34). The potential cardiac toxicity of MyoNovin® was assessed by measuring levels of cardiac Troponin (cTnI), a sensitive marker of myocardial damage (35). Cardiac TnI concentrations in serum samples collected 24 h after MyoNovin® IV administration were not significantly different from baseline controls. Figure 5.13 shows cTnI concentration 24 h post MyoNovin® (20mg/kg IV) compared to those 24 h following a single IV dose of doxorubicin. Although the concentration of cTnI was much higher in the Doxorubicin group, it was not significantly different in from the control concentration, largely due to within-group variability.

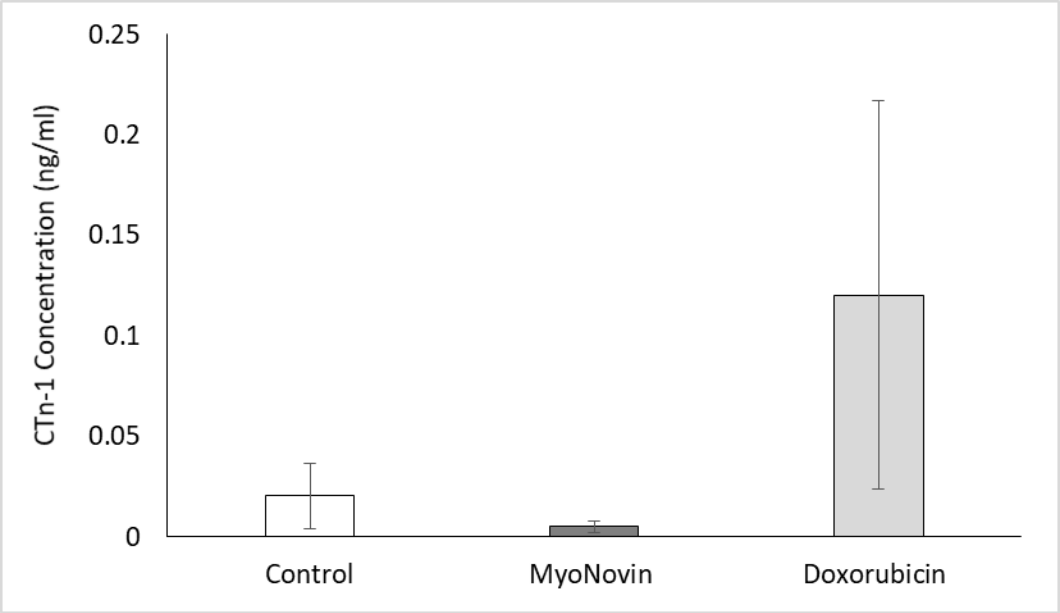

Figure 5.13. cTnI concentration (mean ± SEM) after 24 h of IV administration of MyoNovin® (20mg/kg) and doxorubicin (10mg/kg) compared to control cTnI. Control (n=7), MyoNovin® (n=4), and doxorubicin (n=3). There was no statistical difference observed among groups.

5.5. DISCUSSION

MyoNovin® was designed to deliver nitric oxide to skeletal muscle, thus providing a novel drug-delivery approach by utilizing guaifenesin as a carrier for transporting NO (9). While there are no clinically viable drugs that directly initiate skeletal muscle growth and regeneration, such treatment would be beneficial in restoring muscle mass in atrophic and some disease conditions. Thus, pharmaceutical development of MyoNovin® could lead to a viable pharmacological approach for the treatment of skeletal muscle atrophy associated with aging, disuse and denervation, and for the repair of skeletal muscle after injury or disease. MyoNovin® is a novel drug targeted toward skeletal muscle regeneration and with potentially lower levels of systemic toxicities typically associated with conventional NO donors. As MyoNovin® is an

investigational compound, its physicochemical properties, biodistribution, pharmacokinetics, and safety have not yet been examined. In this report, we characterized MyoNovin® *in silico* using computer software to explore the physiochemical and biopharmaceutical properties. We also developed and validated an HPLC assay to quantitate MyoNovin® concentrations in serum following IV administration, which allowed us to elucidate initial pharmacokinetic profile.

MyoNovin® was designed to deliver nitric oxide to skeletal muscle, thus providing a novel drug-delivery approach by utilizing guaifenesin as a carrier for transporting NO (9). While there are no clinically viable drugs that directly initiate skeletal muscle growth and regeneration, such treatment would be beneficial in restoring muscle mass in atrophic and some disease conditions. Thus, pharmaceutical development of MyoNovin® could lead to a viable pharmacological approach for the treatment of skeletal muscle atrophy associated with aging, disuse and denervation, and for the repair of skeletal muscle after injury or disease. MyoNovin® is a novel drug targeted toward skeletal muscle regeneration and with potentially lower levels of systemic toxicities typically associated with conventional NO donors. As MyoNovin® is an investigational compound, its physicochemical properties, biodistribution, pharmacokinetics, and safety have not yet been examined. In this report, we characterized MyoNovin® *in silico* using computer software to explore the physiochemical and biopharmaceutical properties. We also developed and validated an HPLC assay to quantitate MyoNovin® concentrations in serum following IV administration, which allowed us to elucidate initial pharmacokinetic profile.

In silico characterization of MyoNovin® revealed that it has low predicted water solubility, a log P of ~3.5, reasonable solubility in fed-state gastrointestinal fluids, good intestinal permeability, and a low likelihood of efflux by transporters (Tables 1 and 2). These parameters suggest that MyoNovin® is a potential candidate for oral administration. The fact that

the solubility of MyoNovin® in fed-state simulated gastrointestinal fluids is more than 30-fold higher than in fasted-state fluids suggests that better oral absorption would be achieved when administered with food. Given that MyoNovin® is a neutral compound and that its solubility is generally expected to be unaffected by fluctuations in the pH according to predictions by GastroPlusTM software (Figure 2A), it is possible that MyoNovin® solubility would be compromised in gastric fluids, as predicted by ADMET PredictorTM software (Table 2). Further development of an oral formulation, use of an enteric coated solid-dosage form of MyoNovin® or incorporation of an acid-neutralizing excipient into the formulation may be useful to overcome the limited solubility of the compound in gastric fluids. Moreover, if MyoNovin® is to be administered as a liquid oral formulation, the vehicle used in that formulation may affect MyoNovin® solubility in gastrointestinal fluid and also its absorption from the gastrointestinal tract. In previous studies published by our group, MyoNovin® was administered as a liquid formulation in corn oil by oral gavage to mice at a dose of 80 mg/kg (9) or as a suspension in canola oil (11). Corn and canola oils may have improved the solubility of the lipophilic molecule, MyoNovin®, and could have also facilitated its absorption via the intestinal lymphatic pathway. Most importantly, the oral administration of MyoNovin® did result in the desired pharmacological effect *in vivo*, as evidenced by the increase in DNA synthesis in skeletal muscle 24 h post-dose (9).

Another potential route for MyoNovin® administration could be transdermal. An ointment transdermal formulation of MyoNovin® may be superior to an oral formulation, due to the ease of transdermal application especially in older individuals with swallowing difficulties. A potential therapeutic barrier to transdermal drug delivery is the ability of a drug to permeate across the stratum corneum layer of the skin. Prediction of MyoNovin®'s skin permeability by

ADMET predictorTM software (19.89 cm/s*107) and its high lipophilicity (predicted by GastroPlusTM log P~3.5) renders it a potential candidate for transdermal application. Furthermore, the vehicle and excipients used in a transdermal ointment formulation can also have an effect on the permeability of MyoNovin® through the skin. Administration of MyoNovin® as a 2% ointment formulation in Dermabase on the shaved skin on the back of mice did increase DNA synthesis of skeletal muscles 24 h following application (9), demonstrating the feasibility of transdermal administration, although it is possible that Dermabase itself, may have improved the permeation of MyoNovin® through the skin.

The effects of MyoNovin® on metabolic enzymes were examined *in vitro* using a commercial assay kit. CYP3A4 is the major metabolic enzyme involved in first-pass metabolism. Results demonstrated that MyoNovin® does not inhibit CYP3A4. This observation is also consistent with the in silico observations as predicted by ADMET PredictorTM software (Table 2). Interestingly, the same software program also predicted that MyoNovin® is a substrate of CYP3A4. The high likelihood of MyoNovin® as a substrate of CYP3A4 suggests that it would likely be susceptible to first-pass metabolism, which may decrease its oral bioavailability and require a higher oral dose for treatment efficacy.

To examine the disposition of MyoNovin® in biological fluids and characterize its pharmacokinetics, an HPLC assay was developed and successfully applied to quantitate the concentration of MyoNovin® in rat serum after IV administration. The IV route was chosen for this initial pharmacokinetic study because its pharmacokinetic parameters would not be contaminated by an absorption phase and/or first-pass metabolism that affects the outcome of drug treatment administered orally. Only male rats were used to minimize factors that may contribute to gender-based differences in metabolism and pharmacokinetics (36, 37). Male and

female rats could metabolize MyoNovin® to different extents due gender dependent hepatic metabolism. Non-metabolic gender based differences in clearance and volume of distribution are also present in animal species (38,39) and may affect the disposition of MyoNovin®. Moreover, female rats may have higher fat content (especially subcutaneous fat) due to estrogen levels (40,41) and this may affect the distribution of lipophilic drugs. Gender based differences in pharmacokinetics may affect serum drug levels and thus the minimum toxic dose that could increase cardiac and renal toxicity biomarkers may be different between male and female rats in our study.

In this study, MyoNovin® was detected in rat serum up to 30 min post-dose, with a biexponential disappearance from plasma. The terminal half-life was very fast, with a t1/2 of 0.16 h. The short half-life of MyoNovin® may be anticipated since the compound is designed to release NO in vivo, leading to the formation of a new metabolite. The observed half-life of MyoNovin® is close to the reported half-life of its precursor guaifenesin: 0.82 h in rats (42) and 1.41 h in ponies (43) after IV administration, and 0.6 -1.03 h in humans after oral administration (44). Furthermore, detection of MyoNovin® in serum for up to 30 min post-dosing as well an M1 peak suggested that MyoNovin® stays intact in the systemic vasculature, releasing NO and distributing it to tissues before it undergoes biotransformation.

The reported physiological parameters of a 0.25 kg rat indicate that the total blood volume is approximately 13.5 mL and total body water is 167 mL (45), which translates to 0.054 L/kg and 0.668 L/kg, respectively. The observed V_{ss} of MyoNovin® (0.620 ± 61.58 L/kg) is larger than the total blood volume and is almost equal to the total body water; these findings suggest that MyoNovin® is rapidly distributed beyond the systemic circulation. The fact that MyoNovin® is lipophilic (predicted Log P 3.49, Table 1) and Vss is not greater than total water

volume suggests that MyoNovin® may be distributed to tissues such as skeletal muscles. Also, the observed Vss of MyoNovin® is comparable to the reported V_{ss} values of guaifenesin, 0.79 L/kg in rats (42), 0.79 L/kg in horses (43), and 0.68 L/kg in donkeys (43).

The safety of MyoNovin on cardiac muscles was examined both *in vitro* and *in vivo*. Human cardiomyocytes were cultured *in vitro* to assess the safety of MyoNovin® on heart muscle. RL-14 cells are a commercially available cell line isolated from human ventricular tissue, and are commonly used to investigate toxic effects induced by xenobiotics. Although there were no *in vivo* effects of MyoNovin® on cardiac size noted after 18 days of treatment in dystrophic mice (10), the effects of MyoNovin® on cardiac tissue are not known in any detail. Here, cardiomyocytes were treated with MyoNovin® at several concentrations, 2, 4, 8, 16, and 32 μM to assess safety *in vitro*. Results demonstrated that MyoNovin® did not induce significant cytotoxicity at 4 μM or lower as the percent viability was about 94 % (figure 7). However, cardiomyocytes treated with MyoNovin® at 8 μM showed only 77% cell viability, suggesting that MyoNovin® may be cardiotoxic at concentrations at or above 8 μM. In this study, rats dosed with 20mg/kg MyoNovin showed a maximum circulating concentration of 43.6 μg/mL (151.3 μM). Assuming linear kinetics a dose of 1 mg/kg would give a maximum circulating serum concentration of 8 μM (2.3 μg/mL), which showed cardiac toxicity *in vitro*. Despite the observed cardiotoxic effects of MyoNovin® *in vitro* at 8 μM during the 24 h of incubation, examination of cardiac troponin concentration 24 h after a single IV dose of MyoNovin® (20mg/kg) in rats showed no acute evidence of cardiotoxicity *in vivo* (figure 13). Furthermore, studies of urinary output and NAG 24 h after administration of the same dose of MyoNovin® *in vivo* showed no initial evidence of renal toxicity (figures 12). Findings therefore suggest that a single IV 20mg/kg dose did not induce acute cardiac or renal toxicity up to 24 h post-dosing, despite

reaching a maximum circulating concentration of 43.6 ± 8.82 μg/mL (~150 μM). It is imperative to note that our *in vivo* results are generated only after single doses. Further research is needed to ascertain the effect of MyoNovin® on cardiac cells.

5.6. CONCLUSIONS

MyoNovin® is a novel synthetic skeletal muscle regenerating agent that was developed using guaifenesin as a carrier system to deliver NO to muscle. Given that there are no viable pharmacological treatments for skeletal muscle atrophy, MyoNovin® and analogues we have synthesized could be a feasible therapeutic approach to restore loss of skeletal muscle mass associated with aging, or to treat diseases by promoting normal repair after injury. Use of guaifenesin's molecular skeleton in MyoNovin® was intended to enhance the localization of NO to skeletal muscle, and thus lower its tendency to induce undesirable systemic effects associated with conventional NO donors.

Our preliminary *in silico* and in vitro observations of MyoNovin® in this study, along with in vivo results from our previous reports (9, 10) suggest that intravenous, oral, and transdermal routes might all be feasible for MyoNovin® administration. Pharmacokinetic characterization shows that MyoNovin® has a short plasma half-life with tissue distribution. Previous and current results now provide a basis for further experiments to explore dosing regimen required to achieve optimal therapeutic outcome and delineate the toxicokinetic profile of MyoNovin®. In addition, efforts to study skin flux and optimize MyoNovin® formulations (particularly solubility) are also warranted and are in progress in our laboratory.

5.7. REFERENCES

1. Wozniak AC, Pilipowicz O, Yablonka-Reuveni Z, Greenway S, Craven S, Scott E, Anderson JE. C-Met expression and mechanical activation of satellite cells on cultured muscle fibers. J Histochem Cytochem, 2003;51(11):1437-45.
2. Darr KC, Schultz E. Exercise-induced satellite cell activation in growing and mature skeletal muscle. J Appl Physiol (1985). 1987;63(5):1816-21.
3. Tatsumi R, Liu X, Pulido A, Morales M, Sakata T, Dial S, Hattori A, Ikeuchi Y, Allen RE. Satellite cell activation in stretched skeletal muscle and the role of nitric oxide and hepatocyte growth factor. Am J Physiol Cell Physiol, 2006; 290(6):C1487-94.
4. Wozniak, A. C.; Anderson, J. E. Single-fiber isolation and maintenance of satellite cell quiescence. Biochem. Cell Biol, 2005; 83, 674–6.
5. Anderson JE. Molecular Biology of Cell, 2000;11:1859-74.
6. Miller KJ, Thaloor D, Matteson S, Pavlath GK. Hepatocyte growth factor affects satellite cell activation and differentiation in regenerating skeletal muscle. Am J Physiol Cell Physiol, 2000 ;278(1):C174-81.
7. Mauro A. Satellite cell of skeletal muscle fibers. J Biophys Biochem Cytol. 1961; 9:493-5.
8. Moss FP, Leblond CP. Satellite cells as the source of nuclei in muscles of growing rats. Anat Rec, 1971; 170(4):421-35.
9. Wang G, Burczynski FJ, Hasinoff BB, Zhang K, Lu Q, Anderson JE. Development of A Nitric Oxide Releasing Analogue of the Muscle Relaxant Guaifenesin for Skeletal Muscle Satellite Cell Myogenesis. Mol Pharm. 2009; 6(3):895-904.
10. Wang G, Burczynski FJ, Anderson JE. Composition and methods for enhancing nitric oxide delivery. U.S. Patent 8,106,080 B2 filed June 8, 2006, and issued January 31, 2012.

11. Mizunoya W, Upadhaya R, Burczynski FJ, Wang G, Anderson JE. Nitric oxide donors improve prednisone effects on muscular dystrophy in the mdx mouse diaphragm.Am J Physiol Cell Physiol. 2011;300(5):C1065-77.
12. Tetko IV, Gasteiger J, Todeschini R, Mauri A, Livingstone D, Ertl P, Palyulin VA, Radchenko EV, Zefirov NS, Makarenko AS, Tanchuk VY, Prokopenko VV. Virtual computational chemistry laboratory—Design and description, J Comput Aided Mol Des. 2005;19(6):453-63.
13. Virtual Computational Chemistry Laboratory. Available online: http://www.vcclab.org (accessed on 24 August 2017).
14. Liu Y, Schubert D. Cytotoxic amyloid peptides inhibit cellular 3-(4,5-dimethylthiazol-2-yl)-2,5-diphenyltetrazolium bromide (MTT) reduction by enhancing MTT formazan exocytosis. J Neurochem, 1997; 69(6):2285-93.
15. Maayah ZH, El Gendy MA, El-Kadi AO, Korashy HM. Sunitinib, a tyrosine kinase inhibitor, induces cytochrome P450 1A1 gene in human breast cancer MCF7 cells through ligand-independent aryl hydrocarbon receptor activation. Arch Toxicol, 2013; 87(5):847-56.
16. Lillico R, Sayre CL, Sitar DS, Davies NM, Baron CM, Lakowski TM. Quantification of cefazolin in serum and adipose tissue by ultra high performance liquid chromatography-Tandem mass spectrometry (UHPLC-MS/MS): application to a pilot study of obese women undergoing cesarean delivery. J Chromatogr B Analyt Technol Biomed Life Sci, 2016; 15;1031:94-98.
17. Charles River Laboratories International, Vascular Catheterizations: Handling Instructions, 2012.
18. Naughton, C.A. Drug-induced nephrotoxicity. Am. Fam. Physic, 2008; 78, 743–750.

19. Le JM, Han YH, Choi SJ, Park JS, Jang JJ, Bae RJ, Lee MJ, Kim MJ, Lee YH, Kim D, Lee HY, Park SH, Park CB, Kang JS, Kang JK. Variation of nephrotoxicity biomarkers by urinary storage condition in rats. Toxicol Res. 2014;30(4):305-9.
20. Alrushaid S, Sayre CL, Yáñez JA, Forrest ML, Senadheera SN, Burczynski FJ, Löbenberg R, Davies NM. Pharmacokinetic and Toxicodynamic Characterization of a Novel Doxorubicin Derivative. Pharmaceutics. 2017;9(3):35.
21. www.Drugbank.ca
22. Wallace JL. Nitric oxide as a regulator of inflammatory processes. Mem Inst Oswaldo Cruz. 2005 Mar;100 Suppl 1:5-9.
23. US Food and Drug Administration Guidelines on Analytical Procedures and Methods Validation for Drugs and Biologics, US Food and Drug Administration, 2015.
24. Wong PS, Fukuto JM. Reaction of organic nitrate esters and S-nitrosothiols with reduced flavins: a possible mechanism of bioactivation. Drug Metab Dispos, 1999; 27(4):502-9.
25. Kauert G, von Meyer L, Drasch G. Investigations of guaifenesine metabolism with gas chromatography-mass spectrometry. Arch Toxicol, 1980; 45(2):149-59.
26. Giri SN. The pharmacological action and O-demethylation of glyceryl guaiacolate ether in male and female rats. Toxicol Appl Pharmacol, 1973;24(4):513-8.
27. Vandenheuvel WJ, Smith JL, Silber RH. -(2-Methoxyphenoxy)lactic acid, the major urinary metabolite of glyceryl guaiacolate in man. J Pharm Sci, 1972; 61(12):1997-8.
28. Naito SI, Mizutani M, Kitao K, Nishimura S. Biopharmaceutical studies on guiacol glycerol ether and related compounds. 3. Metabolites of guaiacol glycerol ether and its mononicotinate. 1. Chem Pharm Bull (Tokyo). 1969;17(9):1794-8.

29. Mizutani M, Naito S. Studies on absorption and excretion of drugs. XXIX. Biopharmaceutical studies on guaiacol glycerol ether and related compounds. I. Blood level of guaiacol glycerol ether in rabbit and its binding with serum proteins. Chem Pharm Bull (Tokyo), 1967;15(9):1422-6.
30. Notenboom S, Miller DS, Smits P, Russel FG, Masereeuw R. Role of NO in endothelin-regulated drug transport in the renal proximal tubule. Am J Physiol Renal Physiol, 2002; 282(3):F458-64.
31. Kone BC. Nitric oxide in renal health and disease. Am J Kidney Dis 30: 311–333, 1997.
32. Pickens CL, Milliron AR, Fussner AL, Dversdall BC, Langenstroer P, Ferguson S, Fu X, Schmitz FJ, Poole EC. Abuse of guaifenesin-containing medications generates an excess of a carboxylate salt of beta-(2-methoxyphenoxy)-lactic acid, a guaifenesin metabolite, and results in urolithiasis. Urology, 1999; 54(1):23-7.
33. Le JM, Han YH, Choi SJ, Park JS, Jang JJ, Bae RJ, Lee MJ, Kim MJ, Lee YH, Kim D, Lee HY, Park SH, Park CB, Kang JS, Kang JK. Variation of nephrotoxicity biomarkers by urinary storage condition in rats. Toxicol Res. 2014;30(4):305-9.
34. Ferdinandy P, Schulz R. Nitric oxide, superoxide, and peroxynitrite in myocardial ischaemia-reperfusion injury and preconditioning. Br J Pharmacol, 2003;138(4):532-43.
35. Adamcova, M.; Sterba, M.; Simunek, T.; Potacova, A.; Popelova, O.; Mazurova, Y.; Gersl, V. Troponin as a marker of myocardiac damage in drug-induced cardiotoxicity. Expert Opin. Drug Saf. 2005; 4:457–472.
36. Czerniak R. Gender-based differences in pharmacokinetics in laboratory animal models. *Int J Toxicol*. 2001;20(3):161-3.

37. Lyu C, Zhang Y, Zhou W, Zhang S, Kou F, Wei H, Zhang N, Zuo Z. Gender-Dependent Pharmacokinetics of Veratramine in Rats: In Vivo and In Vitro Evidence. AAPS J. 2016;18(2):432-44.
38. Witkamp RF, Yun HI, van't Klooster GA, van Mosel JF, van Mosel M, Ensink JM, Noordhoek J, van Miert AS.Comparative aspects and sex differentiation of plasma sulfamethazine elimination and metabolite formation in rats, rabbits, dwarf goats, and cattle. *Am J Vet Res*. 1992;53(10):1830-5.
39. Griffin RJ, Godfrey VB, Kim YC, Burka LT.Sex-dependent differences in the disposition of 2,4-dichlorophenoxyacetic acid in Sprague-Dawley rats, B6C3F1 mice, and Syrian hamsters. *Drug* Metab Dispos. 1997;25(9):1065-71.
40. Thibault L. Animal Models of Dietary-Induced Obesity. In Conn PM (Ed.), Animal Models for the Study of Human Disease in. Elsevier Inc., 2013.
41. Jenkins AJ. Toxicokinetics and Factors Affecting Pharmacokinetic parameters. In Karch SB (Ed.), Pharmacokinetics and Pharmacodynamics of Abused Drugs. New York: CRC Press Taylor & Francis group, 2007.
42. Kagan L, Lavy E, Hoffman A. Effect of mode of administration on guaifenesin pharmacokinetics and expectorant action in the rat model. Pulm Pharmacol Ther, 2009; 22(3):260-5.
43. Davis LE, Wolff WA. Pharmacokinetics and metabolism of glyceryl guaiacolate in ponies. Am J Vet Res, 1970; 31(3):469–73.
44. Thompson GA, Solomon G, Albrecht HH, Reitberg DP, Guenin E. Guaifenesin Pharmacokinetics Following Single-Dose Oral Administration in Children Aged 2 to 17 Years. J Clin Pharmacol, 2016; 56(7):894-901.

45. Davies B, Morris T. Physiological parameters in laboratory animals and humans. Pharm Res, 1993; 10(7):1093-5.

CHAPTER 6

SUMMARY, CONCLUSIONS, AND FUTURE DIRECTION

6.1. SUMMARY AND CONCLUSIONS

Much effort has been made towards improving the efficacy and safety of pharmaceuticals yet many of the drugs used clinically still exhibit therapeutic barriers that limit their clinical use. Systemic toxicities, undesirable side effects, and poor oral bioavailability are among the most common therapeutic barriers. Drug delivery strategies such as using nanocarriers (e.g.: micelles and polymeric carriers), antibody directed therapy, chemical derivatization, and using combination therapy have been employed to optimize drug therapy. Chemical derivatization alters the physicochemical properties of the parent drug and subsequently its bio-distribution and pharmacological effects could also change. In this thesis, a chemical derivatization strategy (pro-drug approach) was employed to improve drug delivery of two investigational compounds. Pre-clinical *in silico*, *in vitro*, or *in vivo* studies on DoxQ and MyoNovin® were undertaken to evaluate the utility of the drug delivery strategy and examine their efficacy, safety, and bio-distribution.

Doxorubicin is one of the most commonly used anti-cancer drugs, yet could induce severe cardiac toxicity leading to discontinuation of the therapy. The currently available liposomal formulations of Dox: Doxil™ and Myocet™ provide a sustained release of Dox with a lower C_{max} compared to Dox-HCl, and subsequently result in lower acute cardiac toxicity and are only administered parentally. Dox is also characterized by distribution to tissues resulting in undesirable side effects and possibly toxicities (e.g.: renal toxicity). Therefore, increasing the localization of Dox at the desired tissues while minimizing Dox-induced toxicities would have a significant effect on Dox therapy. In this thesis, the utility of using quercetin as a lymphatic carrier for the delivery of Dox to the lymphatics was investigated for the first time (Chapter 5).

Intestinal lymphatic transport studies of Dox after oral DoxQ and Dox in a mesenteric lymph duct cannulation model as well as cycloheximide model in rats suggest that DoxQ facilitated the intestinal lymphatic transport of Dox as evident by a 2 fold increase in Dox concentration in lymphatic fluid vs Dox and a 1.5 fold decrease in AUC_{last} after blocking intestinal lymphatic pathway by cycloheximide (1).One of the mechanisms by which Dox-induces cardiac and renal toxicities is oxidative stress, so using the antioxidant quercetin to mitigate theses toxicities could improve the safety of Dox therapy. Findings presented in this thesis show that a single equimolar IV dose of DoxQ did not increase levels of cardiac troponin compared to Dox alone in normal rats despite a 4 fold increase in C_0 after DoxQ vs Dox suggesting that DoxQ was not more cardiotoxic than Dox (Chapter 4). These results are also consistent with *in vitro* studies where DoxQ was less toxic to both rat and human cardiomyocytes compared to Dox alone (Chapter 3). DoxQ also retained anticancer activity in a triple negative murine cancer cell line. If DoxQ retains efficacy and is less likely to cause cardiac toxicity then this could possibly allow for more doses of DoxQ (IV) to be administered as Dox-induced cardiac toxicity results from cumulative doses accumulating in the heart. The cardioprotective effects of DoxQ are likely due to the antioxidant activity of quercetin present in DoxQ intact or when released from the conjugate as well as inhibitory effects on CYP1B1 expression and catalytic activity (2). In addition to mitigating Dox induced cardiac toxicity, it is possible that antioxidant activity of DoxQ also had a protective effect on Dox induced nephrotoxicity as levels of NAG were significantly lower after an equimolar IV dose of DoxQ vs Dox. By understanding the protective mechanism of DoxQ against Dox-induced cardiac toxicity, it is possible that DoxQ also exhibits protective effects on other tissues that could be susceptible to Dox induced damage such as the liver.

Another limitation of doxorubicin therapy is that it has poor bioavailability and therefore it is administered parenterally. Oral DoxQ improved the systemic exposure of Dox compared to oral Dox alone in a rat model (Chapter 4). The overall increase in the systemic exposure of Dox after DoxQ by ~1.5 fold compared to Dox after Dox is likely due to reducing the susceptibility of Dox to first pass effect (F=1-E) and also partially shunting Dox to intestinal lymphatics. As Dox is a substrate of CYP3A4 and P-gp efflux pump, reducing effects of Dox on CYP3A4 as well as P-gp when quercetin is released likely reduced E, improved absorption and thus increased the systemic exposure to Dox. Additionally, the presence of the lymphatic carrier quercetin likely facilitated the transport of Dox via intestinal lymphatics pathway partially shunting it from absorption via hepatic portal vein and possibly lowered E and contributed to the overall increase in systemic exposure.

If oral DoxQ improved the systemic exposure of Dox by ~1.5 fold in a rat model, then an oral formulation of DoxQ could be beneficial and warrants consideration for therapeutic use. The 1.5 increase in systemic exposure of Dox after DoxQ was observed when rats where fasted prior to oral dosing, while more than 3 fold increase in the systemic exposure was observed when rats were not fasted in an earlier pilot study (unpublished observations from Davies and Dr. Forrest laboratories). Fasting could have reduced the incoperation of DoxQ into chylomicrons or possibly blocked the intestinal lymphatic pathway and thus reduced the overall systemic exposture in fasting rats compared to non-fasting rats. Therefore, co-administereation of oral DoxQ with food, adding lipids to the oral formulation, or pre-administerion of lipids prior to oral dosing would likely facilitate absorption via intestinal lymphatics, by promoting formation of chylomicrons, and increase the overall systemic exposure to Dox after oral DoxQ. Furthermore, an oral formulation of Dox could provide better patient convenience and improve the overall

quality of life as the invasiveness of the conventional Dox IV therapy and the complications associated with its administration is a major limitations. In addition, oral DoxQ could reduce the cardiotoxicity associated with Dox by partially shunting Dox towards intestinal lymphatics and may also be useful to treat lymphomas and metastatic cancers, which spread through lymphatics.

The utility of using the skeletal muscle regenerator MyoNovin® as a drug delivery strategy for NO transport with emphasis on potential routes of administration, disposition, and safety was investigated (Chapter 5). The guaifenesin skeleton of MyoNovin® is intended to limit systemic effects of nitric oxide to skeletal muscle, hence reducing systemic undesirable effects of NO and improving therapeutic efficacy. Preliminary *in silico*, *in vitro*, *in vivo* studies presented in this thesis (3) as well as promising results of MyoNovin®'s efficacy in normal (4) and dystrophic rodent models (5) suggest that intravenous, oral, and transdermal routes of administration are feasible. Effects of MyoNovin® on metabolic ezymes, antioxidant activity, as well as on cardiac and renal tissues were examined because NO released from MyoNovin® could affect normal physiological levels of NO and thus affect various pharmacological activities. MyoNovin® did not inhibit CYP3A4 nor exhibit antioxidant activity. In silico biopharmaceutical and pharmacokinetics modelling data by ADMET Predictor™ software (Tables 5.2 and 5.3) was used as basis to design the pharmacokinetic study *in vivo*. Pharmacokinetic studies in a rat model showed MyoNovin® has a short half-life of 0.16 h and distributes to tissues following a single IV dose (Table 5.5). To refine and improve the resulting PK data from the *in vivo* study further efforts are needed. Preliminary assessment of cardiac and renal safety revealed that MyoNovin® did not induce cardiac or renal toxicities after a single intravenous dose of 20mg/kg in a rat model.

Findings presented in this thesis provide insight into formulation design, pharmacological effects, and dosing regimen of MyoNovin® and warrants consideration for further pharmaceutical development and therapeutic use especially that there are no clinically viable pharmacological treatments for muscle atrophy. As a skeletal muscle regenerator, MyoNovin® administered transdermally or orally could be useful to treat muscle atrophy and muscle injury by restoring the loss in skeletal muscle mass. In addition, restoring the loss of skeletal muscle in age related atrophy could reduce the likelihood of bone fractures and could also be useful in conditions where skeletal muscle restoration is needed but is refractory to hypertrophy induced by exercise.

6.2. FUTURE DIRECTION

For further pharmaceutical development of DoxQ future efforts will focus on chronic studies and multiple dosing pharmacokinetics to optimize dose frequency and examine the influence of food or lipids co-administration with DoxQ or prior to its administration. In addition, studies to examine anti-cancer activity of DoxQ *in vivo* as well other potential lymphatic carriers for oral drug delivery are warranted. Also, to confirm that DoxQ is shunted into the lymphatic system in the gut, fluorescence imaging techniques could be used as Dox exhibits a fluorescent property rendering it possible to follow *in vivo*.

Future studies on MyoNovin® should be towards optimizing formulations for oral and transdermal administration. *In vitro* skin flux studies would be useful to determine the fraction of the dose could permeate across the skin. The RP-HPLC assay of MyoNovin® described in chapter 5 could be employed to quantitate MyoNovin® concentrations from skin flux studies. These skin flux studies would improve therapeutic efficacy and reduce the dose of MyoNovin®

required as well as provide insight into dosage regimen for transdermal application. Given the short half-life of MyoNovin® and limitation of the analytical assay, further efforts to improve pharmacokinetic modelling data should be considered. One way to refine the pharmacokinetic modelling data, is to collect larger blood volume samples at each time point, which may require terminal blood sample collection or sacrificing rats after each sample collection. Similarly, for future pharmacokinetic studies in humans a larger blood sample will likely be required. Alternatively, a population study or a sparse data approach could be used to improve the pharmacokinetic modelling data. Further studies on MyoNovin® metabolites, multiple dosing and chronic pharmacokinetic and toxicokinetic studies are also need for optimal therapeutic efficacy and safety.

6.3. REFERENCES

1. Alrushaid S, Sayre CL, Yáñez JA, Forrest ML, Senadheera SN, Burczynski FJ, Löbenberg R, Davies NM. Pharmacokinetic and Toxicodynamic Characterization of a Novel Doxorubicin Derivative. Pharmaceutics. 2017;13;9(3).
2. Alrushaid S, Zhao Y, Sayre CL, Maayah ZH, Forrest ML, Senadheera SN, Chaboyer K, Anderson HD, El-Kadi A, Davies NM. Mechanistically Elucidating the In-Vitro Safety and Efficacy of a Novel Doxorubicin Derivative. Drug Deliv Transl Res. 2017;7(4):582-597.
3. Alrushaid S, Davies NM, Anderson JE, Le T, Yáñez JA, Maayah ZH, El-Kadi AOS, Rachid O, Sayre CL, Löbenberg R, Burczynski FJ. Pharmaceutical Characterization of MyoNovin®, a Novel Skeletal Muscle Regenerator: In silico, in vitro and in vivo Studies. J Pharm Pharm Sci. 2018;21(1s):1-18.

4. Wang G, Burczynski FJ, Hasinoff BB, Zhang K, Lu Q, Anderson JE. Development of A Nitric Oxide Releasing Analogue of the Muscle Relaxant Guaifenesin for Skeletal Muscle Satellite Cell Myogenesis. Mol Pharm. 2009; 6(3):895-904.
5. Mizunoya W, Upadhaya R, Burczynski FJ, Wang G, Anderson JE. Nitric oxide donors improve prednisone effects on muscular dystrophy in the mdx mouse diaphragm. *Am J* Physiol Cell Physiol. 2011;300(5):C1065-77.